Hydrothermal Catalytic Deoxygenation of Fatty Acids and Upgrading Algae Biocrude

by

Thomas M. Yeh

A dissertation submitted in partial fulfillment
of the requirements for the degree of
Doctor of Philosophy
(Chemical Engineering)
in the University of Michigan
2015

Doctoral Committee:

Professor Suljo Linic, Co-chair
Professor Phillip E. Savage, Co-chair
Professor Adam J. Matzger
Professor Levi T. Thompson

To my family and friends.

ACKNOWLEDGMENTS

I thank my committee members, Phil, Suljo, and Adam for their guidance and support during my time at Michigan. Each member has asked many thought provoking questions that have resulted in higher quality research. Their contributions have been instrumental to my success.

My wife, Karen, has provided unending support throughout this time. She has been with me every step of the way, and she has never asked me the most dreaded question of the PhD student – "How's your research going?".

My parents helped in the best way parents can – with free food. The skills my parents taught me through maintaining apartments has been used repeatedly in the lab through reactor construction and general equipment maintenance.

Professional statistical analysis, career advice, and general support was always a phone call away. My in-laws support has consistently far exceeded expectations over the years.

The Savage and Linic group members have provided valuable feedback through discussions and thought provoking questions during group presentations.

My friends provided much needed escapes from research. Leonid Pavlovsky introduced me to the art of beer brewing. As a result, I have slowly transformed into a beer snob, and Michelle Przybylek held a birthday party for me every year. Matt Morabito, Julia Faeth, Lilian Hsiao, Chad Huelsman, Ryan Franck, and Luke Griffith played Dungeons & Dragons with me and fulfilled my innate desire to nerd-out. Peter Valdez and I went on many outings to the shooting range, and he offered me training in the art of tact. Youngri Kim provided many rides to the airport and helped fulfill my love of being cheap and not paying for airport parking. Jenn Jocz was a good tennis partner, and she was able to put up with being in my office and not be offended. Yang Guo and Donghai Xu taught me Chinese and corrected my accent. Because of Yang, I also ate more bacon in one year than I have in my entire life thus far.

Lastly, I am grateful for the staff. Kelly Raickovich, Susan Hamlin, Shelley Fellers, Pam Bogdanski, and Laura Bracken have provided a lot of administrative support. Kelly provided copious amounts of free food and literally provided the energy for a lot of this work.

Preface

All work presented was performed at the University of Michigan. This work contains both published and unpublished work that is the original work of the author, Thomas Yeh.
Portions of Chapter 2 are published as a review paper. Some of Chapter 4 and most of Chapter 5 has been published, but Chapter 5 has been modified to include unpublished material. Finally, Chapter 6, has been submitted for publication and is under review at the time of this writing.

TABLE OF CONTENTS

LIST OF FIGURES

LIST OF TABLES

LIST OF APPENDICES

LIST OF ABBREVIATIONS

FID flame ionization detector

GC gas chromatography

HDO hydrodeoxygenation

HTL hydrothermal liquefaction

MS mass spectrometer

TCD thermal conductivity detector

TEM transmission electron microscope

XRD x-ray diffraction

DRIFTS Diffuse reflectance infrared Fourier transform spectroscopy

FTIR Fourier transform infrared spectroscopy

EROI energy return on investment

LHHW Langmuir Hinshelwood Hougen Watson

ATR Attenuated total reflectance

FAMEs fatty acid methyl esters

HDS hydrodesulfurization

DFT density functional theory

SCW supercritical water

ABSTRACT

Hydrothermal Catalytic Deoxygenation of Fatty Acids and Upgrading Algae Biocrude

by

Thomas M. Yeh

Co-Chairs: Suljo Linic and Phillip E. Savage

This work addresses the production of renewable liquid transportation fuels from algae. Pt/C and $PtSn_x$/C were used to deoxygenate free fatty acids, model compounds for components in biocrude oil, from liquified algae. All reactions were conducted in the aqueous phase.

Pt/C is an effective decarboxylation catalyst in the hydrothermal environment, but studies examining catalyst longevity are limited. Catalyst deactivation studies with Pt/C and butyric acid in a continuous flow reactor revealed a first order deactivation rate constant, k_d, of 0.063 ± 0.006 h^{-1}. A combination of coking and molecular poisoning was responsible for the deactivation of the catalyst. Diffuse reflectance infrared Fourier transform spectroscopy (DRIFTS) and gas chromatography (GC) suggested the poison was an unsaturated C_3 molecule.

Pt/C is effective for decarboxylating saturated fatty acids to the alkane products, but it suffers from low selectivity for unsaturated fatty acids, which are more

abundant in plant-derived oils, in the absence of H_2. Rather than decarboxylating the unsaturated feed to a hydrocarbon, the unsaturated acid hydrogenates to the fully saturated fatty acid. $PtSn_x/C$ catalysts showed selectivities up to three times higher than Pt for oleic acid (C18:1) decarboxylation and two times higher for linoleic acid (C18:2) decarboxylation. Even with the addition of Sn into the alloy system, however, catalyst activity and selectivity still declined with increasing fatty acid unsaturation. Interestingly, with both Pt and $PtSn_x$ in the absence of external H_2, the resulting fuel molecule was fully saturated. Experiments in D_2O showed that water served as a source of hydrogen.

More generally, many catalysts are unstable in the hydrothermal environment. To have societal impact, the catalysts need to be both active and stable for biocrude oil rather than just model compounds. Some catalyst metal and support combinations were chosen to upgrade algae biocrude oil based on previous activity towards deoxygenation and denitrogenation of model compounds found in biocrude oils and stability in near critical, supercritical water, and high temperature steam. The presence of H_2 shifted the products from catalytically upgraded biocrude towards heavier, diesel appropriate molecules whereas the absence of H_2 resulted in a wider range of hydrocarbons suitable for liquid fuels from gasoline to diesel.

CHAPTER 1

Introduction

1.1 Background and Motivation

Abundant energy resources have enabled the economic and technological advancements that we as a society have enjoyed. As humanity continues to progress, we increasingly depend on abundant and cheap sources of energy. The total US energy delivered, as opposed to consumed, is projected to increase from 70 quadrillion Btu in 2014 to 77 quadrillion Btu in 2040. Energy use in the US can be broken down into four major sectors composed of residential, commercial, industrial, and transportation use. Respectively, each sector is projected to account for 16, 12, 34, and 38% of the total energy demand for 2014, Figure 1.1[1]. Coal, petroleum, and natural gas are the primary energy sources with petroleum in particular fueling the transportation sector, but these are all fossil fuels and thus finite in nature. Unfortunately, the use of fossil fuels releases greenhouses gases and causes climate change. To address these issues, researchers look to renewable energy sources such as solar, wind, hydropower, geothermal, and biomass.

Petroleum and its products, such as gasoline and diesel, are one of these finite

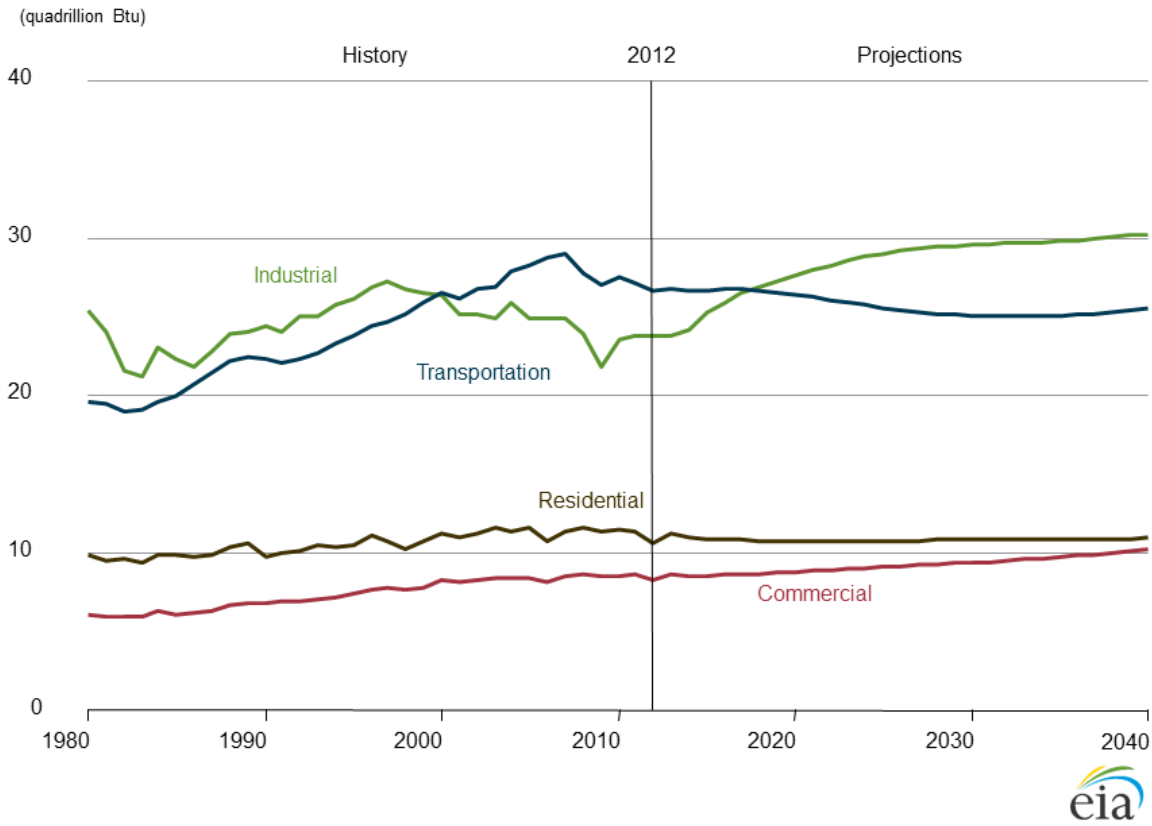

Figure 1.1: Total US energy delivered by sector from 1980 – 2040[1]

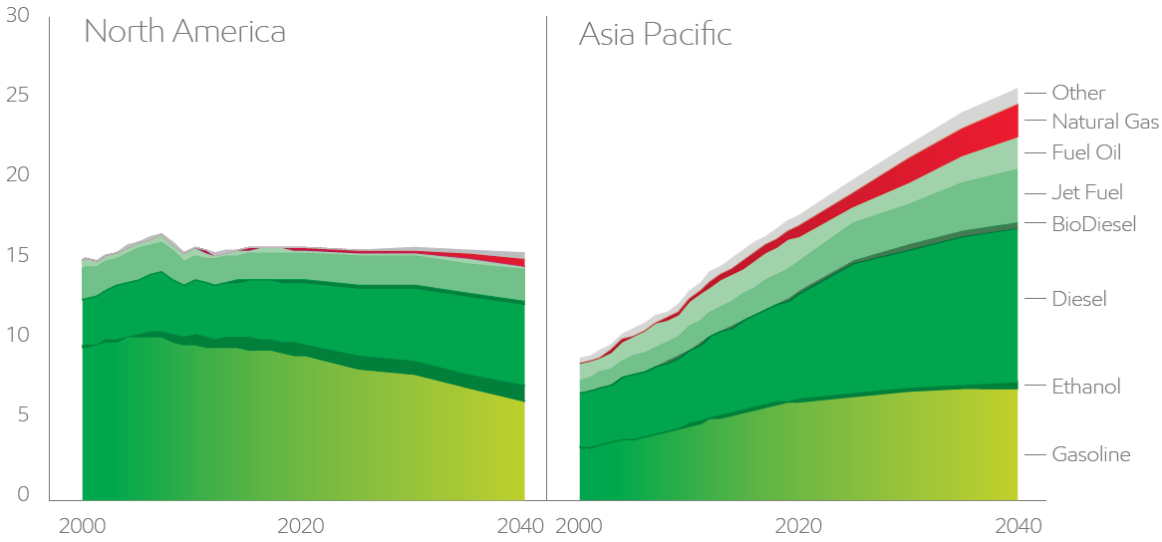

Figure 1.2: Transportation fuel use by type for North America and Asia Pacific (Millions of oil-equivalent barrels per day) [2]

energy resources that has enabled rapid economic growth through transportation. World liquid fuel demand is expected to rise through 2040, but the US is projected to have a slight decrease. However, the demand for diesel fuel is expected to increase for both regions, Figure 1.2 [1, 2].

1.2 Biomass

Biomass is a promising renewable energy source for producing liquid transportation fuels. Many techniques already exist to produce liquid fuels from biomass. Fermentation of corn starch or cane sugar results in ethanol. Oil extraction of seeds such as rape seed or soybeans results in a liquid oil, and pyrolysis of cellulose and lignin yields a liquid biocrude.

1.2.1 First and Second Generation Biofuels

Corn ethanol was one of the candidates in the initial push for biofuels. Initially corn-based fuel was thought to be capable of serving as an energy source (energy return on investment (EROI) > 1) and reduce CO_2 emissions in comparison to gasoline. Reports show a range of EROI for corn between 0.8–1.3, where 1 is the value required to break even, and 3 is the minimum for a sustainable society[3–5]. Corn ethanol can serve as an energy storage medium, but it cannot serve as an alternative energy source due to the low EROI. The growth of corn for both food and fuel production has had unintended consequences. The overuse of fertilizer to grow corn has led to the formation of hypoxic and anoxic deadzones in the Gulf of Mexico and near other areas for fresh water runoff. These hypoxic zones are areas of reduced oxygen content that are incapable of supporting the majority of sea life such as fish or shrimp [6]. Land use also changed due to economic incentives for biofuel production. Life cycle analysis accounting for land use change suggested that through a variety of factors including water use and land use change, corn ethanol may even emit more CO_2 than gasoline [7]. Biodiesel has met some of the same criticisms as corn ethanol, but in general, it is viewed more favorably both in terms of EROI and green house gas emissions[4, 8].

As biofuel technology advances, the focus has shifted from first generation biofuels derived from corn, sugar cane, and oil seeds, which compete for food or feed, to second generation biofuels derived from grasses and corn stover which do not compete with the food/feed supply. Cellulosic ethanol is a promising technology

that can address many transportation fuel use needs while avoiding the issues associated with food versus fuel[9]. Cellulose however, is a complex polymer that requires complicated processing and still suffers from a low EROI around 1[8]. While there are still hurdles to overcome regarding cellulosic ethanol, two commercial cellulosic ethanol plants have recently become operational, and one more is under construction. POET-DSM opened a facility in September that is capable of producing 20 million gallons of ethanol per year [10, 11]. Abengoa currently operates a facility in Kansas capable of producing 20 million gallons of ethanol annually [10, 11]. Dupont is currently building a facility that is projected for completion in early 2015 [10–12]. Altogether, the three ethanol plants will generate 70–80 million gallons of ethanol per year with the 2013 U.S. consumption of gasoline at 135 million gallons [13].

1.2.2 Third Generation – Algae

Microalgae, a unicellular organism hereon referred to as algae, is uniquely poised to address the need for alternative fuels. Algae is an aquatic plant, therefore it can grow in man-made ponds constructed on non-arable lands. Growth ponds can also help mitigate the environmental problems associated with fertilizer runoff. It is a relatively simple organism that does not contain lignin and can simplify processing. Additionally, algae is capable of high productivity in comparison to agricultural biofuels. Low projections of algal productivity, 40,700 L $\cdot$ha$^{-1}\cdot$ year^{-1}, show volumetric fuel production one to two orders magnitude higher than corn,

canola, and oil palm (172, 1190, 5950 $L \cdot ha^{-1} \cdot year^{-1}$) [14].

One major reason for the high productivity of producing liquid fuels from algae is the composition. Algae are composed primarily of three different types of compounds: proteins, carbohydrates, and lipids. On a dry weight basis, the protein, carbohydrate, and lipid content can range from 23–65%, 8–49%, 1–77% respectively depending on the strain selected [15–17]. The lipids contain fatty acid chains that typically range from 14 – 22 carbons long, and 55 – 85% of the fatty acids are unsaturated [15].

While algae are capable of producing high oil yields in comparison to terrestrial biomass, processing the aquatic plant becomes problematic due to the high water content. Algae are typically grown to a concentration of 0.1 wt% or 1 g/L, and can be concentrated to 8 wt% through flocculation or filtering. Conventionally, biomass feedstocks need to be dried to 95% dry weight to be processed, either through oil extraction or pyrolysis, but the large water content in algae makes this energetically and economically unfeasible.

1.3 High temperature water

As enough water cannot be removed from algae in this process to make conventional techniques attractive, an attractive alternative is to process algae in water to avoid drying. One might expect that water, as a polar solvent, is a poor choice for reaction medium when handling non polar compounds such as oils. Hot and compressed liquid water, however, has properties that differ from water at ambi-

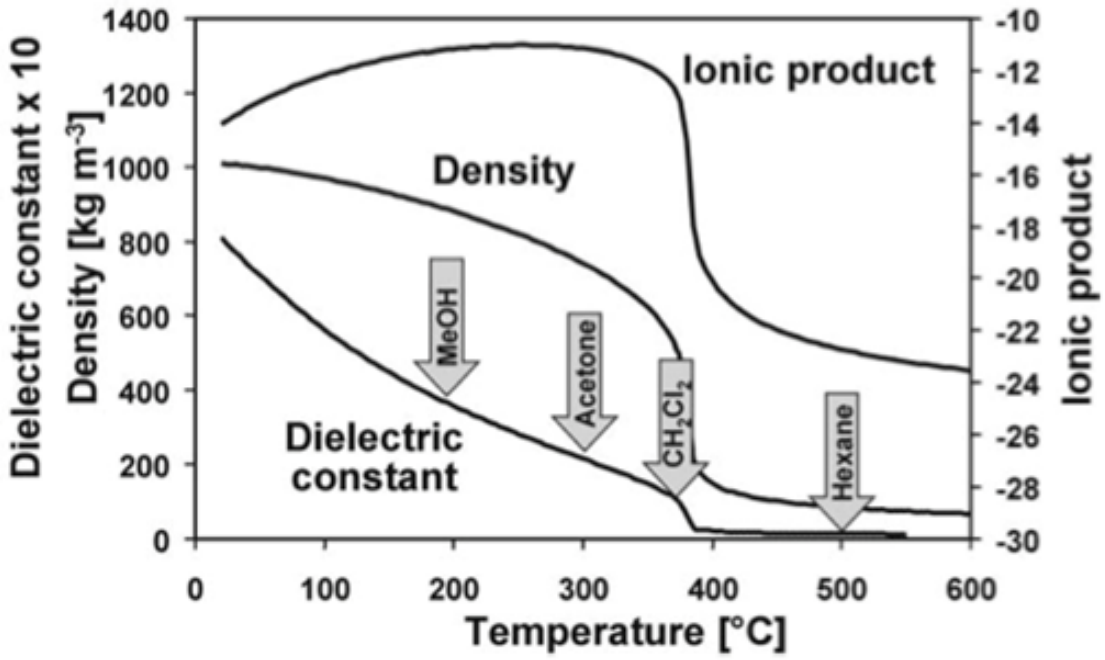

Figure 1.3: Physical properties of water at 24 MPa with respect to temperature [18]

ent conditions. Figure 1.3 shows that with increasing temperature, liquid water has an increasing ionic product which facilitates both acid and base chemistries. More importantly, the dielectric constant decreases with increasing temperature allowing for water to behave as a nonpolar solvent [18]. The increasing nonpolar behavior allows us to process biomass with high water contents without the need for an expensive drying step.

1.3.1 Supercritical Water

Water enters the supercritical region when the temperature and pressure exceed the critical point of water (374 °C, 22.1 MPa). Supercritical fluids have unique properties that make them neither a liquid nor a gas but share properties of both. Figure 1.3 demonstrates that the density of a liquid near the critical point rapidly

decreases with small changes in temperature, thus becoming more gas-like. Although the fluid becomes more gas-like, it still retains its abilities to behave as a solvent. Gases are completely miscible in supercritical fluids allowing for high concentrations that would normally not be accessible in the liquid phase. These properties of supercritical water give desirable properties that might otherwise be unavailable. Supercritical water allows for facile dissolution of biocrude along with complete miscibility of hydrogen as a reactant.

CHAPTER 2

Literature Review

Some of the background information provided here has already been published in a review paper [19].

2.1 Hydrothermal Liquefaction Oil

Hydrothermal treatment of algae ranges in temperature from 200 – 800 °C. At temperatures from 200 – 250 °C, algae carbonizes into a coal-like solid. At temperatures from 300 – 400 °C, the reaction yields a biocrude oil product, and above 350 °C, depending on catalyst selection, gasification of the algae contents dominates to produce gases such as methane and hydrogen [19–28]. This work focuses on the production of liquid transportation fuels, and hydrothermal liquefaction generally shows optimum conditions for bio-oil production around 300 – 400 °C[23–28].

Algae liquefaction can be executed both with and without catalysts. Catalytic liquefaction uses a one-pot technique where the idea is to liquefy the algae while simultaneously removing heteroatoms from the resulting oil.

This work focuses on the non catalytic liquefaction process which requires a cat-

alytic treatment as a separate process. The composition of the raw algae impacts the quality and composition of the resulting products from liquefaction. When algae is hydrothermally liquefied, the products fractionate into four separate phases: the aqueous phase, organic phase, gas phase, and solids phase.

The aqueous phase contains most of the original nitrogen as ammonia and phosphorus as phosphate [29, 30]. The nitrogen fractioning to the aqueous phase as NH_3 is consistent with work concerning amino acid model compounds in 300 °C water,[31] and liquefied protein-containing biomass[32]. The aqueous-phase from hydrothermal liquefaction (HTL) of *Nannochloropsis* sp. contained small polar compounds such as citric acid, glucose, glycerol, lactic acid, and pyruglutamic acid. The concentration of aqueous phase organic carbon also increases with HTL temperatures up to 350 °C, but the concentration drops as the HTL temperature reaches 400 °C [30]. The likely explanation is that these temperatures are in the regime where gasification is expected to occur, and the the aqueous-phase organic compounds are gasified to hydrogen and light hydrocarbon gases such as methane and ethane.

The solids from reaction contain the ash and other salts that remain from algae processing. Elemental analysis shows the ash resulting from algae combustion to contain metals such as Co, Mn, Fe, Cu, Zn, Mo, Cr, Mg, Al, Na, K, Ca, and Cl [30]. Other work suggests that the solid phase contains N and P compounds that can be redissolved and recycled [33].

The organic phase contains the product of the most interest for this work, the biocrude oil. Biocrude oil contains many different types of compounds, and one

Element	Petroleum Crude[34]	Algal Biocrude[16]	Upgraded Bio-oil
Carbon	83.0 – 87.0%	68 – 73%	86%
Hydrogen	10.0 – 14.0%	8 – 9%	10%
Nitrogen	0.1 – 2.0%	5%	1%
Oxygen	0.05 – 1.5%	10 – 15%	1%
Sulfur	0.05 – 6.0%	<1%	<1%

Table 2.1: Petroleum crude, algal hydrothermal liquefaction biocrude, and target upgraded biocrude elemental composition

way to simplify the analysis of the HTL biocrude is through the use of the elemental composition. Algal HTL biocrude contains 10-15 wt% oxygen and has a lower energy density than petroleum crude. Table 2.1 shows that in terms of carbon and hydrogen, biocrude oil contains less than petroleum crude [16, 34]. However, if oxygen and nitrogen are reduced to the levels in petroleum crude, the elemental composition of the upgraded biocrude will be in the expected ranges for petroleum crude.

Biocrude oils from liquefaction have been characterized in terms of molecular composition in addition to the elemental composition. Molecular characterization of these biocrude oils shows that the chemical composition of the oil changes with respect to the algae strain selected. The oil is composed of the products of reactions involving lipids, proteins, and carbohydrates. The lipids are hydrolyzed to free fatty acids. Proteins become nitrogen-containing heterocycles and amides, and carbohydrates become oxygen-containing compounds such as phenols and ketones [16]. The production of the nitrogen heterocycles begins to occur as temperatures exceed 300 °C due to the degradation of the protein content[35]. As the proteins and carbohydrates reform, the nitrogen content is partitioned into the oil

phase [35]. Although these reactions increase the oil yield of the reaction, the resulting oil is not high quality and requires further treatment to remove nitrogen. Naturally, the quality of the biocrude resulting from liquefaction is directly impacted by the original composition of the algae. Vardon et al. showed that the the compounds in the biocrude oil differ depending on the composition of the original feedstock although the elemental composition is similar[36]. Although there are numerous compounds present, the compounds present can be grouped through similar chemical properties. The bio-oil contains large amounts of heterocyclic nitrogen-containing compounds, alkanes, alkenes, phenols, hydroxylamines, and free fatty acids [23, 36, 37].

2.2 Deoxygenation of Fatty Acids

Free fatty acids are often a major component of the resulting oil and have the potential to be transformed into a high quality hydrocarbon fuel through deoxygenation. Deoxygenation of a fatty acid is generally performed through hydrodeoxygenation (HDO) where the oxygen is removed as water, Equation 2.1, or where oxygen is removed as carbon dioxide through decarboxylation, Equation 2.2. Both HDO and decarboxylation are effective means of removing oxygen. Though HDO produces a hydrocarbon that is one carbon atom longer than decarboxylation, it also requires an external H_2 supply. Decarboxylation on the other hand produces a shorter carbon chain, but the carbon is lost as CO_2 so the heating value of the molecule is essentially unchanged. We focus on decarboxylation because stoichio-

metric amounts of H_2 are not required and there is effectively no loss of energy content.

$$R\text{–}COOH + 3\,H_2 \longrightarrow RCH_3 + 2\,H_2O \tag{2.1}$$

$$R\text{–}COOH \longrightarrow RH + CO_2 \tag{2.2}$$

2.2.1 Decarboxylation of Saturated Fatty Acids

Fatty acid deoxygenation has been primarily studied in the organic or gas phase. Limited work was performed investigating the noncatalytic, thermal decarboxylation of saturated fatty acids. Thermal decarboxylation to alkanes is thermodynamically possible, but the rates are prohibitively slow, on the order of a few percent conversion at 300 °C for 6 hours[38]. Supercritical water at 454 °C showed faster decarboxylation rates (10% with a 13 min residence time) for potassium butyrate, but the presence of potassium may have contributed catalytic effects [39]. While fatty acids can be thermally decarboxylated, overall, the reaction rates are slow in comparison to catalyzed reactions.

Heterogeneous catalysts are used in a process called Ecofining to perform a combination of hydrogenation, hydrodeoxygenation, decarboxylation, and isomerization [40]. The expected order of steps in ecofining are first hydrogenation of the usaturated vegetable oil, then the other upgrading steps [41–43]. Ecofining demonstrates that decarboxylation of a saturated lipid can be part of a commer-

cially viable process, but the process does not specify which catalyst is used[40, 44]. Different monometallic catalysts have been studied for this deoxygenation chemistry. One study in particular screened many different catalytically active metals and showed that in terms of conversion, the most to least active metals were Pd, Pt, Ni, Rh, Ir, Ru, and Os [38]. Ni in particular was active for production of cracking products. On the topic of supports, they found that the higher surface area carbon support resisted deactivation more than the other lower surface area supports.

Pd-based catalysts are the most active for decarboxylation in the organic phase, and therefore, they are the most heavily studied [38, 41, 45–49]. Pd/C is active and shows selectivities greater than 90% for decarboxylation of stearic acid towards C_{17} hydrocarbons [38, 46, 47]. Long-term use however, shows that the Pd catalysts are subject to deactivation after only several hours [46, 47]. When Pd deactivates, it still maintains a high selectivity towards the desired C_{17} products.

Deoxygenating fatty acids in the hydrothermal environment is also of interest due to processing concerns. The water content can be easily removed after the HTL processing step through a reduction in temperature such that the biocrude oil and water separate. The biocrude can then be upgraded in an environment with little water present. Alternatively, the biocrude can be upgraded directly from HTL without performing this separation. After upgrading, the water and upgraded oil solution would undergo separation through a reduction in temperature. In both cases, separation of the oil product must be performed, but in the latter method, the system does not have to be reheated to reaction temperatures. Additionally, the separation in the latter method will result in an oil with a lower water content

because the oil will have a reduction in polar functional groups. Fu et al. showed that Pt/C is an effective catalyst for removing O atoms from palmitic and stearic acids [43, 50], which represent common fatty acids present in the biocrude. The authors reported an 80% yield to pentadecane from palmitic acid in 1 hr at 350 °C. Pd/C was also an effective catalyst for decarboxylation, but it had lower activity in the hydrothermal environment than did Pt/C. As discussed earlier, this is the reverse trend for catalytic activity of Pt/C and Pd/C in an organic solvent [38], thereby demonstrating that catalyst behavior in hot compressed water cannot simply be inferred from catalyst behavior in organic media.

While Pt/C primarily promotes monomolecular decarboxylation, metal oxides have been reported to promote bimolecular decarboxylation [51, 52]. Of the materials investigated, ZrO_2 shows the highest activity with approximately 68% conversion of stearic acid at 400 °C for 30 minutes. KOH was also studied as a catalyst used to decarboxylate stearic acid. Larger products appeared, and the activity was inferior to heterogeneous catalysts. Regardless of whether the catalyst was a precious metal, metal oxide, or simply activated carbon, the main products from stearic acid were CO_2 and C_{17} alkanes [42, 43, 50, 51].

From a theoretical standpoint, Lu et al. and Lamb et al. suggested possible mechanisms for the decarbonylation and decarboxylation of propanoic acid (C3:0) and butanoic acid (C4:0) on a Pd(111) surface[53, 54]. Lu et al. found that the reaction energy is independent of alkyl chain length when the tail contains at least 3 carbon atoms. The most favorable decarbonylation pathway results in a lower activation energy than the most favorable decarboxylation pathway[53]. The de-

carboxylation pathway proposed by Lu et al. requires O–H scission and direct decarboxylation, or the α-carbon fully dehydrogenates prior to decarboxylation. Lamb et al. offer other possible decarboxylation pathways using butanoic acid. They offer an intramolecular pathway where the acidic H directly transfers to the α-carbon, a pathway that involves the dissociation of H and diffusion to the same α-carbon, and finally a pathway with a propylidene intermediate. The difference in conclusion may stem from the different model systems used. Lu et al. used a repeating slab of Pd(111) whereas Lamb et al. used a Pd_{42} cluster[53, 54]. The presence of a water environment may also influence the energies of intermediates, thus changing the mechanism in hydrothermal systems.

2.2.1.1 Decarboxylation of Saturated Fatty Acid Literature Analysis

The only prior information on catalyst activity maintenance for hydrothermal decarboxylation of fatty acids is from a few experiments done previously in our lab. Pt/C and Pd/C were used in three successive 90 min batch experiments. The Pd/C catalyst showed reduced activity after each run, whereas the Pt/C catalyst was recycled without measurable loss of activity during the 4.5 h of use [50].

Taken collectively, the literature suggests that catalyst deactivation during hydrothermal decarboxylation of fatty acids may be a potential problem for this route to renewable transportation fuels. To our knowledge, there has been no prior work dedicated to quantifying and understanding causes of catalyst deactivation in such systems. Because Pt is an active and selective decarboxylation catalyst for saturated fatty acids in both organic and hydrothermal environments [38, 43, 50, 55],

and because Pt/C was the more stable material in the previous batch reactor studies, a study of Pt/C deactivation characteristics for decarboxylation in a continuous flow hydrothermal system would be valuable. Chapter 5 reports such a study.

2.2.2 Decarboxylation of Unsaturated Fatty Acids

Deoxygenation of saturated fatty acids has shown that there are highly effective catalysts both in terms of activity and selectivity to desired deoxygenated products. However, the fatty acids in most plant sources are dominantly unsaturated [15, 56]. Commonly studied oils in literature include those derived from algae, sunflower, linseed or flax, soy, jatropha, cottonseed, oiticica, palm, and tung. Excluding selected strains of algae, these oils are mainly composed of fatty acids with one, two, or three degrees of unsaturation, and the ratio of unsaturated:saturated fatty acids ranges from 3:1 for cottonseed to 18:1 for tung oil. The algae oil composition ranges from 0.8-6:1 for unsaturated:saturated fatty acids, depending on the algal strain selected [15]. While the studies with saturated fatty acids address one of the major components of plant-derived oils, this paints an incomplete picture and deoxygenation chemistry of unsaturated fatty acids should be addressed.

Multiple methods are capable of deoxygenating unsaturated fatty acids. As briefly discussed in Section 2.2.1, fatty acids can be decarboxylated through a purely thermal process. Noncatalytic pyrolysis of oleic acid at 390 and 450 °C over 4 hours shows 93-100% conversions. The thermal process, however, suffers from low selectivity to fuel range hydrocarbons with 7 and 34% of the yield go-

ing towards gaseous hydrocarbons, 43 and 35% as alkanes, alkenes, aromatics, and cracked fatty acids with the remainder unidentifiable [57]. While pyrolitic deoxygenation effectively removes oxygen, much of the resulting product would be undesirable to use as fuel.

Alternatively, catalytic HDO is a robust process that gives high yields for conversion of both saturated and unsaturated fatty acids to paraffins [58]. The ecofining process mentioned in Section 2.2.1 hydrogenates unsaturated free fatty acids to saturated free fatty acids, and ultimately will hydrodeoxygenate the fatty acids to paraffins [40]. Although the ecofining process is effective for conversion of unsaturated fatty acids to paraffins, the process has a large stoichiometric hydrogen demand of at least one molecule of hydrogen per degree of unsaturation.

Examining decarboxylation, Arend et al. observed that conversion of gaseous oleic acid (C18:1) over Pd/C was enhanced in the presence of H_2, and that the presence of H_2 pushed the selectivity towards the saturated decarboxylation product, *n*-heptadecane, rather than the direct decarboxylation product, hexadecene. The selectivity of the reaction shifted towards heptadecene with decreasing H_2 pressure. Snåre observed high conversion of both oleic and linoleic acid over Pd/C catalyst in mesitylene (condensed organic phase) under an inert atmosphere over a 6 h reaction time, but rather than obtaining the desired decarboxylation product the major product was stearic acid. Some heptadecenes were observed, and *n*-heptadecane was also present to a lesser extent (<10%) [59]. Similarly, Immer et al. observed that in alkane solvent, the deoxygenation rate of oleic acid in the absence of H_2 was inhibited to achieving only 11% conversion to alkenes and alkanes

compared to a complete conversion for stearic acid [48]. The binding of the C=C to the Pd surface is the likely culprit of the slowed reaction kinetics.

The addition of H_2 to reactions involving unsaturated fatty acid feeds improves the decarboxylation activity for Pd/C catalysts. Performing decarboxylation of oleic acid in the presence of sufficient H_2 increases the activity and selectivity of the Pd catalyst such that the results are indistinguishable from a reaction with stearic acid [48]. The reaction in hydrogen pushes the product profile to fully saturated alkanes as opposed to unsaturated alkenes because decarboxylation of an unsaturated fatty acid sequentially hydrogenates to stearic acid and subsequently decarboxylates. High selectivity and activity are also demonstrated with linoleic and linolenic acids, but the study did not isolate individual feeds for direct comparison. [60].

Fu et al. showed that in hydrothermal media, activated carbon was capable of converting oleic acid to alkanes and olefins [42]. Interestingly, most of the products detected were fully hydrogenated compounds including cracked alkanes and ketones, but no external hydrogen was added to the system. Oleic and linoleic acid suffered from poor selectivity towards the C_{17} hydrocarbon. After a one hour reaction, the stearic acid feed showed a 95% molar yield of the C_{17} alkane whereas oleic and linoleic showed 10 and 5% molar yields of the C_{17} alkane. The major product in both the cases was the saturated stearic acid. Stearic, oleic, and linoleic acid have 0, 1, and 2 degrees of unsaturation, and as the unsaturation of the fatty acid increases, the corresponding selectivity of heptadecane from the decarboxylation reaction over Pt/C decreases from 95%, 10%, and 5%. For decarboxylation

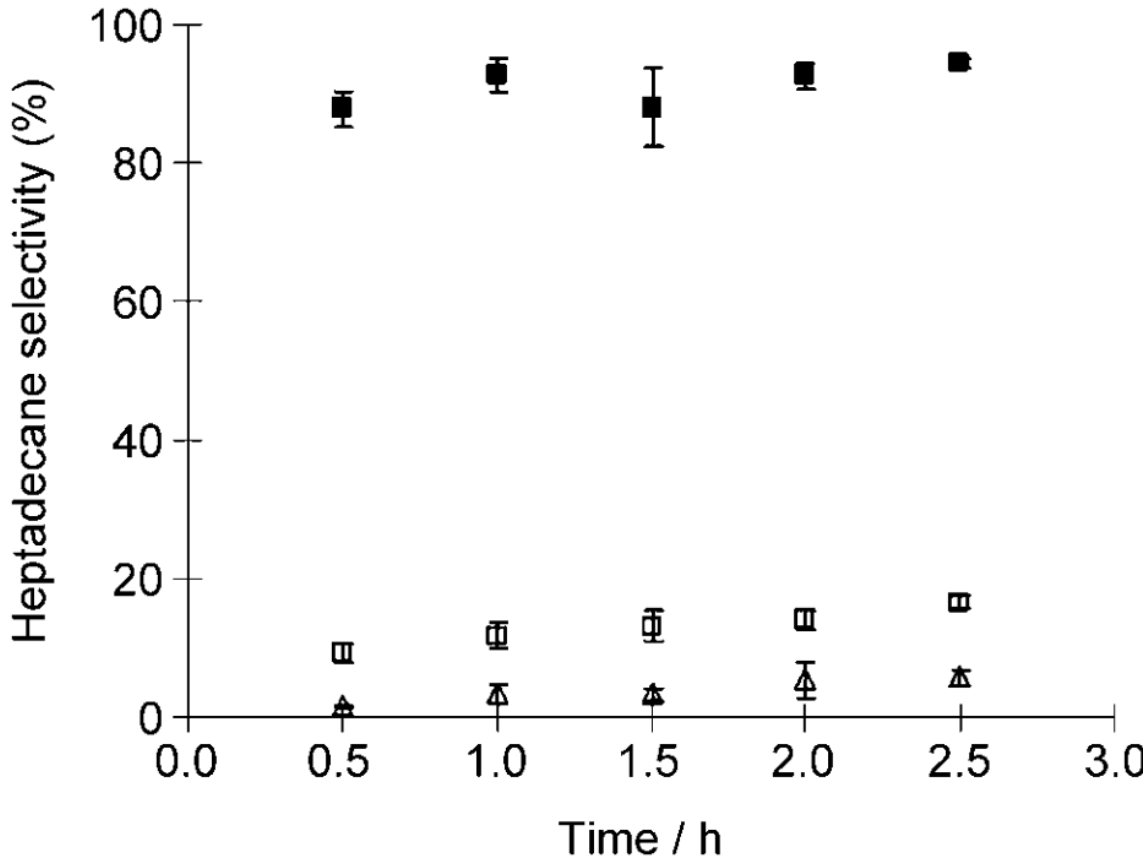

Figure 2.1: Pt/C selectivity to *n*-heptadecane for stearic (■), oleic (□), and linoleic acid (△) feeds in water [42]

over Pt/C, both oleic and linoleic acid performed worse than stearic acid. Figure 2.1 shows the decreasing selectivity towards heptadecane with increasing unsaturation of the fatty acid reactant[42].

2.2.2.1 Decarboxylation of Unsaturated Fatty Acid Literature Analysis

These studies show that Pt and Pd catalysts, which are effective for decarboxylating saturated fatty acids, are ineffective for the same reaction with unsaturated fatty acids in the absence of hydrogen in both aqueous and organic solvents. It is clear that improving catalyst performance for decarboxylation of unsaturated fatty acids in the absence of external hydrogen is worthy of further study [61]. Chapter

6 reports on such a study.

2.3 Upgrading of Biocrude from Hydrothermal Liquefaction and Model Compounds

Crude HTL bio-oil contains numerous compounds that complicate processing and upgrading. In addition to saturated and unsaturated fatty acids, biocrude oil assessment revealed identities of other major compounds that can be further be selected for model compound work[23, 29, 33, 36]. Pyrolysis oils share many of the same types of compounds found in HTL biocrude. The literature presented here will also include hydrothermal heteroatom removal of pyrolysis oils and its model compounds. The compounds present can be grouped into a few different categories such that a representative model compound can be chosen and tested for the sake of simplicity. This section will discuss the current field of hydrothermal heterogeneous catalytic deoxygenation, denitrogenation, desulfurization, and finally the hydrothermal catalytic upgrading of real biocrude oils.

2.3.1 Catalytic Hydrothermal Deoxygenation

HTL biocrude contains oxygenated compounds in forms other than the fatty acids that have been extensively discussed in Section 2.2. Brown et al. demonstrated that heterocyclic oxygen compounds, phenolics, and ketones are also present in abundance[23].

Dumesic's group has studied the synthesis of hydrocarbons from platform chemicals such as sugars and lactones. Kunkes et al. investigated a process for converting a sugar or polyol over a Pt-Re/C catalyst. Through reforming of the sugar or polyol, the system can generate enough hydrogen to perform controlled hydrodeoxygenation for the production of monofunctional compounds [62]. Chia et al. examined a Rh-ReO_x/C using a combined experimental/theoretical approach with density functional theory (DFT). The experimental results showed that Rh-ReO_x/C was more selective than Rh/C for the hydrogenolysis of secondary C–O bonds. DFT suggested that the hydroxyl groups on Re were acidic and thus promoted the formation of a carbenium ion suitable for ring-opening or dehydration [63]. Wang et al. showed that γ-valerolactone could be deoxygenated to a linear 1-butene using SiO_2–Al_2O_3 and WO_x–Al_2O_3. They showed that the Brønsted acid sites were important for achieving a high selectivity towards the linear alpha olefin[64]. Dumesic's group has demonstrated through experimental and theoretical work that transition metals are capable of deoxygenating polyols, ethers, and lactones into hydrocarbon fuels or monofunctionalized organics.

Dickinson et al. studied the hydrodeoxygenation of benzofuran over Pt/C in supercritical water at 380 °C. They reported the effects of batch holding time, hydrogen loading, catalyst loading, and water loading on the reaction products. Ethylbenzene and ethylcyclohexane were the main deoxygenated products, and the selectivity to ethylbenzene could be increased by increasing the water loading or decreasing the hydrogen loading. Experiments with the oxygen-containing reaction intermediates (e.g. ethylphenol) showed that benzofuran had an inhibitory

effect on the hydrogenolysis of the hydroxyl group on ethylphenol to produce ethylbenzene. The authors put forth a reaction network and developed a kinetic model that was consistent with the experimental findings. The model suggested that water was not an important source of hydrogen for this reaction under the conditions studied [65].

Phenolic compounds are common in these HTL biocrudes. Ohta et al. demonstrated that 4-propylphenol effectively underwent HDO [66] over precious-metal catalysts at 280 °C in water. They tested Pd, Pd, Ru, and Rh on different carbon supports, ZrO_2, TiO_2, CeO_2, γ-Al_2O_3 and demonstrated that Pt/C catalysts were the most active and selective for the fully saturated HDO product of propylcyclohexane with selectivities greater than 90 %[66]. The major side products were 4-propylcyclohexanol and propylbenzene [66]. Non precious-metals such as sulfided-CoMo catalysts are also active for HDO of 2-ethylphenol in steam at 350 °C [67]. The deoxygenation occurs through hydrogenation, direct deoxygenation, or acid catalyzed isomerizations that lead to further deoxygenation. The main products are ethylcyclohexane, cyclohexane, benzene, and ethylbenzene, and these deoxygenated products account for about 80% of the products observed [67]. They demonstrated that steam causes irreversible deactivation of the catalyst. Dickinson and Savage further performed HDO on o-cresol. They showed that NiCu catalysts, which reduce gasification activity in comparison to Ni, were capable of producing 60–70% yield of liquid hydrocarbons at 100% conversion in near and supercritical water conditions [68]. Lercher's group investigated the hydrothermal deoxygenation of lignin-derived oxygenates such as phenolic monomers

and dimers. Zhao and Lercher used Pd/C and HZSM-5 catalysts to hydrodeoxygenate phenolic monomers and dimers to cycloalkanes. At 200 °C, the catalysts demonstrated 95 – 100% conversion of the phenolic monomer with nearly 100% selectivity to the cycloalkane and the corresponding methanol from the hydrogenolysis of the C–O–C bond. Similarly, with phenolic dimers, both Pd/C and HZSM-5 yielded the cycloalkanes with 100% conversion and 100% selectivity [69]. Subsequently, Zhao et al. studied the kinetics and stability of Ni/HZSM-5 and Ni/Al_2O_3-HZSM-5 for phenol HDO. They determined that the sequence of steps transforming the phenol to the fully saturated cyclohexane first involved hydrogenation of the phenol to cyclohexanone. The cyclohexanone hydrogenated to cyclohexanol. Cyclohexanol dehydrated to cyclohexene which finally hydrogenates to the cyclohexane. In this four step reaction sequence, Ni/Al_2O_3-HZSM-5 gave a higher overall phenol HDO rate in comparison to Ni/HZSM-5 due to higher Ni dispersion. Both catalysts deactivated from sintering, and there was some leaching of Ni from both catalysts [70].

These studies show that both noble and non-noble metals can catalyze HDO of phenolics and ether linkages in the hydrothermal environment.

2.3.2 Catalytic Hydrothermal Denitrogenation

Heterocyclic N-containing compounds are major carriers of nitrogen in bio-oil produced from hydrothermal liquefaction [23–25, 29, 35, 71, 72]. Hydrothermal heterogeneous catalytic denitrogenation of model heterocyclic N-containing com-

pounds has been the focus of two recent studies [72, 73]. Yuan et al. used the partial oxidation of heptane in supercritical water (SCW) to produce hydrogen for the hydrodenitrogenation of quinoline [73]. The researchers found that N was removed from quinoline at 350 and 450 °C over a sulfided NiMo/γ-Al_2O_3 catalyst. Interestingly, this work also found that partial oxidation of the heptane occurred even without adding O_2 to the reactor, although O_2 did enhance the reaction rate. This result indicated that the SCW provided a strong enough oxidation environment to produce CO and the subsequent CO_2 and H_2 through the water gas shift reaction.

Duan and Savage examined the denitrogenation of pyridine in a hydrothermal medium with added H_2 [72]. They examined a variety of catalysts (Pt/C, Pd/C, Ru/C and Rh/C, sulfided-Pt/C, Pt/γ-Al_2O_3, sulfided-CoMo/γ-Al_2O_3, Mo_2C, and Mo_2S) at temperatures between 250 and 450 °C. Most interestingly, this article found that performing reactions in a hydrothermal medium significantly alters the reaction pathway of pyridine when using Pt/γ-Al_2O_3. In the absence of water, pentane was the major reaction product and the yield of butane was about one fourth that of pentane. In the presence of water at 0.025 g/cm^3, the yields of butane and pentane were equal. Increasing the water density to 0.1 g/cm^3 caused a further reduction in pentane yield, such that the ratio of butane to pentane was about 3:1. In all cases (with or without water) the yield of ammonia was always around 100% indicating that complete denitrogenation had occurred.

Nitrogen can be effectively removed through the use of both noble and non-noble metal catalysts.

2.3.3 Catalytic Hydrothermal Desulfurization

The final major heteroatom that is present in aquatic biomass and bio-oils produced from their liquefaction is sulfur. Valdez et al. showed that sulfur can be present in HTL algal biocrude as dimethyl sulfide.

Most work on hydrothermal hydrodesulfurization (HDS) has focused on processing heavy petroleum oils. Benzothiophene and dibenzothiophene have been studied as model sulfur compounds for desulfurization in supercritical water for bitumen pyrolysis oils and tar pitch[74, 75]. Yuan et al. reacted benzothiophene between 350 and 450 °C using a sulfided-CoMo/γ-Al_2O_3 catalyst. Under these conditions, no sulfur-containing products were detected in the resulting oil. The only compounds present after reaction were ethyl benzene and toluene while sulfur was released as hydrogen sulfide [74]. Dibenzothiophene can also undergo hydrodesulfurization using a NiMo/γ-Al_2O_3 catalyst. Desulfurization of dibenzothiophene was accomplished using a variety of reductants (H_2, CO, CO and H_2, and HCOOH), and suprisingly, all the alternative reductants provided higher conversions of dibenzothiophene than did H_2. The authors suggest that an active chemical species is formed from the water gas shift reaction causing the higher conversion of dibenzothiophene [75, 76].

Sulfur is the heteroatom that appears to be the easiest to remove from hydrothermal liquefaction biocrudes. Treatment of crude bio-oil in supercritical water, even without a catalyst, reduced the sulfur content to below detection limits [55].

2.3.4 Hydrothermal Catalytic Upgrading of Real Biocrude Oils

While model compound studies offer valuable insight, they may fail to capture interactions between different compounds. Ultimately, the success of a certain catalyst or technique ultimately needs to evaluate performance on the actual oil itself.

Duan and Savage performed several studies on hydrothermal upgrading the bio-oil obtained from the noncatalytic liquefaction of *Nannochloropsis* sp. at 320 or 340 °C [55, 77, 78]. These studies determined that bio-oil upgrading in supercritical water at 400 °C for 4 h was most effective when a Pt/C catalyst was used in a hydrogen atmosphere. The oxygen content of the bio-oil dropped from 6.5 to 4.5 wt%, the nitrogen content decreased from 4.9 to 2.2 wt%, and the sulfur content decreased from 0.7 wt% to below the detection limits for the elemental analysis. Furthermore, the viscosity of the bio-oil was reduced, producing a freely flowing liquid at room temperature [55]. The total ion chromatograms, shown in Figure 2.2, indicate the bio-oil upgraded with Pt/C has an increased abundance of volatile (early eluting) compounds and a decreased abundance of compounds with low volatility (late eluting). This finding agrees with the observed decrease in viscosity. In a follow up article [78], the authors used an optimization algorithm to examine the effects of catalyst loading, catalyst type, reaction time, and temperature on upgrading of the same crude bio-oil. This study showed that Mo_2C, HZSM-5, and Pt/C were all effective for upgrading crude bio-oil into a product that had a significant reduction in heteroatom content for all the temperatures examined (430, 480, and 530 °C). At 480 and 530 °C, there was a significant reduction

in the H/C ratio of the upgraded bio-oils indicating the increased presence of aromatic compounds. Table 4 shows the optimum conditions for various properties of the bio-oil, and the relative importance of each process variable as determined by the optimization algorithm. In the parameter space examined, a reaction at 430 °C for 6 hours with a Mo_2C catalyst was found to be the most effective for upgrading [78]. Lastly, using 5 wt % Pd/C at 400 °C, these authors examined the effects of catalyst loading (5 to 80 wt %) and batch holding time (1 to 8 hr) on the composition of the upgraded bio-oil. They determined that increasing the batch holding time and catalyst loading generally had positive effects on the upgraded bio-oil by decreasing the O/C and N/C ratios, and increasing the HHV (44 MJ/kg) and H/C ratio of the product oil [77].

Duan et al. asessed Pt/γ-Al_2O_3 for upgrading algal HTL biocrude from Chlorella pyrenoidosa in supercritical water and high pressure H_2. They varied the catalyst loading as well as adding a formic acid coreagent. The Pt/γ-Al_2O_3 alone increased the higher heating value of the biocrude from 35.6 MJ/kg to 38.7 – 40 MJ/kg. The final heating value of the upgraded crude oil seems to be independent of the catalyst loading, but the oil yield decreased and the gas yield increased with increasing amounts of catalyst. Adding formic acid also allowed for the control of coke formation, but led to an oil with a lower heating value in comparison to oils resulting from Pt/γ-Al_2O_3 treatment alone[79].

Duan et al. also studied the hydrothermal upgrading of HTL biocrude from duckweed and compared the results to a previous study on algae discussed in the previous paragraph [80]. Pt/C-sulfide (Pt/C-S) effectively upgraded HTL biocrude

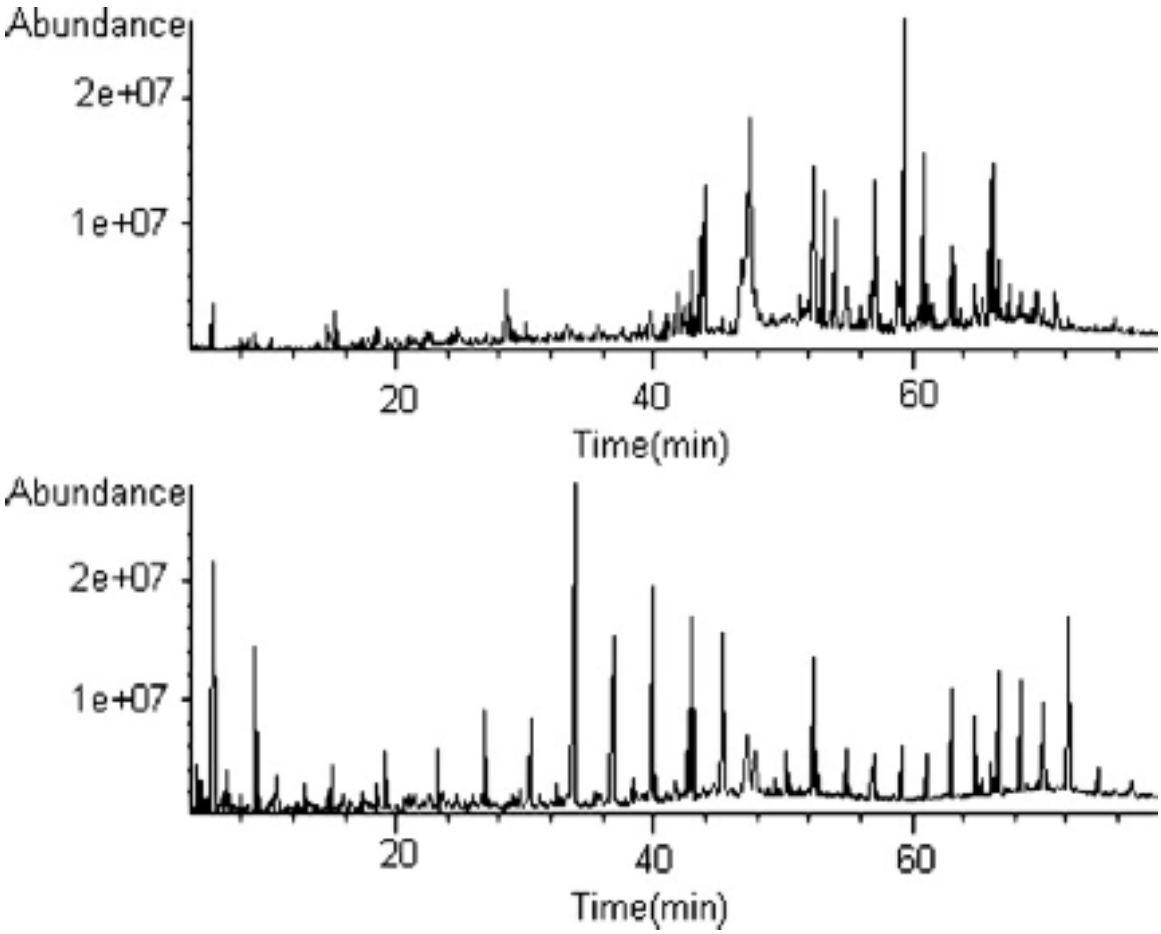

Figure 2.2: Total ion chromatograms from crude bio-oil (top) and upgraded product oil (bottom) obtained from SCW treatment with Pt/C, H_2 [55]

from duckweed in both sub (350 °C) and supercritical water (400 °C) with both H_2 and CO added to the reactions. In all cases, the Pt/C-S catalyst upgraded the biocrude in terms of removing nitrogen, and oxygen with longer reaction times resulting in a lower presence of the heteroatoms. The sulfur content was removed to below detection limits without the presence of a catalyst. High temperatures also produced a higher quality oil in terms of energy density and lower heteroatom content in comparison to the lower temperature conditions. The higher temperatures however, resulted in a lower oil yield with an increasing amount of coke detected [80].

Bai et al. investigated hydrothermal upgrading of algal biocrude oil at 350 °C using monometallic catalysts. They also used a combination of two catalysts, Ru/C and Raney-Ni, and they found that the combination of these two catalysts was more effective for oxygen and nitrogen removal than the individual performance for either catalyst. The final oil had the N and O content reduced from 4.1% and 3.6% down to 2.0% and 2.0% [81].

All the catalysts studied for upgrading of biocrude in batch reactors showed activity towards favored products that would be more suitable for fuel than the original feed. However, the resulting oils seen here are still unsuitable for direct use in transportation and may be unsuitable in terms of a drop-in source for an existing refinery. Further upgrading needs to be performed to these oils in terms of oxygen and nitrogen removal.

In contrast to batch studies, Elliott et al. demonstrated the catalytic conversion of algae using a continuous flow reactor. Their reactor system was a multistep

reaction that first liquefied the algae, then performed pretreatment to remove sulfur, and finally performed upgrading of the oil. They employed Co promoted MoS/Al_2O_3 and showed high oxygen, nitrogen, and sulfur removal when cofeeding greater than stoichiometric amounts of H_2 [33].

2.4 Hydrothermal Catalyst Stability

Most of what we know about catalyst degradation during fuel production comes from R&D related to the petroleum industry. Catalysts in the oil industry normally experience either gas phase or liquid hydrocarbon environments. For hydrothermal catalytic reactions, however, the reaction environment is much different as it is either hot compressed water or supercritical water. There have been only a few studies on catalyst stability and activity maintenance for reactions related to aquatic biomass in hydrothermal media, and these are reviewed in this section.

The use of high temperature or supercritical water as the reaction environment introduces challenges related to catalyst stability. Elliott and coworkers tested different metals for gasification activity in water, and many of the metals underwent oxidation. The metals tested include Zn, W, Mo, Zn, Cr, Re, Sn, Pb, Ni, Cu and Ru. All were oxidized except for Ni, Cu, and Ru. Thus, much of the catalyst development work has focused on working with the base metals that did not oxidize under those conditions [82].

Catalyst deactivation typically stems from three main issues: the presence of chemical poisons in the feed stream, a reduction in the number of exposed metal

atoms in the catalyst itself, and support issues. All three can be important when hydrothermally processing aquatic biomass.

For the first issue, sulfur is a widely known catalyst poison. Sulfur irreversibly binds to the surface of some metals making the active sites unavailable to perform the desired chemistry. Researchers have studied sulfur poisoning of Ru due to the effectiveness of Ru as a gasification catalyst. All forms of sulfur examined to date, including elemental sulfur, sulfates, organic sulfides, and thiols, poison Ru catalysts [83, 84]. Guan et al. presented modeling evidence that Ru deactivation during algae gasification was due to sulfur poisoning [85]. Waldner et al. showed that Ru irreversibly binds to the sulfate ion to form a Ru(III) complex [86]. Methods to deal with sulfur poisoning include developing sulfur-tolerant catalysts, sulfur removal from the feed stream via HDS, or via formation of sulfur salts. One group proposed dealing with sulfur by transforming it into a non-poisoning form [87].

The second major cause of catalyst deactivation is loss of catalyst surface area due to crystallite growth, or sintering. Elliott examined the long-term catalyst stability for low temperature hydrothermal gasification (350 °C, 21 MPa) using Ni and Ru catalysts to treat a 10% solution of phenol in water. When Ni is doped with Ru, the catalyst is stabilized in terms of crystallite growth. The pure Ni crystallites grew to 700-1000 Å compared to a stable 400 Å for Ni doped with Ru [88]. Doping Ni with Ag and Cu was even more effective than doping with Ru as the stable crystallite sizes were 214 and 104 Å, respectively. The ruthenium catalyst was found to be stable as the base metal. Skeletal NiRu stability was studied at 400 °C at 30 MPa in a continuous flow system with synthetic liquefied wood – a mixture of formic

acid, acetic acid, ethanol, anisole, and phenol. The crystallites showed evidence of sintering from 9 nm to 45 nm in 90 hours which corroborates Elliott's work [86].

The third major issue with catalyst deactivation deals with support degradation. While this does not directly affect the active catalyst material, it is still important because it affects the effective surface area and pore structure of the catalyst. Supports that are stable in organic solvents may not be stable in aqueous environments. γ-Al_2O_3, in particular, degrades rapidly to boehmite in supercritical conditions (450 °C, 40 MPa) and loses 1 – 2 orders of magnitude of surface area in 1 hour [74]. Recently, Ravenelle et al. investigated Pt/γ-Al_2O_3 and the effects of the Pt precursors on the stability and reactivity of the catalysts in water at 200 °C. While 200 °C is too low to be effective for algae liquefaction, catalyst degradation that can occur at 200 °C will also occur at higher temperatures. Ravenelle found that Pt synthesized from H_2PtCl_6 led to dissolution of alumina whereas Pt from $H_2Pt(OH)_6$ did not. The supporting γ-Al_2O_3 eventually changed to boehmite, but the rate of change varied depending on the Pt precursor used. Pt-OH changed faster than Pt-Cl [89, 90]. The stability of Pt/γ-Al_2O_3 was further studied in the presence of oxygenated biomass solutions. The presence of polyols (sorbitol and glycerol) in water at 225 °C inhibited the phase change of γ-Al_2O_3 to α-Al_2O_3. The sorbitol solution was better able to inhibit the degradation of γ-Al_2O_3 to α-Al_2O_3 as only 2% of the catalyst support changed phase compared to 15% with the glycerol solution. The inhibition of degradation can also be seen from the BET surface area of the support as shown in Figure 2.3. The proposed reason for this inhibition of support degradation is that carbonaceous deposits stabilize the γ-Al_2O_3[91]. In

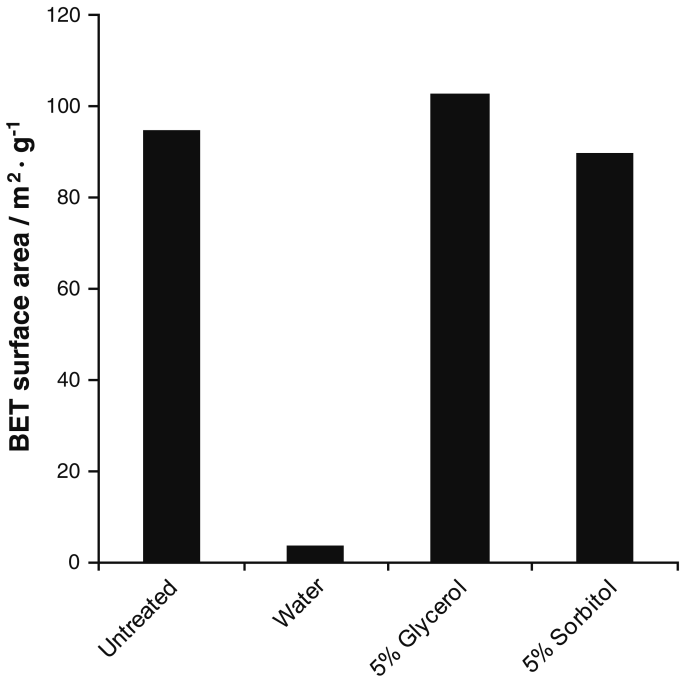

Figure 2.3: BET surface area of untreated 1 % Pt/Al_2O_3 and after 10 h treatment at 225 °C in different solutions [91]

general, stable supports in HTW were found to be monoclinic ZrO_2, rutile-titania (anatase transforms to rutile), α-Al_2O_3, and carbon.

This overview of hydrothermal stability of catalysts indicates that there is a need for more work on the long-term stability of liquefaction, upgrading, and gasification catalysts in high temperature water. Additionally, because sulfur is present within algal biomass, sulfur-resistant catalysts would be very useful. Otherwise, sulfur removal steps will have to be implemented to maintain the longevity of the catalysts. Fortunately, significant sulfur removal from algal bio-oils appears to be possible even by noncatalytic treatment in supercritical water. The stability of catalyst supports is also an important factor in determining the useful life of a catalyst. Research is needed to develop stable supports in high temperature water.

Lastly, the stabilization of metals on the supports such that sintering and dissolution can be avoided or minimized is important. Though researchers have studied this topic, it is primarily limited to Ru and Ni catalysts for gasification. The overall improvement of catalysts for hydrothermal conditions will be important for making hydrothermal processing of algal biomass economically viable.

CHAPTER 3

Research Objectives

3.1 Objectives

The literature review from Chapter 2 has outlined some areas that can serve as suitable research topics.

Pt/C catalysts have shown to be highly effective for decarboxylation of saturated fatty acids, however, the deactivation studies are limited to repeated batch reactions that test the catalyst for approximately 4.5 hours of time on stream [50]. Work by Luo et al. on glycerol reforming shows that Pt deactivation may be an important consideration, but the issues associated with aqueous-phase reforming may be different than the issues associated with hydrothermal decarboxylation [92].

Although Pt/C is effective for decarboxylating saturated fatty acids, it shows decreased selectivity towards the decarboxylation product for unsaturated fatty acids without added H_2.[41, 43, 48, 50]. Interestingly, the hydrocarbons formed in the hydrothermal environment are saturated, and the source of H_2 is unclear [43].

Finally, identifying a catalyst that is stable on the order of several hours or days

in the hydrothermal environment remains a challenge. The combination of many active metals oxidizing in water and the general instability of supports in the hydrothermal environment makes the development of a hydrothermally stable catalyst a challenging task [82, 93].

This dissertation seeks to:

1. Verify deactivation of Pt/C and characterize modes and kinetics of deactivation in the decarboxylation of a fatty acid.

2. Improve Pt-containing catalysts for the decarboxylation of unsaturated fatty acids, and identify the source of H_2 that hydrogenates the double bond during hydrothermal treatment.

3. Identify catalysts that may be stable and active in hydrothermal upgrading of algal biocrude.

CHAPTER 4

Experimental Methods

The materials used throughout the projects described hereon are discussed here. The experimental methods used to execute the reactions both in flow for butyric acid decarboxylation and in batch for unsaturated fatty acid decarboxylation and HTL biocrude upgrading reactions are detailed here. Lastly, this section describes the analytical techniques used to analyze the reactor effluent and the catalyst characterization techniques.

4.1 Materials

All materials were used as received. $H_2PtCl_6 \cdot 6\,H_2O$ with ≥ 37.50% Pt basis and $SnCl_2 \cdot 2\,H_2O$ – reagent grade were from Sigma Aldrich, Vulcan XC-72R carbon black with a particle size of 50 nm[94] was from Cabot Corp., P25 aeroxide titania with a particle size of < 25 nm was from Evonik Industries, and all gases (i.e., ultra high purity H_2, 1% N_2 in Ar, 1% H_2, 4% H_2 in N_2) were from Cryogenic Gases. Deionized water was produced in-house and sparged with Ar prior to use.

The reagents used in this work are butyric acid, stearic acid, oleic acid, linoleic

acid, *n*-octane, *trans*-4-octene, and D_2O. Butyric acid ≥ 99% was from Sigma Aldrich. Stearic acid was obtained from Sigma with a purity of ≥ 98.5%. Oleic acid was supplied by Fisher Scientific, and linoleic acid (99%) was purchased from ACROS. *n*-Octane (99+%) and *trans*-4-octene (90+%) were purchased from Aldrich. D_2O (99.8 atom %) was purchased from ICON ISOTOPES. Preservative-free algal paste (Nanno 3600) with 32.5 wt% solids was obtained from Reed Mariculture.

4.2 Catalyst Synthesis

Supported Pt catalysts were prepared using incipient wetness impregnation. An aqueous solution of the metal precursor, $H_2PtCl_6 \cdot 6\,H_2O$, was added dropwise to the continuously stirred support, either carbon or titania. The wet support was dried in a drying oven at 70 °C overnight, and the dried catalyst was subsequently crushed using a mortar and pestle. The reduction step placed the catalyst in a tube furnace at 500 °C for 6 h under flowing 1% H_2 with a balance of N_2. After reduction, the catalyst was stored until ready for use.

Supported $PtSn_x$ catalysts were prepared in a similar manner to the Pt catalysts. The amount of Pt was kept constant such that the Pt metal was always 5 wt% with respect to the support. The Pt precursor was mixed with the appropriate amount of Sn precursor dissolved in 1.0 N HCl in solution. The resulting solution was added dropwise to a continuously stirred carbon support. The drying and reduction steps for the $PtSn_x$ catalyst are identical to the steps used for preparation of the monometallic Pt catalyst.

4.3 Reactor Procedures

4.3.1 High Pressure Flow Reactor for Catalyst Deactivation Studies

Reactions studying catalyst deactivation were performed in a continuous flow reactor system assembled from stainless steel tubing and Swagelok parts. The reactor feed, an aqueous solution of 0.2 M butyric acid, was held in a vessel pressurized with Ar to 100 kPa. The feed stream passed through a 0.2 μm filter and was pumped into the reactor system using a ChromTech Series III HPLC pump. The preheating zone was a 1.8 m section of 1/16 in diameter thick-walled tubing. It was connected to the catalyst bed (150 mg), consisting of a 1/4 in diameter tube and metal frits to contain the catalyst, by two reducing unions. The preheater and reactor resided in a Techne SBL-2D fluidized sandbath with a Techne TC-8D temperature controller and a type K thermocouple. The reactor effluent traveled through a 5 ft. long 1/8 in diameter tube to a water-cooled heat exchanger. The pressure of the cooled effluent then was reduced from 21 MPa to ambient pressure using a Tescom back-pressure regulator. After the pressure let-down, Ar with 1% N_2 flowing at 5 mL/min at STP (21.1 °C and 1 atm) was added to the product stream using a mass flow controller. Figure 4.1 shows a schematic of the key components of the flow reactor system.

Prior to each run, we leak tested the entire reactor system to at least 28 MPa at room temperature. The reactor was then placed into the sand bath at 250 °C, and

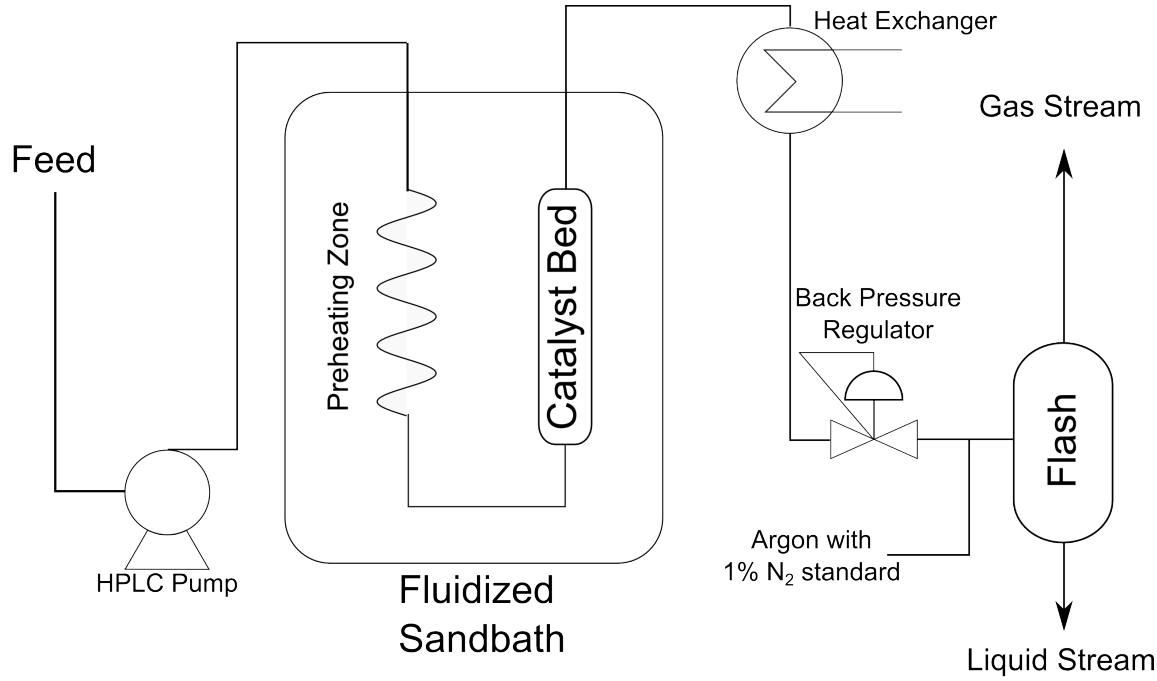

Figure 4.1: Flow reactor schematic

hydrogen flowed through the reactor system for an hour to reduce the catalyst. After reduction, we set the back-pressure regulator to 21 MPa and the sandbath temperature to 350 °C. We initiated flow of the 0.2M butyric acid solution when the sandbath reached 340 °C. The ratio of the volumetric flow rate of the reactor feed (ν) to the mass (W) of the catalyst (support included) was 300 mL/mg min at ambient conditions. The reaction was run continuously at this nominal steady state for 24 h to investigate the effect of aging on the catalysts.

4.3.1.1 Product Analysis

The product gases flowed to an online Agilent 6890 GC with a thermal conductivity detector (TCD) equipped with a Porapak Q packed column. The experimental details of the porapak column are given in section 4.4.1.1. The sample collection

was automated with a Lego mindstorms robot designed in-house and controlled using an RCX 2.0 controller.

Liquid samples were taken using a Gilson 223 sample changer and analyzed on an Agilent 7890 GC with a flame ionization detector (FID) equipped with a DB-FFAP column. The experimental details are given in section 4.4.1.5.

4.3.2 Batch Reactions for Platinum Tin Studies with Unsaturated Fatty Acids

We used batch reactors to perform the reactions that used $PtSn_x$ catalysts

4.3.2.1 Reactor Construction

Batch reactors are fashioned from one 3/8-in Swagelok cap, the corresponding port connector, and either another cap or a 3/8-in to 1/8-in reducing union, and 23 cm of 1/8-in thick-walled tubing that connects to a right angle valve from High Pressure Equipment Company.

4.3.2.2 Reactor Loading

The reactor was filled with water such that 95% of its volume would contain liquid water at subcritical (T < 374 °C) reaction conditions, and approximately 5 mg of catalyst was added in addition to this amount of water. The reactor was then sealed to 45 ft-lbs and placed in a preheated fluidized sand bath. After the desired time had elapsed, the reactors were removed from the sand bath and submerged

into room-temperature water to quench the reaction. The reactors were charged with 100 psig of Ar upon cooling, and the gaseous products were analyzed chromatographically as described in Section 4.4.1. After gas analysis was performed, the caps were removed, and the reactor contents were extracted using acetone such that the final volume was 10 mL. The contents were placed into a falcon tube and centrifuged to separate the catalyst particles from the effluent. The liquid GC samples were then prepared and analyzed as described in Section 4.4.1.

4.3.3 Algal Biocrude Upgrading Studies

4.3.3.1 Biocrude Oil Production

Nannochloropsis sp., raw paste was purchased from Reed Mariculture. The raw algal paste and deionized water, produced through an in-house reverse osmosis filter, were loaded into a Parr reactor with an internal volume of 283 ± 5 mL such that the resulting slurry, 15 wt%, would occupy 90% of the internal volume at the reaction temperature, 350 °C. The Parr reactor is fitted with a magnetically driven impeller and was stirred at 800 rpm. The reactor was heated using an induction heater, and the reaction was allowed to proceed for 20 min after initially reaching the 350 °C setpoint. After reaction, the reactor cooling water was turned on, the induction heater was removed from the reactor, and the reaction vessel was cooled by immersion in water until the temperature read 100 °C.

The reactor contents were emptied out into a separatory funnel and enough dichloromethane was added such that the biocrude oil would enter the solvent.

The funnel was gently agitated through inversion multiple times to ensure the biocrude mixed with the dichloromethane. The mixture was then allowed to settle overnight. The organic layer containing the biocrude was then separated and subsequently centrifuged to facilitate further separation of any entrained aqueous products and solids that result from liquefaction. The biocrude was dried under flowing N_2 to obtain the mass, and then it was redissolved in dichloromethane and stored in a refrigerator for later use.

4.3.3.2 Supercritical Reactor Loading

The reactors described in Section 4.3.2.1 were used again for catalytic upgrading reactions of HTL biocrude oil.

The reactors were loaded with a mixture of biocrude and dichloromethane such that after drying in N_2, 25 mg of biocrude oil would remain. The reactors are then dried in flowing N_2, and then they are loaded into a glovebox for catalyst loading. The reactors are sealed with parafilm after loading, and they are removed from the glovebox. 250 μL of water is injected into the reactor using a syringe, and the parafilm is removed, and the reactor is quickly capped with either a cap or a gas valve torqued to 45 ft-lbs. The reactors were then evacuated and filled with N_2 at 100 psig 3 times to ensure that the headspace was completely N_2. Some reactors were then filled with 150 psig H_2 so that the resulting H_2 pressure was 50 psi. The reactors were placed into a sand bath that was preheated to 400 °C, reacted for 1 h, and then immersed into a water bath to quench the reaction. The gases in the reactor were analyzed according to the methods described in Section

4.4.1. After gas analysis was performed, the reactor contents were extracted using 10 mL of dichloromethane. Several drops of concentrated HCl was added to the aqueous phase to ensure the organic acids remained protonated and improve the solubility in the organic phase. The samples were then vortexed and centrifuged. The organic phase was then separated for further analysis.

4.4 Analytical Chemistry

4.4.1 Gas Chromatography

Gas chromatography accomplishes separation of different compounds through the interaction of a stationary phase (a thin stationary phase coated on the wall or column packing) and the mobile phase (the vaporized products). Unfortunately, no one column is capable of separating all the compounds that one might be interested in detecting, so the proper selection of a column is paramount to achieving good separations for analysis.

4.4.1.1 Gas Analysis

The gas analysis was performed using an Agilent 6890N GC equipped with a TCD.

4.4.1.2 Light Permanent Gases

A Carboxen 1000 packed column (Supelco) that has dimensions of 15 ft. x 1/8 in was used for detecting gases up to C_2. The Ar carrier gas flowed through the

column at 44 mL/min. The temperature program held constant at 40 °C for 10 min, and it increased to 225 °C at 10 °C/min for a total run time of 28.5 min.

4.4.1.3 Heavier gases

An 80/100 Porapak Q 6 ft. x 1/8 in packed column was used for detecting gases up to C_6, but is incapable of performing separations for the light permanent gases. The Ar carrier gas flowed through the column at 44 mL/min. The oven temperature was held at 40 °C for 10 min and then increased to 225 °C at 10 °C/min.

4.4.1.4 Liquid Analysis

The liquid analysis was performed using either an Agilent 6890N or 7890 GC equipped with a FID.

4.4.1.5 Fatty Acid Analysis

Fatty acid analysis was carried out in a 30 m x 0.32 mm x 0.25 μm DB-FFAP column installed in an Agilent 7890 GC equipped with a FID. The GC inlet was set to a split ratio of 50:1 with a temperature of 220 °C. The carrier gas flow rate through the column was set to 20 mL/min. The oven temperature started at 50 °C and increased to 100 °C at a rate of 5 °C/min, and the FID was set to 300 °C with an H_2 flow rate of 40 mL/min, an air flow rate of 345 mL/min, and a makeup flow of N_2 at 5 mL/min.

4.4.1.6 Biocrude Analysis

The nature of biocrude oil involves many different compounds, but most of the compounds analyzed are non polar organics. Because of the large variety of compounds, many are too heavy to be resolved by GC. To protect the longevity of the GC column, an inert glass guard column was installed to capture non eluting compounds. The guard column was trimmed as needed. To analyze the non polar compounds, a low polarity wax column was chosen. The HP-5ms column, 50 m x 200 μm x 0.33 μm, was installed into an Agilent 6890N GC with a mass spectrometer (MS). The GC flowed He through at 0.9 mL/min. The oven temperature started at 35 °C and increased to 50 °C at 1 °C per minute. Upon reading 50 °C, the temperature increased to 300 °C at 3 °C per minute. Finally, the temperature was held constant for 15 minutes resulting in a total run time of 113.33 min. A solvent delay was put in place to ensure a long operating life for the MS filament, and thus the chromatography data are unavailable at elution times below 8 minutes.

4.4.2 Infrared Spectroscopy

4.4.2.1 Diffuse Reflectance Infrared Fourier Transform Spectroscopy

DRIFTS is a technique for performing Fourier transform infrared spectroscopy (FTIR) on opaque solid samples. DRIFTS was performed using a Nicolet 6700 FTIR from ThermoScientific equipped with a praying mantis cell. A blank was first taken with no sample. The sample cup was filled with solid sample such that it was flush with the top edge of the cup. The resulting spectra subtracted the

blank from the sample to remove any background signal.

4.4.2.2 Attenuated Total Reflectance

Attenuated total reflectance (ATR) is a technique for performing direct measurement of solid or liquid samples. A Smart iTR accessory from ThermoScientific was installed onto the FTIR. A blank scan without sample was taken prior to scanning the samples. Approximately 50 μL of sample extracted from a GC sample was dried directly on the ATR crystal. Scans were taken in absorbance mode, and the blank was subtracted to remove background signal.

4.4.3 Catalyst Characterization

The catalysts themselves were characterized using mainly x-ray diffraction (XRD) and transmission electron microscope (TEM).

XRD was performed on either a Rigaku Miniflex 600 or a Rigaku Rotaflex. The powder samples were put into an amorphous glass sample holder and prepared such that the powder was flush with the walls of the glass. Scans were performed at 2° per minute from 30° – 90°. The resulting data was analyzed on the Jade software package.

TEM was performed on a JEOL 2010F with a 200 kV accelerating potential. The powder samples were dispersed in a high vapor-pressure solvent such as ethanol or acetone. The dispersed catalyst was dropped onto a 200-mesh holey formvar carbon copper TEM grid from Ted Pella. The samples were imaged in bright-field mode.

CHAPTER 5

Pt/C Deactivation in the Decarboxylation of Butyric Acid

This work has previously been published in ACS Sustainable Chemistry & Engineering. This presentation of results is apportioned into three main subsections. We first discuss the various reaction products observed during the hydrothermal decarboxylation of butyric acid and from these data infer the existence of different side reactions that accompany the desired decarboxylation reaction. We then present data for catalyst activity as a function of time on stream and use the data to model quantitatively the catalyst deactivation kinetics. The final section discusses different mechanisms of catalyst deactivation and experimental results that allow discrimination among several of the possibilities.

5.1 Introduction

The literature in Chapter 2 suggests that catalyst deactivation during hydrothermal decarboxylation of fatty acids may be a potential problem for this route to

renewable transportation fuels. To our knowledge, there has been no prior work dedicated to quantifying and understanding causes of catalyst deactivation in such systems. Because Pt is an active and selective decarboxylation catalyst for saturated fatty acids in both organic and hydrothermal environments [38, 43, 50, 55], and since Pt/C was the more stable material in the previous batch reactor studies, we decided to use Pt/C in this present study. Additionally, because prior work examined activity in a batch system and just for 4.5 h of use, we decided to examine activity in a flow reactor system for much longer times on stream. The purpose of this work is to determine deactivation characteristics of Pt catalysts during the decarboxylation of carboxylic acids in hot compressed water. We selected naturally occurring butyric acid, rather than a longer fatty acid, as the reactant for experimental convenience. Butyric acid enjoys a sufficiently high solubility in water at ambient conditions that a feed solution for the flow reactor could be prepared conveniently. One can reasonably expect the catalytic decarboxylation chemistry for butyric acid to mimic that of larger fatty acids since the reaction of interest at the COOH group is not likely to be affected by additional methylene units that are far removed. We also note that butyric acid has been used previously in a detailed mechanistic study of decarboxylation [54], which provides an opportunity to connect the experimental results in this study with those from DFT calculations in the prior work.

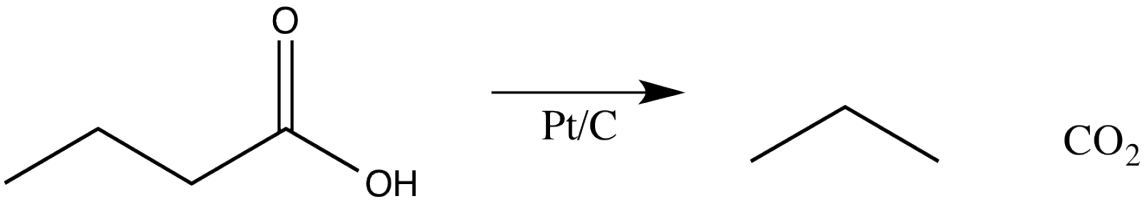

Figure 5.1: Butyric acid decarboxylation

5.2 Reaction Products

We monitored the reaction products in both the gas and liquid phases that emerged from the flow reactor. The liquid phase contained only unreacted butyric acid whereas the gas phase products were H_2, CO_2, CH_4, C_2H_6, and C_3H_8. No ethylene or CO was observed. The most abundant products were C_3H_8 and CO_2, indicating that Pt/C is selective for the desired decarboxylation reaction shown in Figure 5.1.

This outcome is in agreement with other work [43] on the hydrothermal conversion of saturated fatty acids over Pt/C. Over 90% of the converted butyric acid was converted to propane, and the selectivity to the decarboxylation products remained high throughout the duration of the reaction. Figure 5.2 shows that the gas and liquid phase products together accounted for 95 ± 3% (excluding the point at t = 0.07 h) of the total carbon of the feed stream, thus effectively closing the carbon balance.

The product stream contained H_2, a product that is not formed in the decarboxylation reaction. Additionally, the H/C atomic ratio for the gas-phase products, (Figure 5.3), modestly exceeds 2.0, the H/C ratio in butyric acid. Figure 5.3 also shows that the molar ratio of CO_2/C_3H_8 exceeds the stoichiometric ratio of 1.0. These results are consistent with the existence of one or more side reactions

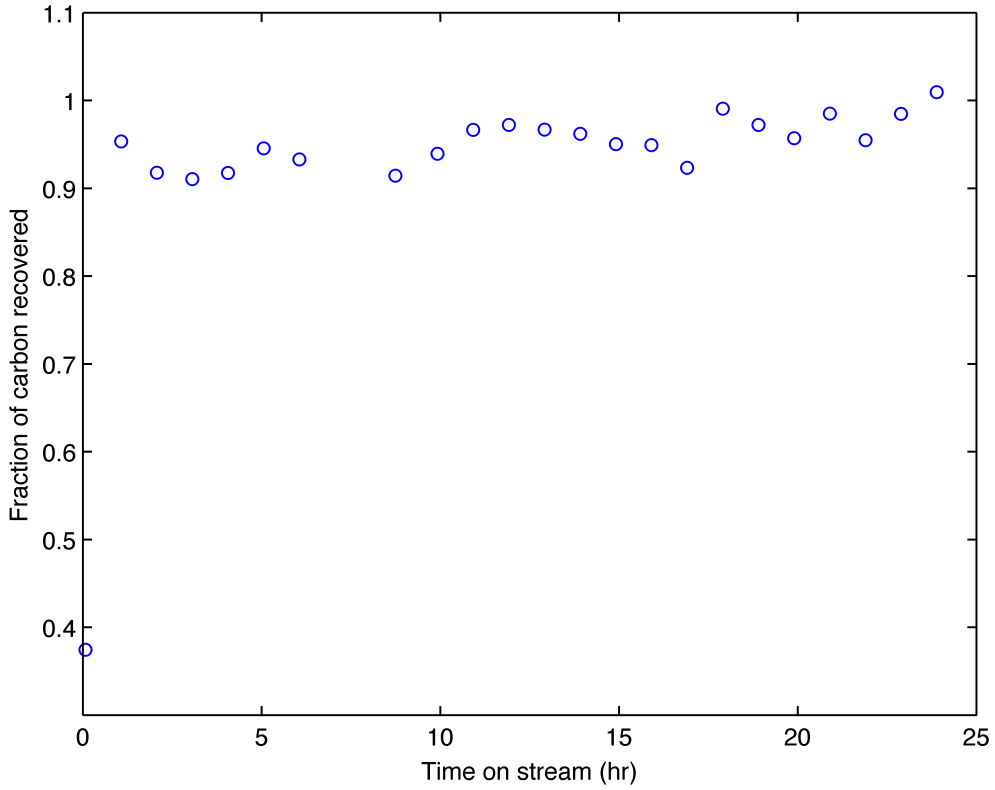

Figure 5.2: Carbon recovery in gas and liquid phase reactor effluent from hydrothermal treatment of 0.2 M butyric acid over Pt/C at 350 °C with W/ν = 300 mg min/mL.

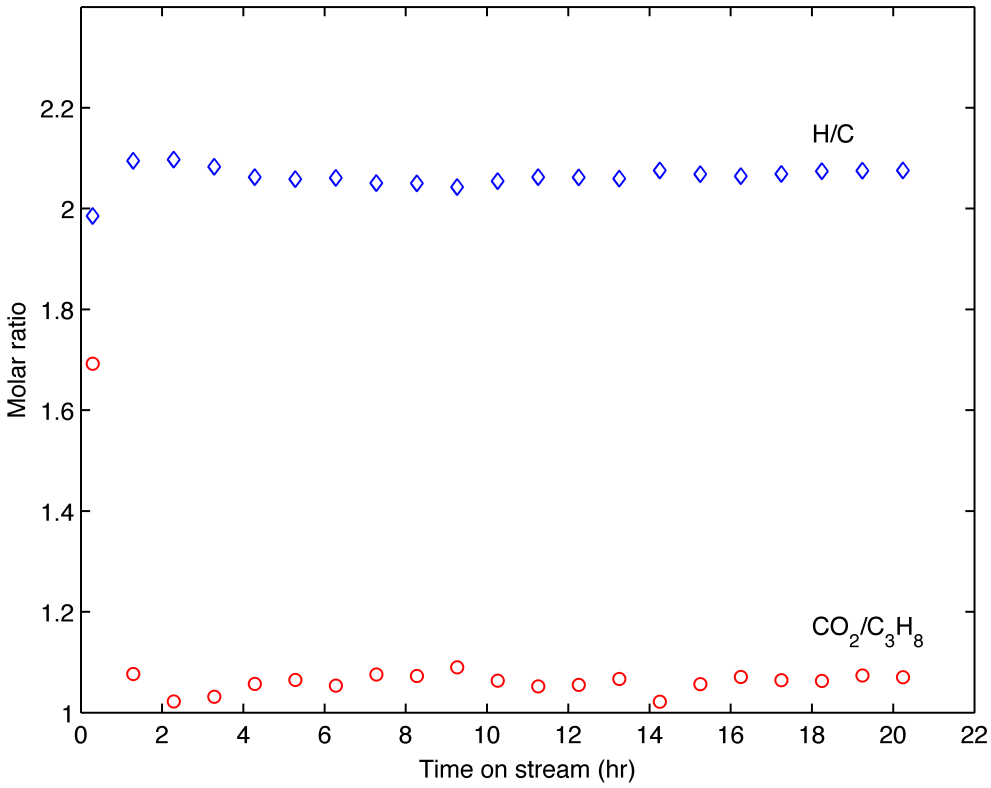

Figure 5.3: H/C and CO_2/C_3H_8 ratios from hydrothermal treatment of 0.2 M butyric acid over Pt/C at 350 °C with W/ν = 300 mg min/mL.

that produce modest amounts of H_2 and/or CO_2.

There are several such potential side reactions and we consider two here. The first is steam reforming of the butyric acid reactant or the propane product. Equation 5.1 shows the stoichiometry for the case of butyric acid, and it is clear that such a reaction could produce H:C atomic ratios well in excess of two.

$$CH_3CH_2CH_2COOH + 6\,H_2O \longrightarrow 4\,CO_2 + 10\,H_2 \tag{5.1}$$

We used Aspen Plus process simulation software to calculate the equilibrium compositions of butyric acid and its anticipated reaction products with water, namely

Species	Mole Fraction (dry basis)
H_2	0.044
CO	<0.002
CO_2	0.360
CH_4	0.593

Table 5.1: Equilibrium composition of products from hydrothermal decomposition of butyric acid at 350 °C and 3000 psig.

C_1, C_2, and C_3 hydrocarbons, CO_2, CO, and H_2 at the reaction conditions. We selected the thermodynamic package, SRK-KD, because of its ability to handle interactions between organic molecules and water at elevated temperatures and pressures. The RGIBBS block, which minimizes the Gibbs free energy for the system, was chosen to calculate the equilibrium compositions for a 0.1 M aqueous stream of butyric acid at 3000 psig and 350 °C. Table 5.1 shows the results, which indicate that the gaseous products would have an H/C ratio of 2.6 at equilibrium and that CO_2 is formed. Both of these outcomes are consistent with the experimental observations. The equilibrium calculation gave no evidence for the presence of C_2 or C_3 hydrocarbons.

A second possible side reaction is degradation of the carbon support as shown in equation 5.2

$$C + 2\,H_2O \text{-> } CO_2 + 2\,H_2 \tag{5.2}$$

Carbon is generally considered a stable support in hydrothermal environments, though carbon gasification in supercritical water has been documented [95]. The results presented thus far clearly show that the main decarboxylation reaction is

accompanied by one or more minor side reactions that may involve the reactant, a product, or the catalyst support. The number of potentially significant side reactions is larger in this hydrothermal system due to the presence of water, which is reactive at elevated temperatures. Side reactions appear regularly in hydrothermal catalytic reaction systems and frequently complicate the interpretation of experimental results. Minor hydrocarbon products that appeared during the nominal decarboxylation reaction include ethane and methane. These saturated alkanes are completely analogous to the *n*-alkanes Fu et al. [43, 50] reported as minor products from the hydrothermal treatment of palmitic acid over Pt/C. Figure 5.4 shows that the yields of ethane and methane were about a factor of 30 – 200 lower than the yield of propane. The carbon contained in these C_1 and C_2 hydrogenolysis products accounts for less than 2% of the carbon in the gas-phase reaction products with Pt/C. The scatter in experimental data is due to the concentrations of methane and ethane in the reactor effluent being near the lower detection limits of the GC-TCD.

5.3 Deactivation Kinetics

Previous work showed that fatty acid hydrothermal decarboxylation at 380 °C with Pt/C occurred in the intrinsic kinetics regime [50]. Additionally, the catalyst bed in the present experiments is essentially isothermal with a calculated temperature change of less than 1 °C. Therefore, we do not expect heat or mass transfer effects to be influencing the rates measured in the present experiments. Moreover, we do not expect the carbon support to be a major contributor to the decar-

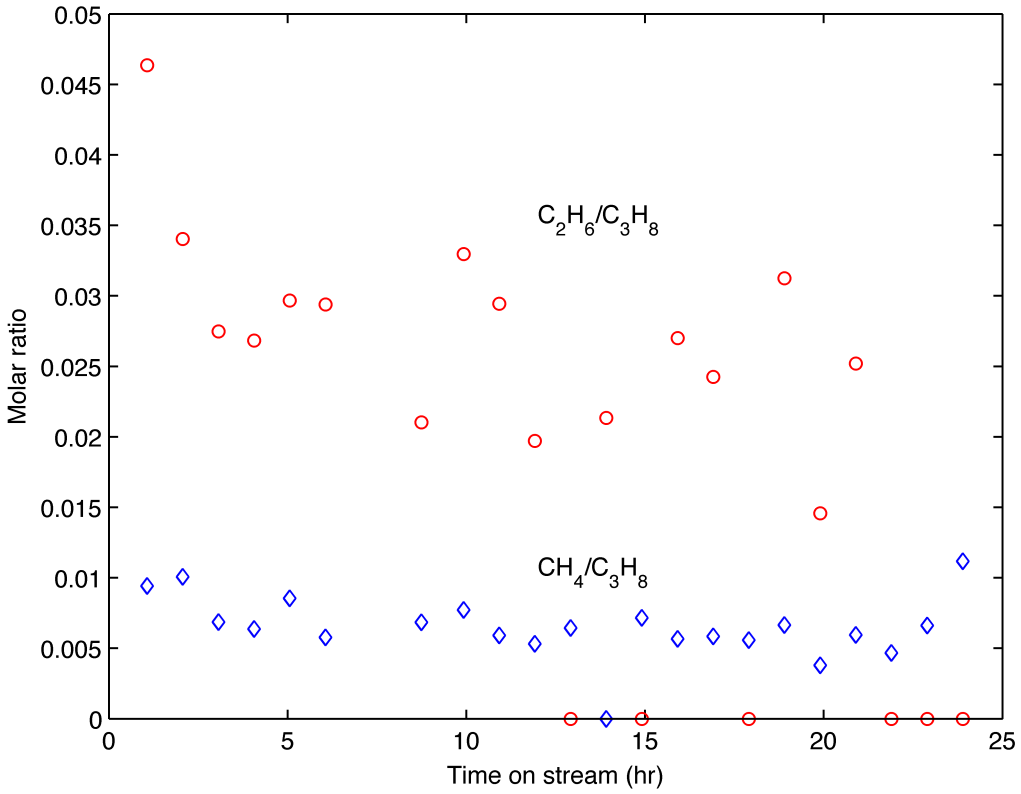

Figure 5.4: Molar ratios of lower alkanes to propane for hydrothermal treatment of 0.2 M butyric acid over Pt/C at 350 °C with W/ν = 300 mg min/mL.

boxylation activity as previous work showed that activated carbons were much less active than Pt/C for hydrothermal decarboxylation. Comparing activated carbon catalyzed decarboxylation of stearic acid and Pt/C catalyzed decarboxylation of palmitic acid show rate constants at 350 °C of 0.00075 min^{-1} and 0.024 min^{-1}, respectively[42, 50]. The difference in rate constants shows that catalytic effects from carbon are negligible in comparison to Pt. The literature indicates that first-order kinetics adequately describes the hydrothermal decarboxylation of long-chain saturated fatty acids over Pt/C [50]. Combining a first-order rate equation with the design equation for the plug-flow, packed-bed, catalytic reactor used in the experiments and rearranging leads to equation 5.3 where k'_0 is the first-order rate constant, ν is the volumetric flow rate, W is the catalyst mass, and X is the conversion of butyric acid. The conversion was calculated as the ratio of the molar flow rate of carbon in the effluent gas stream divided by the molar flow rate of carbon into the reactor.

$$k' = -\frac{\nu}{W} ln'(1 - X) \tag{5.3}$$

Figure 5.7 shows the first-order rate constant as a function of time on stream for three independent runs performed under nominally identical reaction conditions. The rate constant serves as a proxy for the catalyst activity. The data at times longer than 10 h provide information about the rate of catalyst activity decay. The data at shorter times on stream are not as useful. These data seem to show that the catalyst activity increases for the first six hours on stream and then it begins

to decrease. This initial apparent increase in activity is not physical, but rather an artifact due to a time lag in the flow system downstream of the reactor bed and the mixing of the initial reactor effluent with residual gas in the flash column. That is, it takes several hours after starting the experiment for the gas being analyzed by the GC to have the same composition as the gas leaving the catalyst bed. We verified this explanation by modeling the reactor as having a continuously decreasing activity and treating the flash column, which has a residence time of about 30 min under the experimental conditions, as two perfectly mixed stirred tanks with exchange between the two tanks, Figure 5.5. The model is mathematically described with Equations given in 5.4 where C_i is the concentration, ν_i is the volumetric flow rate, and V_i is the volume of the individual tank of the partitioned flash column. This simple dynamic model was used to show the exiting concentration profiles for both a constant inlet concentration (i.e. no catalyst deactivation) and an unsteady inlet concentration where the concentration decreases with time. This unsteady inlet concentration can be used to model a concentration profile with a deactivating catalyst. The model using a steady and constant inlet concentration shows a concentration profile where the initial concentration increase roughly matches the experimentally observed concentration increase. However, the experiment observes a deactivating catalyst meaning that the concentration entering the flash column cannot be constant. The unsteady inlet concentration model uses the k_d measured experimentally to calculate the concentration entering the flash column to determine the final exit concentration profile. The results clearly showed that one expects to observe an initial increase in the product concentration in the efflu-

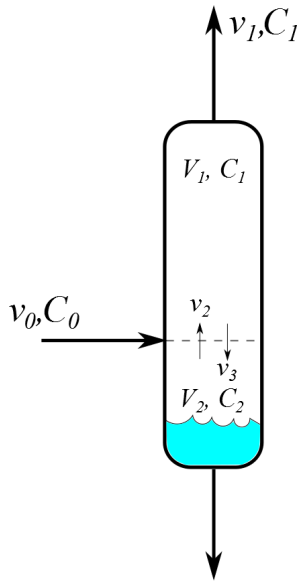

Figure 5.5: Flash column modeled as two stirred tanks with exchange between tanks. $V_1 = V_2 = 200mL$, $\nu_0 = \nu_1 = 5\frac{mL}{min}$, $\nu_2 = \nu_3 = 3\frac{mL}{min}$, $k_d = 0.06h^{-1}$

ent with time on stream before observing the decrease with time that accurately reflects the catalyst activity loss occurring in the catalyst bed, Figure 5.6. The effect of mixing downstream of a catalytic flow reactor leading to an apparent increasing catalyst activity has also been observed elsewhere [92].

$$\begin{aligned} \frac{dC_1}{dt} &= \frac{1}{V_1}[\nu_1 C_0 - (\nu_1 + \nu_3)C_1 + \nu_2 C_2] \\ \frac{dC_2}{dt} &= \frac{1}{V_2}[\nu_3 C_1 - \nu_2 C_2] \end{aligned} \tag{5.4}$$

Because the subset of the data wherein the activity appears to increase with time does not reflect what is occurring in the catalyst bed, we exclude those portions of the data in Figure 5.7 from consideration when analyzing the deactivation kinetics. We consider only the data after ten hours on stream because the rate constant is decreasing within that region. We treat the rate of catalyst activity loss as being first-order. With this model for the deactivation kinetics, one expects the

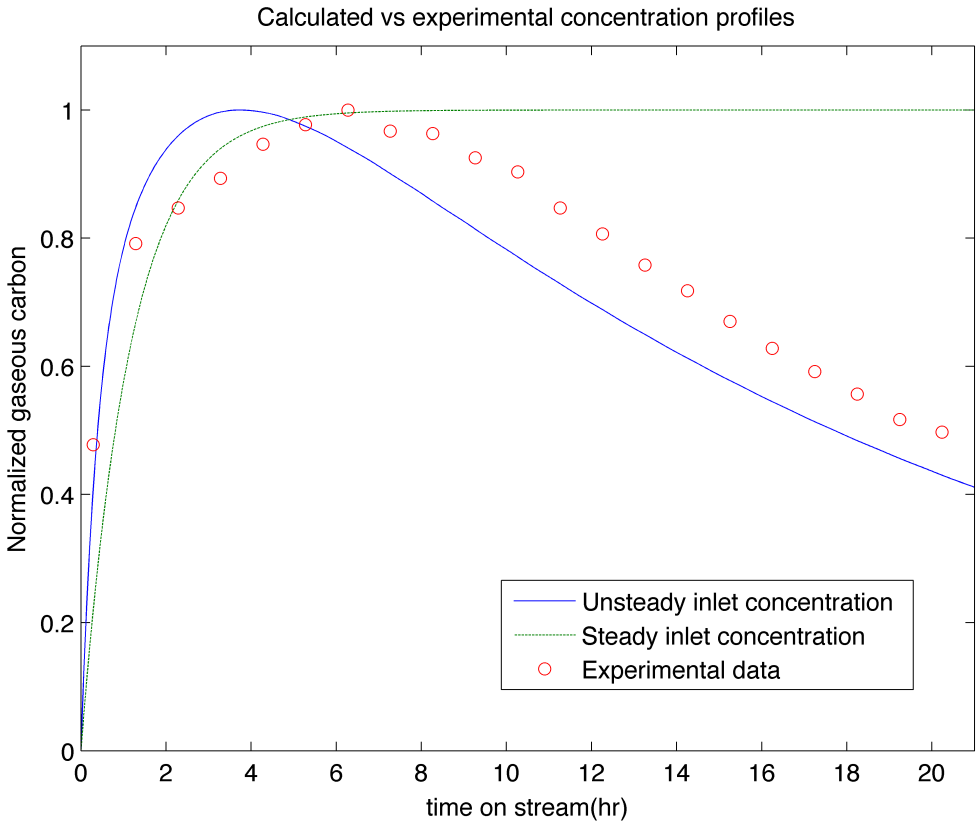

Figure 5.6: Deactivation data with model incorporating mixing in flash column.

rate constant for butyric acid conversion to decrease exponentially with time on stream, as indicated in Equation 5.5.

$$k'(t) = k'_0 e^{-k_d t} \tag{5.5}$$

k_d is the rate constant for catalyst deactivation and k'_0 is the decarboxylation rate constant expected for a fresh catalyst. Both k_d and k'_0 were calculated by fitting $ln(k'(t))$ to linearized data. This model captures the trends in the three independent runs in Figure 5.7 and gives a reasonable representation of the experimental data for the deactivation of the Pt/C catalyst. The deactivation rate constants determined from the three independent runs are 0.059, 0.062, and 0.070 h^{-1} with the respective k'_0 values of $1.58 \cdot 10^{-4}$, $1.84 \cdot 10^{-4}$, and $2.19 \cdot 10^{-4}$ mL mg^{-1} min^{-1}. These values are all similar, which suggests that the three independent experiments provided reproducible results regarding the rate of catalyst activity decay. The best estimate (i.e., the mean value) for the deactivation rate constant and k'_0 value at 350 °C are 0.063 ± 0.006 h^{-1} and $1.9 \cdot 10^{-4} \pm 0.3 \cdot 10^{-4}$ mL mg^{-1} min^{-1}. The results in Figure 5.7 provide new insights into the hydrothermal activity maintenance of Pt/C catalysts for fatty acid decarboxylation. Previous work in batch reactors [50] showed little decline in activity when Pt/C was re-used in subsequent experiments, but the total time the catalysts were in use under reaction conditions was just 4.5 h. Moreover, the process used to recover the catalyst after each batch experiment and prepare it for the next may have altered the catalyst in some way and restored its activity. The present experiments, wherein the same catalyst parti-

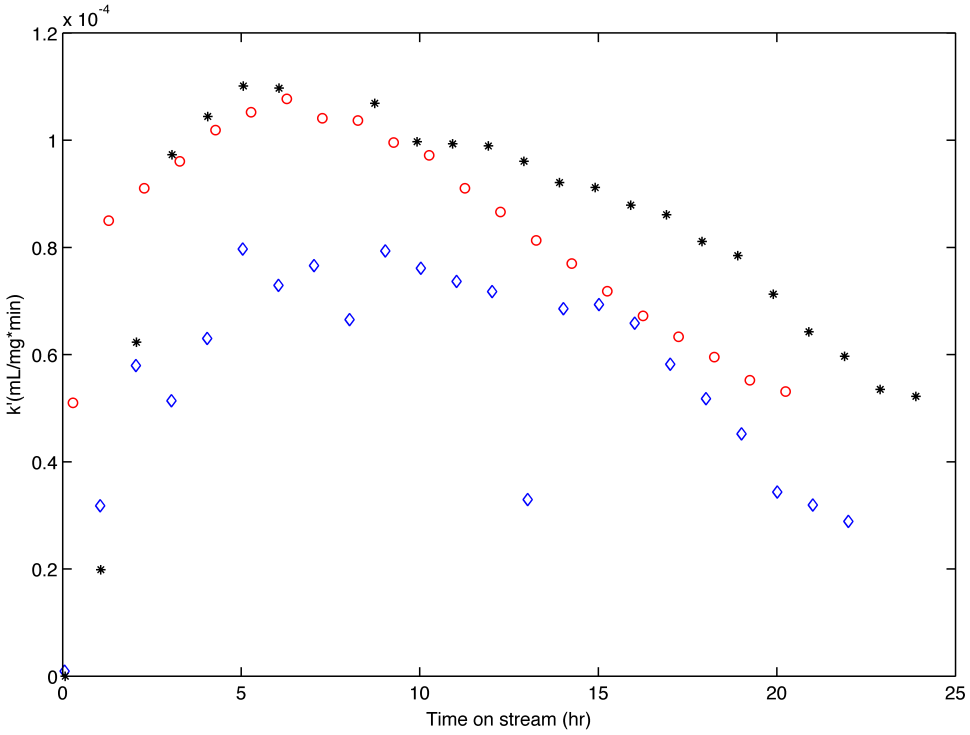

Figure 5.7: Variation of first-order rate constant with time on stream for hydrothermal decarboxylation of 0.2 M butyric acid feed over Pt/C with at W/ν = 300 mg min/mL at room temperature with a reaction temperature of 350 °C

cles were used continuously for 24 h, provide results that are more meaningful as they more closely mimic the mode of operation anticipated at a commercial scale.

5.4 Cause of Deactivation

Having demonstrated that the Pt/C catalyst loses activity with time on stream, we next consider several potential causes of the catalyst deactivation. The catalyst synthesis method was chosen, in part, to produce Pt particles larger than those in commercial catalysts to ameliorate potential sintering effects. The possibility of sintering, the combination of Pt crystallites to form larger particles with fewer

exposed metal atoms, however, still needs to be investigated. XRD is one method of estimating the average size of the metal crystallites in a catalyst. Figure 5.8 shows the XRD spectra of the fresh Pt/C catalyst and the material recovered after 24 h on stream in the flow reactor. The crystallite size, τ, was calculated using the Scherrer equation (5.6).

$$\tau = \frac{K\lambda}{\beta cos\theta} \tag{5.6}$$

We took the shape factor, K, to be 0.9. The wavelength of the x-ray radiation, λ, was 1.5406 Å. The full width at half max, β, and the Bragg angle, θ are obtained from the XRD spectrum. From the Pt(111) XRD peaks in Figure 5.8, which appear at $2\theta = 40$ °, the Scherrer equation showed the crystallite sizes in the fresh and used catalyst to be 13.7 nm and 12.3 nm, respectively. The crystallite sizes being similar in both the fresh and used catalysts suggests that loss of active area through sintering was not a major contributor to deactivation during hydrothermal decarboxylation. TEM images in Figure 5.9 show that the Pt particles were 9.3 ± 3.5 nm for the fresh catalysts, and 9.2 ± 3.1 nm for the used catalyst supporting that sintering was not responsible for deactivation. This combination of XRD and TEM analyses show catalyst sintering is not a likely cause of the observed deactivation.

Another possible cause of catalyst deactivation is poisoning, which is the very strong adsorption of molecules onto the catalyst sites. Carbon-containing molecules on metal surfaces can be detected by different spectroscopic techniques. Because the catalyst support itself was carbon, however, we could not perform these tra-

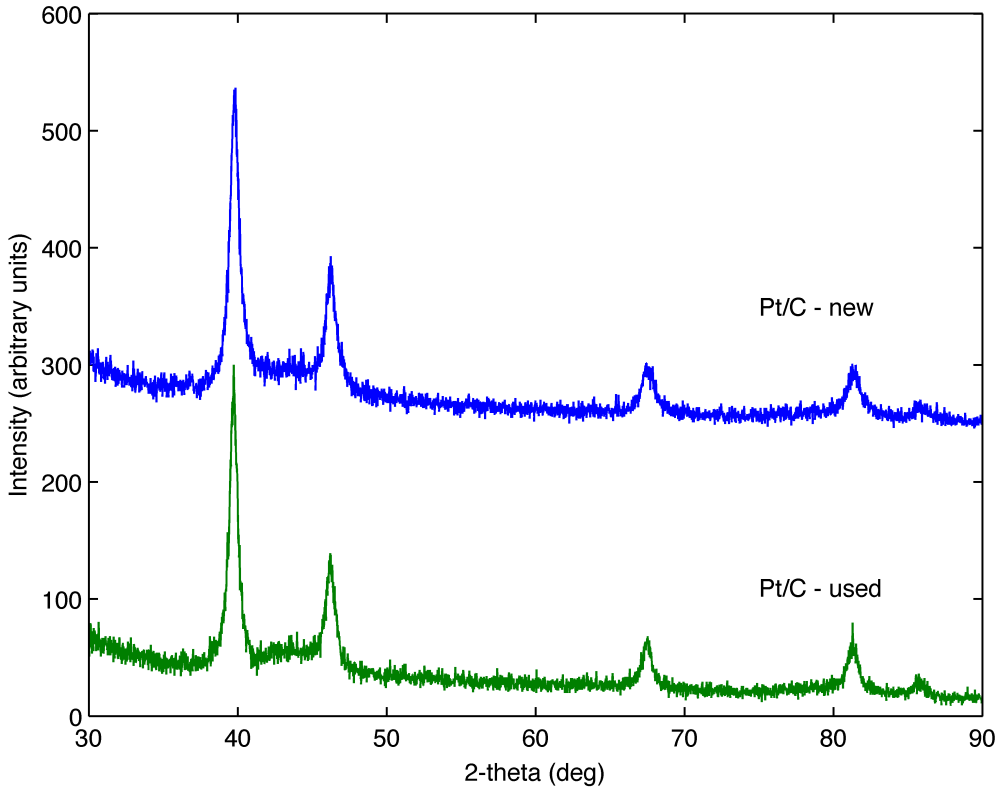

Figure 5.8: XRD spectra of fresh and used (24 h time on stream at 350 °C) Pt/C catalysts

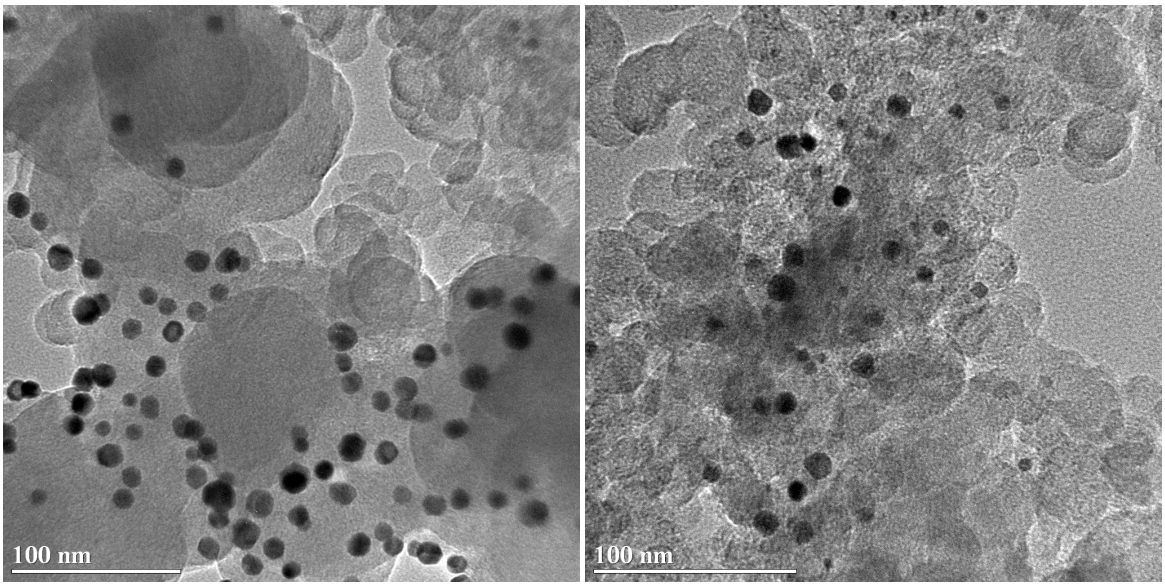

(a) Fresh Pt/C (b) Pt/C after 24 h time on stream at 350 °C

Figure 5.9: TEM images of Pt/C

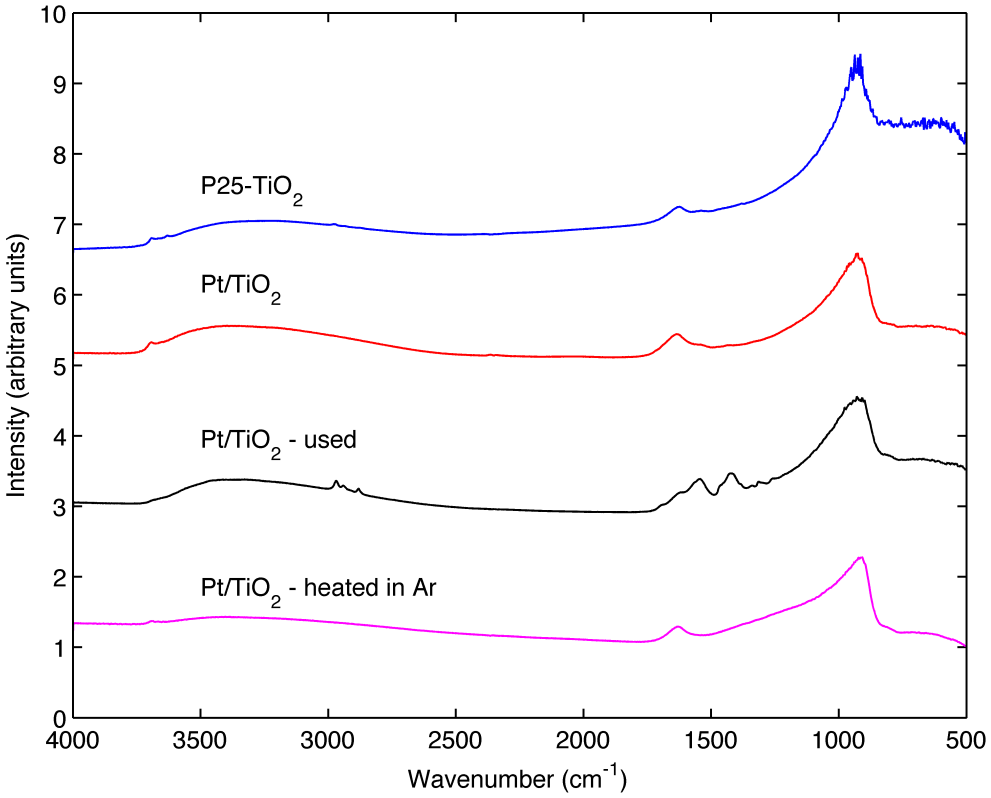

Figure 5.10: DRIFTS spectra for TiO_2 and Pt/TiO_2 catalysts. From top to bottom: P25 titania as received, unused Pt/TiO_2, Pt/TiO_2 after 24 h time on stream at 350 °C with 0.2 M butyric acid feed with W/ν = 300 mg min/mL, Pt/TiO_2 heated in Ar at 700 °C

ditional tests on the Pt/C catalyst. Therefore, to test the hypothesis that poison molecules might have contributed to the decrease of catalytic activity, we synthesized a catalyst containing Pt nanoparticles supported on P25 TiO_2 (80% anatase with the balance of rutile). We chose TiO_2 as an alternative support to elucidate the deactivation mechanism. TiO_2 would also allow for oxidative regeneration of the catalyst.

One possible issue arising from choosing TiO_2 as a support is the strong metal-support interaction. Tauster et al. demonstrated that under the the synthesis conditions with a reduction of $H_2PtCl_6 \cdot 6\,H_2O$ under H_2 at 500 °C, the formation of $TiPt_3$ is thermodynamically favorable[96]. The formation of this intermetallic species may confound the chemistry obtained from the characterizations of the deactivating compounds, but the Pt/TiO_2 catalyst showed similar deactivation characteristics to the Pt/C catalyst (i.e. first-order deactivation).

Figure 5.10 displays DRIFTS spectra of the P25 TiO_2 support, the fresh Pt/TiO_2 catalyst, the used Pt/TiO_2 catalyst as recovered from the flow reactor at the end of a 24 h run, and the same material after being heated in Ar at 700 °C for 2 h. The spectra for the support and the fresh catalyst are largely indistinguishable, whereas the spectrum for the used catalyst shows stretches at 2900, 1530, and 1440 cm^{-1} that were absent in the fresh material. The peak at 2900 cm^{-1} is characteristic of C–H stretches, and the peaks at 1530 and 1440 cm^{-1} are characteristic of unsaturated C–C bond stretches. The appearance of these new peaks indicates the presence of organic compounds on the catalyst surface. These organic molecules could range from being individual small molecules to being large, condensed aro-

matic structures that adhere strongly to the surface. To assess whether the organic compounds would simply desorb, we heated the used Pt/TiO_2 catalyst to 700 °C in flowing Ar. The resulting DRIFTS spectrum is nearly identical to that of the fresh catalyst, and the peaks at 1500 and 2900 cm^{-1} present in the used catalyst are now absent. This result suggests that the organic surface species desorbed during the high-temperature treatment. Larger molecules, such as large carbon networks associated with coke formation, would not be expected to desorb in an inert environment. Typically, an oxidizing environment is needed to burn coke off a catalyst surface. These results suggest that poisoning may play a role in catalyst deactivation during hydrothermal decarboxylation of butyric acid.

Possible poisons in this system are propylene or some other C_3 hydrocarbon. Propane is the main hydrocarbon product, and Pt is known as a good dehydrogenation catalyst. To test the hypothesis that propylene or some variant thereof was a poison, we conducted an experiment wherein a Pt/C catalyst used in the flow reactor for a 24 h reaction. Subsequently, the Pt/C was reduced in place by flowing hydrogen over the catalyst at 350 °C for one hour. We collected the reduction gases emerging from the reactor system and analyzed them by GC. The gas contained trace amounts of propane, suggesting that unsaturated hydrocarbons had been adsorbed on the surface of the catalyst and then hydrogenated to propane during the reduction of the catalyst in flowing hydrogen. The presence of propane could indicate an unsaturated C_3 hydrocarbon present on the surface, although the propane could result from some other larger molecule transforming into the observed propane upon hydrogenation. The presence of propylene or

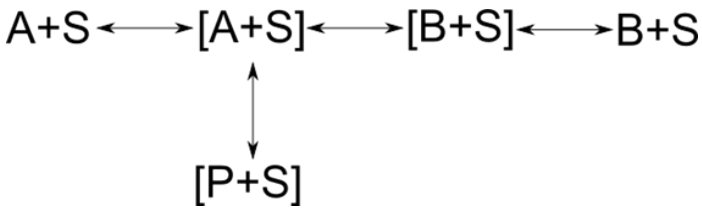

Figure 5.11: LHHW model for catalyst deactivation [97]

some other unsaturated hydrocarbon on the catalyst surface could be consistent with features of the DRIFTS spectrum shown in Figure 5.10 for the used Pt/TiO_2 catalyst.

The prominence of molecular poisons and the first-order deactivation suggest that the catalyst may be undergoing deactivation through the Langmuir Hinshelwood Hougen Watson (LHHW) deactivation model. Figure 5.11 shows that the model is characterized by the reagent (A) binding to a surface site (S) and becoming [A+S]. [A+S] then transforms to the surface-bound product ([B+S]) and desorbs, but there is a side reaction that involves the transformation of [A+S] to a poison ([P+S]).

Following the DRIFTS experiment and the capturing of hydrogen gas with traces of propane, we investigated the reversibility of the deactivation of a Pt/TiO_2 catalyst. Results for a 24 h run with fresh catalyst appear in Figure 5.12. The used catalyst was then treated at 350 °C under flowing H_2 for 12 h to remove any C_3 poison molecules. Figure 5.12 shows that this treatment in 350 °C H_2 restored some decarboxylation activity, but the activity was still lower than that of the fresh catalyst. Next, we treated the Pt/TiO_2 catalyst in flowing H_2 at 500 °C for 12 h to remove poisons up to C_6. Again, the treatment restored activity with similar efficacy

to the treatment at 350 °C. These results show that poisoning does play a role in deactivation, but the loss of activity due to poisoning is minor. Lastly, we performed controlled oxidation of the used catalyst at 500 °C for 12 h under 1% O_2 with the balance of N_2 to remove any carbon-containing species that were resistant to the H_2 treatments. Controlled oxidation restored the majority of the decarboxylation activity. Therefore, we suspect that coke formation is another cause of deactivation during hydrothermal decarboxylation of butyric acid over supported Pt catalysts. Deactivation by coking, which is reversible by controlled oxidation of the coke, typically exhibits deactivation orders of one or less [98].

A final cause of deactivation in this system is collapse of the pore structure in the Pt/C catalyst. Pt/C in water alone at 350 °C produced 0.018 ± 0.002 μmol H_2 and 0.0062 ± 0.0019 μmol CO_2/mg Pt/C indicating that the support reacted with water under the experimental conditions. BET measurements of a used Pt/C catalyst and the fresh carbon support also show that the surface area of the used catalyst (220 m^2/g) was essentially the same as that of the fresh Vulcan XC-72 carbon (229 ± 6 m^2/g). The pore volume of the used catalyst, however, was 0.55 cm^3/g whereas the original pore volume of the support is 1.42 ± 0.2 cm^3/g. The pore volume decreased during the reaction, and this decrease may have contributed to some of the lost activity.

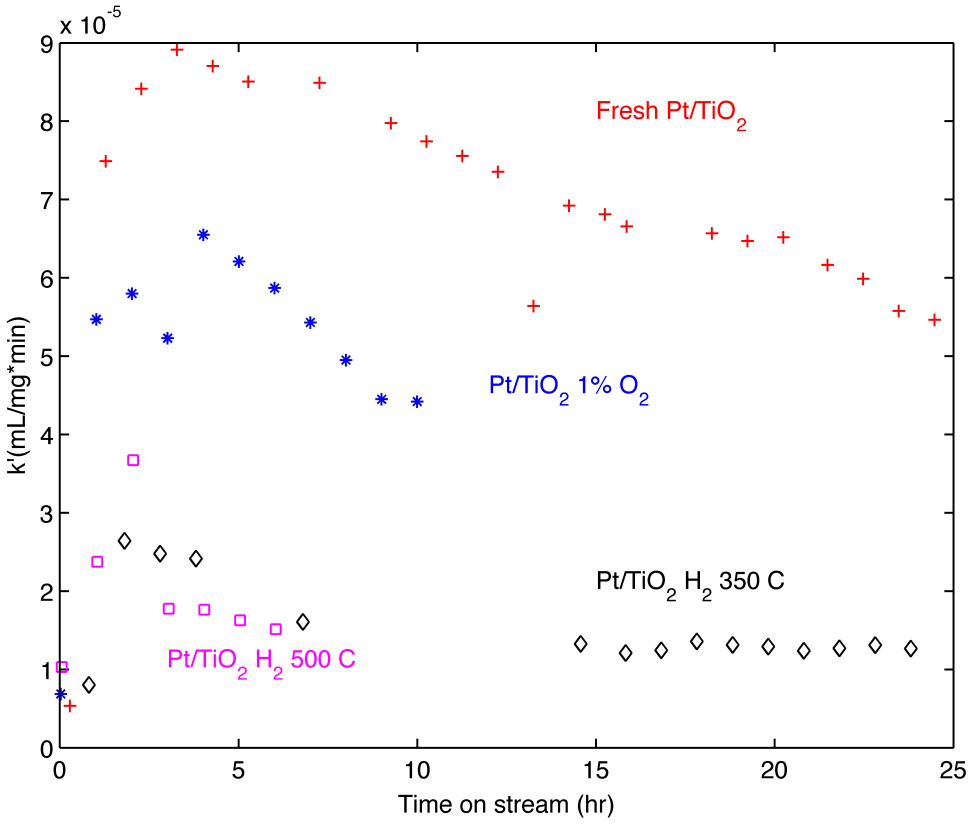

Figure 5.12: Rate constant for fresh and used Pt/TiO_2 catalyst after undergoing different treatments. Initial activity - Fresh Pt/TiO_2 reacted at 350 °C with W/ν = 300 mg min/mL at room temperature. Second recovered activity after 350 °C reduction for 1 hour. Third recovered activity after 500 °C reduction for 1 hour. Fourth recovered activity after oxidation in 1% O_2 overnight.

5.5 Conclusions

The Pt/C catalyst experienced deactivation during decarboxylation of butyric acid in hot compressed water at 350 °C over the course of 24 h on stream. The deactivation of the catalyst is due to three separate phenomena. The carbon support, which typically is considered to be stable in hydrothermal environments, experienced loss of pore volume, indicative of pore collapse within the material. The Pt/TiO_2 was synthesized and characterized to show that Pt/TiO_2 experienced deactivation through a combination of poisoning and coking. We expect these modes elucidated from Pt/TiO_2 to be applicable to Pt/C These modes were operative because of the tendency of Pt to dehydrogenate hydrocarbons. We believe that some unsaturated hydrocarbon molecular compound is responsible for catalyst poisoning, possibly an unsaturated C_3 such as propylene [54]. Thus catalyst poisoning, coking, and structural degradation of the support all contributed to deactivation of the catalyst during hydrothermal decarboxylation of butyric acid. The first-order deactivation rate constant for Pt/C at 350 °C was $0.063 \pm 0.006\ h^{-1}$. As the catalyst deactivation occurred, however, the selectivity of the catalyst toward the desired decarboxylation product, propane, remained high. The research presented herein shows that Pt catalysts have potential for longevity in this application, but the hydrothermal conditions introduce complications not encountered in organic- or gas-phase decarboxylation processes. It is likely that adding a hydrogen source, whether internal or external, and/or modifying the catalyst to weaken the binding of unsaturated hydrocarbons could alleviate the issues of coking and catalyst

poisoning. The irreversible catalyst deactivation noted here stemmed from degradation of the support, so identifying a more stable support can also contribute to a longer catalyst life.

5.6 Acknowledgements

We gratefully acknowledge the National Science Foundation (Grant EFRI-0937992 and award DMR-9871177), the Rackham Graduate School at the University of Michigan, and the Michigan College of Engineering for their financial support. We also thank Ryan Franck for experimental assistance.

CHAPTER 6

PtSn Catalysts for Decarboxylation of Unsaturated Fatty Acids

6.1 PtM alloy catalysts

Pt alloys have been studied for chemistries such as electrooxidation, aqueous-phase reforming, alkene interactions, and deoxygenation. The electrooxidation literature is not included here because our batch reactions will not have a potential difference to affect chemistry. Pt alloyed with mid-transition metals including Fe, Co, Ni, and Re are suitable reforming catalysts where carbon bond scission is necessary for H_2 production [99, 100]. Pt alloys of Fe, Co, and Ni have been tested for aqueous-phase reforming of ethylene glycol. The alloys were superior to the base metals on a mass basis for the production of H_2 [100]. Salciccoli et al. demonstrated that binding energies of ethylene glycol intermediates on monometallic Pt and Ni-Pt alloys can be related through simple linear scaling relationships, and that dehydrogenating was preferred over cleaving C–O bonds [101]. Many different bimetallic Pt alloys have been studied. The alloying metals appear earlier

on the periodic table, in comparison to Pt, and effectively catalyze reforming reactions where C–C bond scissions are favorable. For the purpose of decarboxylating fatty acids and preserving the carbon chain length, C–C bond scissions are undesirable, and alloying Pt with a metal that occurs later on the periodic table may be beneficial.

$PtSn_x$ has been studied as a dehydrogenation catalyst both experimentally and theoretically [102–105]. Experimentally, $PtSn_x$ shows improved selectivity to olefin formation from the alkane [104, 105]. On the theoretical end, Xu et al. investigated ethanol dehydrogenation using Pt_3M clusters consisting of four total atoms where M is Pt, Ru, Sn, Re, Rh and Pd[106]. Their simulations showed that the rate determining step for dehydrogenation was the adsorption of the α-hydrogen to the Pt in the metals studied[106]. Sn was the only metal to enhance dehydrogenation of ethanol [106]. The d-band center of $PtSn_x$ being lower in comparison to Pt results in a lower binding energy of an olefinic adsorbate to the catalyst surface [102, 103]. Their result is corroborated by the decrease in binding energy from the addition of Sn into a Pt surface for ethylene, propylene, and butylene in UHV[107]. Additionally, coke precursors may not be as deactivating for a Sn-modified Pt surface due to increased carbon mobility [108]. $PtSn_x$ has also exhibited the ability to transform paraffinic methyl esters into olefins in organic solvents [109]. The ability of $PtSn_x$ to tolerate alkenes and coke suggests that $PtSn_x$ may be better suited for decarboxylation of unsaturated fatty acids than elemental Pt catalysts.

Sn alone has been documented to effectively hydrogenate carboxylic acids into the corresponding aldehydes [110]. Sn/SiO_2 can selectively hydrogenate an unsat-

urated crotonaldehyde to the unsaturated crotyl alcohol thus leaving the unsaturated C=C untouched. Sn-MCM-41 will convert ketones into esters in the presence of peroxyacids [111], but activity more relevant to the desired decarboxylation reaction here has not been documented.

Results in this section are from experiments that were repeated at least three times. We report the mean values and use the standard deviations as the experimental uncertainty. We first discuss the effect of the Pt:Sn ratio and the degree of unsaturation of the fatty acid on the carbon recovery for each experiment. We then examine the effect of varying levels of Sn on the activity and selectivity towards the desired C_{17} hydrocarbon product, and hypothesize the possible catalytic surface through XRD data and knowledge of the atomic composition of the catalysts. Lastly, this section investigates the source of hydrogen involved in the hydrogenation of the unsaturated fatty acids through the use of D_2O.

6.2 Carbon Balances

Table 6.1 gives the average carbon balance, or recovery, for experiments with each catalyst-fatty acid combination. Experiments involving stearic acid, which is saturated, showed average carbon recoveries of 88 – 100%, effectively demonstrating closure of the carbon balance for the system. Experiments involving oleic acid, which has one C=C double bond, had carbon recoveries of 71 – 79% and those involving linoleic acid, with two C=C double bonds, were 50 – 70%. It is clear that C=C double bonds in the fatty acid reduced the carbon recoveries regardless of

Catalyst	Stearic acid	Oleic acid	Linoleic acid
Pt/C	88 ± 6	79 ± 10.	50 ± 2
Pt_3Sn/C	100 ± 7	71 ± 15	–
PtSn/C	94 ± 6	72 ± 8	60 ± 15
$PtSn_3/C$	95 ± 4	71 ± 4	70 ± 13

Table 6.1: Carbon balances (%) for fatty acid decarboxylation experiments at 350 °C and 1 hour with 5 mg of catalyst, 100 μmoles of fatty acid.

the catalyst type, though an increasing presence of Sn appears to have improved carbon recoveries for linoleic acid. Dimerization or oligomerization of the unsaturated chains is a likely explanation for the lower carbon recoveries with the unsaturated fatty acids. The larger molecules that would form in this route would be undetectable by GC due to their low vapor pressures.

6.3 Reaction Products

Figure 6.1 shows the conversion of stearic acid over different catalysts and the resulting molar yields of heptadecane and fatty acids with one (C18:1) and two (C18:2) double bonds. Heptadecane is the decarboxylation product from stearic acid. The molar yield is calculated as the number of moles divided by the number of moles of fatty acid loaded into the reactor. Figure 6.1 shows that all catalysts tested showed high activity towards the decarboxylation product for the saturated fatty acid. Pt/C, in agreement with literature, produced primarily heptadecane, and the $PtSn_x/C$ catalysts behaved similarly [43]. Pt_3Sn/C and PtSn/C outperformed Pt/C for activity towards the decarboxylation product while $PtSn_3/C$ showed a slightly lower molar yield of heptadecane. Figure 6.1 shows that an un-

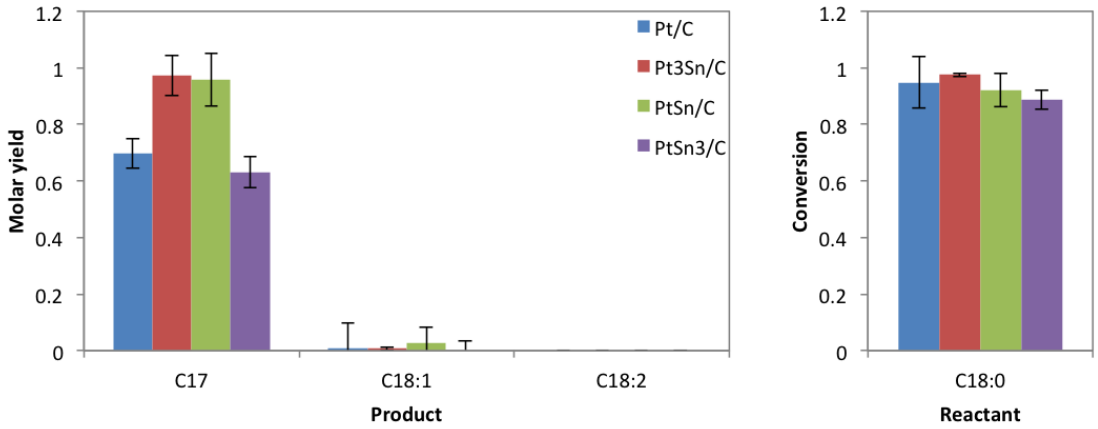

Figure 6.1: Molar yields of products and conversion of stearic acid from hydrothermal treatment over $PtSn_x/C$ catalysts at 350 °C for 120 min.

saturated C_{18} fatty acid was also among the reaction products. This unsaturated fatty acid must have formed from dehydrogenation of the stearic acid reactant. Cracking products were also detected but these were all present in lower yields than heptadecane and C18:1.

Figures 6.2 and 6.3 show that Pt/C was not as active towards the decarboxylation product when oleic and linoleic acid were the reactants. With Pt/C, the yield of decarboxylation product was about 70% when treating stearic acid, but just 16% and 8% when treating oleic and linoleic acids, respectively. Although the yield of C_{17} product, heptadecane, increases with the addition of Sn to the catalyst for all of the C_{18} fatty acids examined, Figure 6.2 and Figure 6.3 show that the overall ability of the catalysts to generate C_{17} products decreases with increasing unsaturation of the fatty acid. Figure 6.4 shows the influence of both the degree of unsaturation of the fatty acid and the catalyst composition on the selectivity to decarboxylation products. We define selectivity as the moles of product formed divided by the

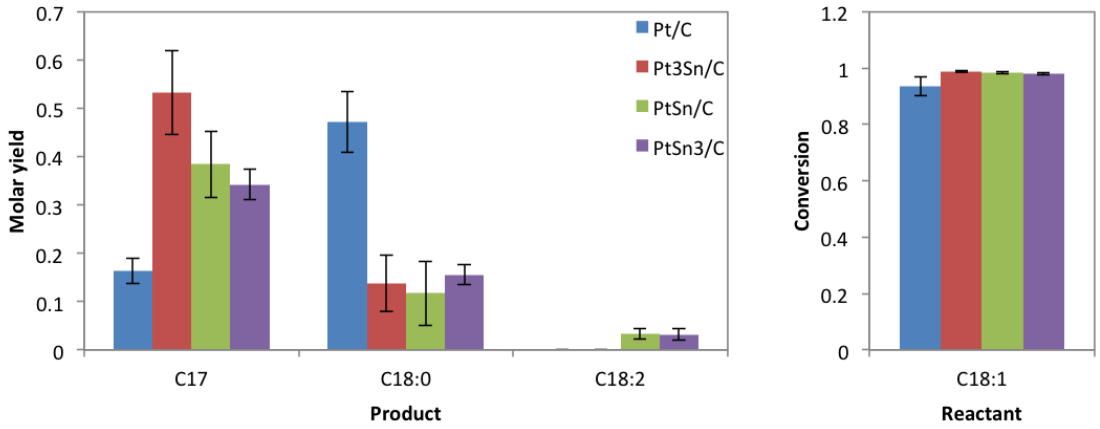

Figure 6.2: Molar yields of products and conversion of oleic acid from hydrothermal treatment over $PtSn_x/C$ catalysts at 350 °C for 120 min.

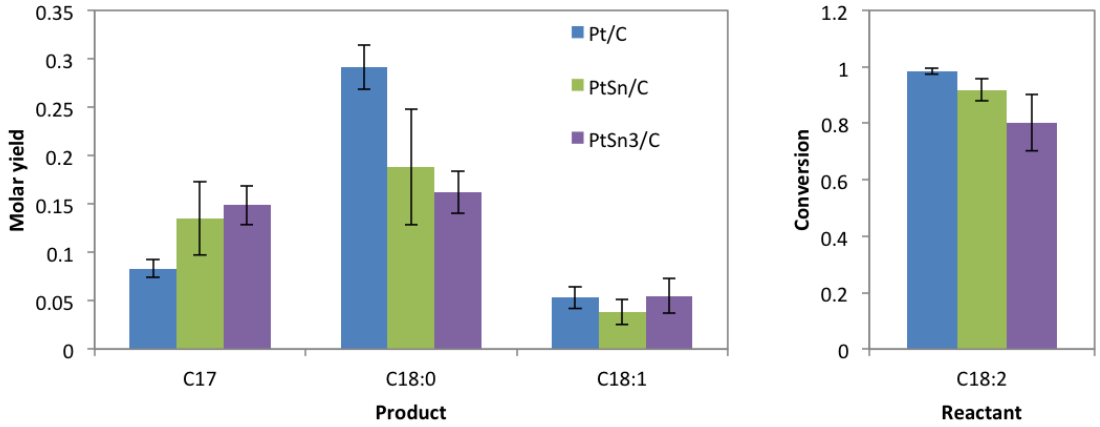

Figure 6.3: Molar yields of products and conversion of linoleic acid from hydrothermal treatment over $PtSn_x/C$ catalysts at 350 °C for 120 min.

moles of fatty acid that have reacted (i.e., molar yield divided by conversion). In all cases, alloying Sn into the Pt catalyst at various levels increases the selectivity towards the C_{17} product in comparison to the performance of Pt alone. With respect to the unsaturated fatty acid reactants, the Pt/C catalyst favored hydrogenation to stearic acid rather than doing decarboxylation, an observation that is in agreement with literature [43].

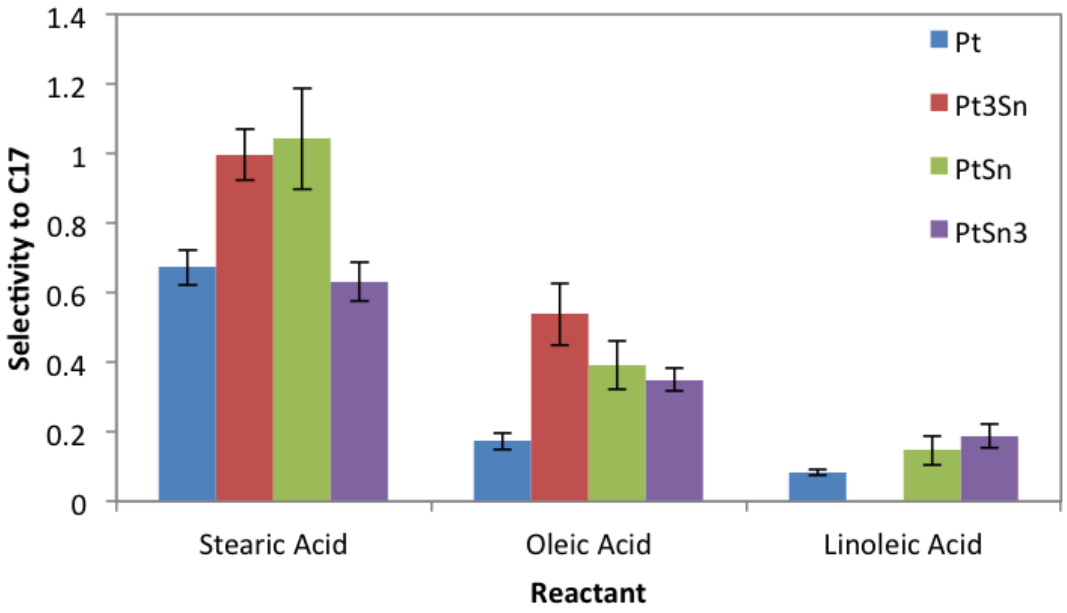

Figure 6.4: Selectivity of $PtSn_x/C$ catalysts for decarboxylation of different fatty acids at 350 °C for 120 min.

6.4 Catalyst Characterization

Figure 6.5 shows XRD spectra for the four fresh catalysts along with vertical lines indicating the locations of expected reflections for different $PtSn_x$ crystal phases. Unfortunately, the diffractograms have a significant amount of noise making the analysis of other crystal phases that may be present to lesser degrees difficult to discern. The peaks in the XRD spectra for Pt/C and Pt_3Sn/C are consistent with the blue and green vertical lines respectively, which show the expected reflections for Pt and Pt_3Sn. On the other hand, the spectrum for PtSn/C does not show strong reflections for PtSn – the vertical red lines. A small peak at 42° shows some evidence of PtSn, but the strongest reflections match those of Pt_3Sn. The $PtSn_3/C$ spectrum shows only reflections corresponding to PtSn. None of the spectra show

evidence of metallic Sn or SnO_2. The bulk structures deduced from XRD for PtSn and Pt_3Sn cannot account for all of the Sn used to synthesize the catalyst. For example, Pt and Sn were added in a molar ratio of 1:1 for PtSn, but XRD shows a molar ratio of 3:1. XRD is a bulk characterization technique, however, so it cannot detect surface features. One possible explanation is that the surface of the catalyst is enriched with Sn. If the stoichiometric PtSn catalyst were taken as having a 3 nm core of Pt_3Sn and a shell of $PtSn_3$ and assuming a uniform bond length in the two alloys, the resulting shell would have a thickness of 0.4 nm which is below the detection limit of the XRD. This surface rich phase that is too thin to be detected would satisfy the Sn balance and also be consistent with the bulk phases detected by XRD. Alternatively, one might suppose that there are small Sn islands, but the synthesis technique heats the catalyst to 500 °C, and this temperature is well above the melting point of Sn. At temperatures above the melting point, we would expect very large Sn particles which result in sharp and tall peaks in XRD that are not observed here.

In summary, XRD shows that Pt and Pt_3Sn were present in the two catalysts, as expected. Meanwhile, the PtSn and Pt_3Sn catalysts show the Pt_3Sn phase and the PtSn phase respectively leading to Sn enrichment elsewhere, possibly on the surface of the catalyst.

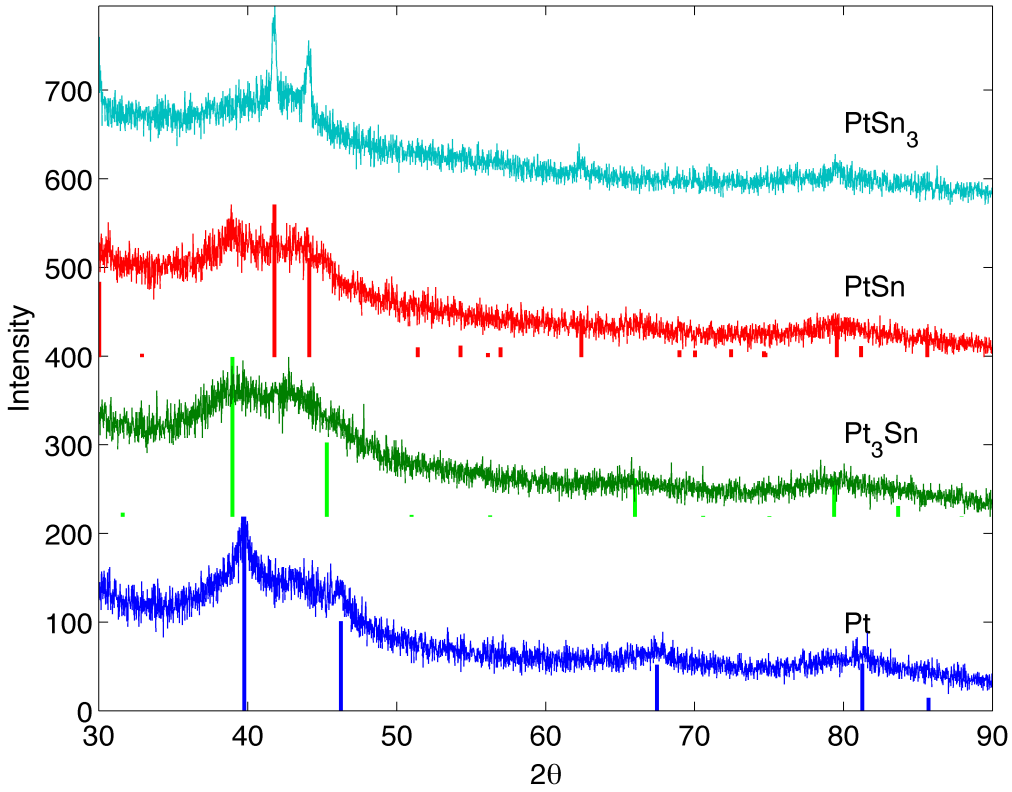

Figure 6.5: XRD spectra of fresh $PtSn_x/C$. The vertical lines denote crystal phases. Blue – Pt, Green – Pt_3Sn, Red – PtSn

6.5 Source of Hydrogen

The primary hydrocarbon product was always the saturated alkane, heptadecane, regardless of the degree of unsaturation of the fatty acid. A hydrogen source is required to make heptadecane with oleic or linoleic acid as the reactant. This hydrogen must arise from water, the organic reactant, or a combination of the two. This section examines the source of the hydrogen atoms that add to the unsaturated fatty acids during hydrothermal treatment.

6.5.1 From H_2O Reacting With Pt/C

We consider whether H_2O could be the sole source of hydrogen for saturating the fatty acids. H_2 could be produced by the catalyst alone through oxidation of the carbon support with water. For example, Xu et al. showed that coconut shell activated carbon alone generated hydrogen in SCW [112]. Likewise, our previous work showed that Pt/C directly reacted with water (350 °C, 2 h) to produce 0.018 ± 0.002 μmol H_2/mg Pt/C and 0.0062 ± 0.0019 μmol CO_2/mg Pt/C [113]. This H_2 can serve as a potential hydrogen source for saturating the C=C bonds in oleic and linoleic acids. However, the H_2 is produced in insufficient amounts to account for all of the hydrogenation observed in the present experiments. Catalyst in water alone produced 0.018 μmoles of H_2/mg Pt/C, but the reactors contained 20 μmoles of fatty acid per milligram of catalyst. Clearly, H_2 production from gasification of the carbon support is not playing a major role in fatty acid hydrogenation.

6.5.2 From Reactant Alone

The literature suggests that hydrogen atoms liberated from dehydrogenation of an olefin can accomplish hydrogenation of a subset of the olefin reactant molecules so that the products include both a saturated and an even more unsaturated product. For example, Crittendon and Parsons show that cyclohexene reacts over Pt/C in supercritical water at 375 °C for 20 minutes to produce benzene and cyclohexane in a roughly 2:1 molar ratio [114]. Figure 6.1 and Figure 6.2 show that stearic acid produces measurable yields of a mono-unsaturated C_{18} fatty acid and that oleic acid produces measurable yields of a doubly unsaturated C_{18} fatty acid. Though these yields of dehydrogenation products are much lower than that reported by Crittendon and Parsons for cyclohexene in SCW, dehydrogenation clearly occurs in this reaction system and this dehydrogenation would produce H_2. Pt and PtSn are both hydrogenation and dehydrogenation catalysts.

As alkenes are also known to undergo oligomerization reactions, the pathway of dehydrogenation followed by oligomerization could serve as a route that provides sufficient hydrogen for the hydrogenation observed during hydrothermal treatment of the unsaturated fatty acids. Moreover, the *missing* carbon evident in Table 6.1 could reside in oligomerization products that went undetected in our analytical protocol. One mole of oleic or linoleic acid could provide up to 7 or 6 moles of H_2, respectively, when dehydrogenating to a fully conjugated alkene. This pathway would generate sufficient H_2 to account for the hydrogenation observed in this system. Since this pathway is viable on the basis of stoichiometry, we per-

formed additional experiments to determine whether hydrogen from the organic reactant alone is the source of H atoms used to hydrogenate the fatty acids.

We chose *n*-octane and 4-octene to test whether the organic reactant could be the sole source of the hydrogen observed in the present reaction system. *n*-octane and 4-octene represent the hydrocarbon tails of the fatty acids. The double bond in oleic acid is sufficiently distant from the –COOH group that the chemistries of the two groups can be treated separately. *n*-octane and 4-octene reacted in water in 1.67 mL batch reactors at 350 °C with Pt/C for two hours. The results for *n*-octane showed no detectable compounds other than the original *n*-octane. There was no detectable dehydrogenation of this alkane. This low conversion is consistent with Crittendon and Parsons reporting just 2% conversion (to benzene) for the reaction of cyclohexane in SCW with Pt/C [114]. The reactions for 4-octene, on the other hand, showed multiple products including *n*-octane, 4-octanone, and small amounts of heptane. The production of 4-octanone points to water playing a role as the oxygen source, and thus also potentially a hydrogen source for the reaction. At supercritical conditions, water can add across the double bond to form an alcohol, and the subsequent oxidation of the alcohol to a ketone is catalyzed by Pt.

To probe further the possibility of the reactant acting as the sole H_2 source in this system, we examined the reaction of 4-octene in D_2O (rather than H_2O) at 280 °C for 1 hour. If H atoms from the reactant are the H atoms used to hydrogenate the double bond, one expects octane with 2 or fewer deuterium atoms as Pt will facilitate H-D exchange across the double bond [115].

The products resulting from the reaction of 4-octene in D_2O were analyzed us-

ing gas GC-MS. The fully protonated products from reaction were separable by GC, but the addition of deuterium shortened the retention times in comparison to the fully protonated parent molecule. The altered retention times caused overlapping of the reaction products. Examining the mass spectrum of the peak that appeared where *n*-octane is expected to elute from the GC revealed that fully protonated *n*-octane was not among the products. Rather, Figure 6.6 shows the presence of compounds with mass to charge ratios greater than 114. We observe m/z = 43, 59, 75, 89, and 118 which corresponds to characteristic peaks associated with *n*-octane-4,5-d4 as given in Table 6.2. The spectrum also shows peaks at m/z = 115, 116, and 117 which correspond to the m/z values expected for *n*-octane with one, two and three D atoms on the 4 and 5 carbons. There was no evidence for the presence of fully deuterated octane, which suggests that H-D exchange between the alkane and water was not a complicating factor in this experiment. Given these results, it appears that H atoms from the reactant are not directly added to double bonds in this system. Of course, we cannot rule out the possibility that H_2 liberated from the reactant underwent H-D exchange with water and then later added across the double bond in a different reactant molecule. Even in this scenario, however, the reactant would not be acting alone as water molecules would also be involved in the series of steps leading to hydrogenation. Thus, we conclude that hydrogen atoms from the reactant alone are not solely responsible for the hydrogenation observed in this system.

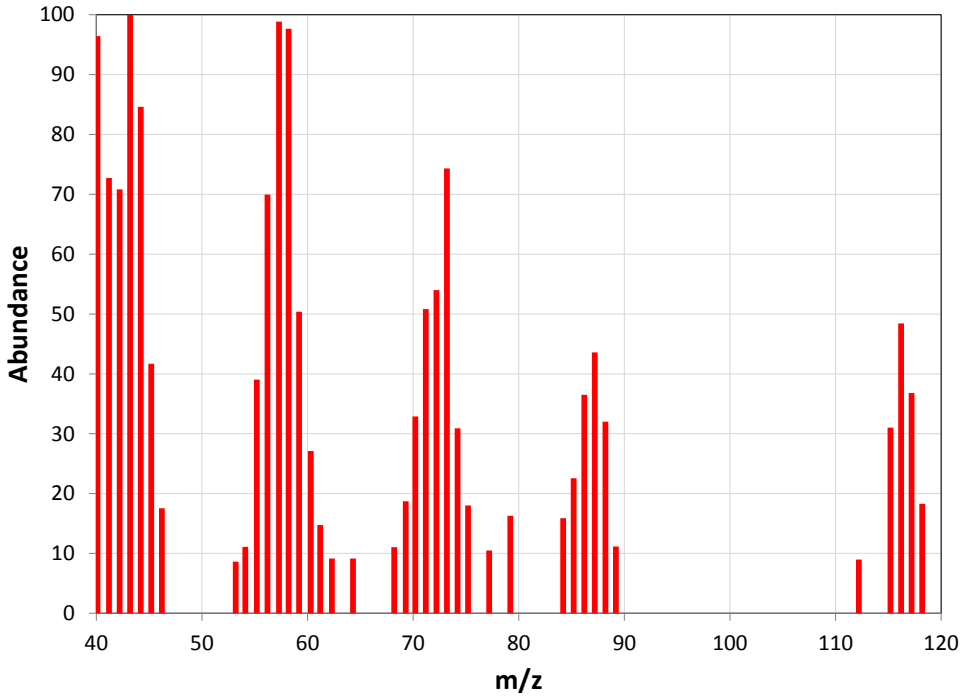

Figure 6.6: Mass spectrum of the reaction products from 4-octene $\overset{D_2O}{\underset{Pt/C}{\rightleftharpoons}}$ deuterated octanes at 280 °C for 15 minutes where protonated *n*-octane is expected to elute

Compound	Characteristic m/z values					
4-octene	41	55	56	70	83	112
n-octane	41	43	57	71	85	114
n-octane-4,5-d4	41	43	59	75	89	118

Table 6.2: m/z values for 4-octene and deuterated *n*-octane

6.5.3 From Water Alone

The presence of D from D_2O in the resulting *n*-octane molecules indicates that H_2O plays a role in the hydrogenation of the unsaturated fatty acids. Water alone is not the sole source of H atoms, however, since the product spectrum included octane with 1, 2, 3, and 4 deuterium atoms. If water alone were the source of hydrogen, then only D atoms should be on the surface (no H atoms). Water can dissociate on Pt surfaces, so D atoms from deuterated water molecules could be on the Pt surface in proximity to an adsorbed olefinic group. In that case, one would expect *n*-octane-4,5-d4 to be the major reaction product. We expect *n*-octane-4,5-d4 as the major product in this scenario because the literature reveals that olefinic hydrogen atoms undergo facile H-D exchange on Pt [115]. Therefore, one can expect these two H atoms to be exchanged with D atoms prior to hydrogenation. The *n*-octane that forms in the reaction will have also been hydrogenated across the 4 and 5 carbons during hydrogenation to yield *n*-octane-4,5-d4 if hydrogen is generated from water. Since other levels of deuteration were detected, we eliminate water alone being the hydrogen source.

6.5.4 From Both H_2O and Reactant

Having eliminated the reactant alone and water alone as hydrogen sources, both water and hydrogen together remains the sole possibility. The literature shows that Pt can catalyze the hydrothermal gasification of organic compounds and the production of H_2 [82, 116]. Our previous study on hydrothermal decarboxylation

of butyric acid over a Pt/C catalyst showed that steam reforming of the fatty acid is likely under these conditions [113]. In the presence of D_2O one would expect formation of H_2, HD, and D_2 from steam reforming/hydrothermal gasification in the system. Thus, both H and D atoms could be on the Pt surface and available for hydrogenation, which would lead to octane molecules containing 0, 1, 2, 3, or 4 deuterium atoms.

We performed a control experiment with n-octane and D_2O (280 °C, 1 h) to determine whether H-D exchange occurs over the Pt/C catalyst. The product spectrum showed just a single peak, which we identified as fully deuterated n-octane. The complete deuteration of n-octane under conditions where the octane formed from hydrogenation of 4-octene contained no more than four deuterium atoms requires explanation. We hypothesize that the alkene functional group in 4-octene has such a high affinity for the Pt surface that the surface is essentially completely covered with 4-octene. The molar ratio of 4-octene to Pt atoms was 100:1 in this experiment. Even if the catalyst dispersion were 100%, there is more than enough 4-octene to occupy all of the surface sites. In this scenario, octane would not be able to compete with octene for access to the catalyst sites, so it would not be further deuterated after leaving the surface. When no octene is present however, octane molecules have unimpeded access to the Pt surface and can readily undergo H-D exchange. This explanation is also consistent with the lower decarboxylation activity and selectivity observed for unsaturated fatty acids during treatment over Pt catalysts [43, 48, 117].

6.6 Conclusion

$PtSn_x/C$ catalysts decarboxylated stearic, oleic, and linoleic acids to various degrees of effectiveness. Increasing degrees of unsaturation, i.e. more C=C decreased catalyst activity and selectivity towards the decarboxylation product. The addition of Sn as an alloying agent for the Pt catalysts decreased the overall activity of the catalyst, but the lower activity was more than compensated for through increased selectivity towards the C_{17} decarboxylation product. Interestingly, the resultant C_{17} products were completely saturated, i.e. heptadecane, rather than the direct decarboxylation product of heptadecenes. Experiments involving D_2O support that a source of this hydrogen was water through steam reforming.

6.7 Acknowledgements

The authors thank the National Science foundation (Grant EFRI-0937992), the Rackham Graduate School at the University of Michigan, and the Michigan College of Engineering for their financial support.

CHAPTER 7

Activity Screening of Potential Hydrothermally Stable Catalysts

The purpose of this work is to explore catalyst candidates that may be able to maintain HTL biocrude upgrading activity in harsh hydrothermal conditions. As discussed in Section 2.4, catalyst stability in the hydrothermal environment represents an ongoing challenge. I selected various catalyst active metal and support combinations based on literature reports showing promise of stability in the hydrothermal environment.

7.1 Catalyst Selection

The catalyst selection considered three primary factors: the activity of the material, the stability of the catalytically active material, and the stability of the support.

7.1.1 Metal Catalyst

The most important factor in choosing the catalyst is that the catalyst itself will perform the desired chemistry. Ideally, the catalyst will be active for oxygen, nitrogen, and sulfur removal. Ni-based catalysts are less active and selective than noble metals such as Pt and Pd for deoxygenation reactions, but the low cost of Ni makes it attractive [68, 118–120]. In addition to Ni, Ru, Pt, and Pd catalysts are effective for upgrading as discussed in Chapter 2. The stability criteria included resistance to oxidation in water, and resistance to leaching. Many metals are not stable in water, but Ni, Cu, and Ru catalysts were stable in the tests performed by Elliott et al. [82]. Furthermore, from liquefaction experiments, we know that Pt and Pd are effective catalysts that are also resistant to oxidation [82, 113]. These works showed that Ni, Cu, Ru, Pt, and Pd are stable in hydrothermal conditions. Due to these considerations, we chose Ni, Ru, Pt, and Pd as candidates for the screening study.

7.1.2 Catalyst supports

Catalyst supports are primarily used as a low cost carrier to hold a more expensive catalytically active metal. This allows for high dispersion of the catalytic metal which translates to a high fraction of the active metal being exposed to the surface. The support stability would affect the dispersion of the catalyst. As the surface area of a support decreases, there is less area for the catalyst metal to be dispersed on to. The support can also play a functional role such as providing acid sites that

can influence reaction pathways.

7.1.2.1 Aluminates

A collaboration with Miron Landau's group at Ben-Gurion University in Israel encouraged the investigation of hexaaluminate materials. These hexaaluminates are typically used as combustion catalysts where high temperature steam would be present, so they may be suitable for use in high temperature water or supercritical water.

γ-Al_2O_3 is a commonly used support for many catalytic applications. This support is a natural choice due to its high surface area and resistance to thermal degradation. However, in the harsh aqueous environment of near critical or supercritical water, γ-Al_2O_3 degrades to boehmite, $Al(OH)_3$. Single component metal oxides such as γ-Al_2O_3 and SiO_2 suffer from sintering at high temperatures and steam assisted degradation. γ-Al_2O_3 degradation in steam leads to a low surface area α-Al_2O_3 as an end product. Figure 7.1 proposes that a high surface area γ-Al_2O_3 that underwent hydroxylation to yield Al–OH will further dehydrate with adjacent particles to result in a low surface area single particle joined by Al–O–Al bonds [93, 121].

La, Ba, Si, Sn, and P inhibited the rate of sintering [93]. Interestingly, all inhibitors performed equally well on a mole-basis for the stabilization of alumina. There seemed to be no effect with respect to the inhibitor type. Arai et al. suggested two different causes for the inhibition of sintering through Si addition. The first is that sintering stems from the inhibitor reacting with Al_2O_3 to occupy va-

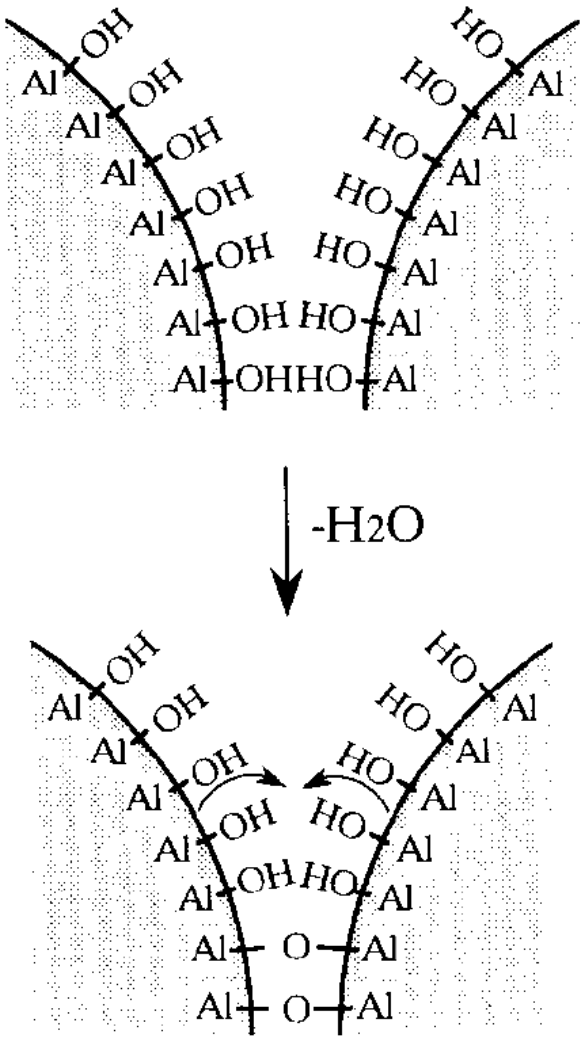

Figure 7.1: Formation of α-Al_2O_3 through dehydration of $Al(OH)_3$ [93, 121]

cant anionic sites that are responsible for thermal sintering. The other is simply that Si replaces surface hydroxyl groups making the surface of the alumina unable to sinter [93, 121].

Hexaaluminate materials can be synthesized such that larger ions can be inserted into the structure. These hexaaluminate materials, similar to the previously mentioned aluminas modified by different metals, have also shown resistance to thermal degradation. Some of these materials also show catalytic enhancement in these combustion processes, and Ba-hexaaluminates have shown high surface areas (100 m^2/g) [122].

We selected the hexaaluminate materials as supports because of their potential to maintain high surface areas in the supercritical water environment. The ability to insert larger ions into the crystal structure may also allow for the insertion of active metal ions rather than supporting the metal externally.

7.1.2.2 TiO_2-SiO_2 Supports

TiO_2 is also a commonly used low-cost support. However, at high temperatures, the high surface area anatase-TiO_2 will degrade to the more thermodynamically stable, but low surface area rutile phase.

TiO_2, in a similar fashion to Al_2O_3, also experiences stabilization through interaction with silica. Anatase titania shows improved resistance to transformation to the rutile phase at temperatures in excess of 1100 °C. The degree of resistance to transformation is dependent on the silica loading with the transition from anatase to rutile delayed until 1300 °C [123]. The major limitation of this study for our

purposes is that the conditions it used are not hydrothermal. The heating was performed in absence of water.

Conversely, TiO_2 is capable of stabilizing silicas. MCM-41, a mesoporous silica, suffers pore collapse at mild aqueous conditions such as being subject to boiling water. Titania deposited on MCM-41 demonstrates resistance to pore structure collapse. 20 wt% TiO_2 essentially stopped pore structure collapse after 6 days in boiling water[124].

Due to the improved resistance to high temperature transformation from anatase to rutile TiO_2 and resistance to pore structure collapse of MCM-41 obtained from mixing TiO_2 and silica, we have chosen both TiO_2 and TiO_2–SiO_2 as support materials.

In summary, we chose TiO_2, TiO_2–SiO_2, Ba and La hexaaluminates, MgO, and HY zeolite as support materials. The catalysts tested in this work were all synthesized by Miron Landau's group at Ben-Gurion University of the Negev and shipped to our lab for upgrading studies. The catalysts tested are summarized in Table 7.1

7.2 Results and Discussion

Here, we evaluate the biocrude. Then we evaluate the activity for deoxygenation and denitrogenation for the catalysts both with and without added hydrogen in the reactor. The efficacy of removing oxygen and nitrogen is characterized through the use of GC-MS and FTIR. The GC-MS results give information regarding the

Catalyst	Reduction Temp(°C)	Reduction time (min)
Pt/TiO_2	275	75
Pd/TiO_2	275	75
Ru/TiO_2	150	60
$LaPtAl_{12}O_{19}$	150	80
$LaPdAl_{11}O_{19}$	150	80
$LaRuAl_{12}O_{19}$	150	80
$BaPtAl_{12}O_{19}$	280	70
$BaPdAl_{11}O_{19}$	100	60
Ru/MgO	280	60
Pt/HY	280	80
Pd/HY	280	80
$Ni/TiO_2–SiO_2$	280	80
Ni/TiO_2	280	80
$BaNi_3Al_9O_{19}$	280	80
$LaNi_3Al_9O_{19}$	280	80

Table 7.1: Table of Catalysts Tested (400 °C for 1 h)

molecular identities and the weight or volatility of the molecule based on the elution time. Data obtained from FTIR indicates potentially which atom and bond type are present based on the wavenumber of the absorbance.

All GC-MS samples presented here were analyzed at the same concentration of initial biocrude to total volume, and the FTIR spectroscopy samples were dried from the same GC-MS samples such that the remaining oil was no longer mobile on the ATR crystal. The compounds identified by MS have match factors (quality) of at least 80 (0 – 100). A match factor is essentially a rating of how closely the fragmentation pattern for an unknown compound matches the NIST computer library where a match factor of 100 is a complete match, and 0 is no match. In cases where there are multiple compounds with a match factor of at least 80, the compound with the highest match is given. In some cases, this treatment will show a unique

compound eluting from the GC with multiple elution times which is impossible, but compounds of the same type (e.g. alkanes) will have similar mass spectra and therefore may be misidentified. The tables in A with compounds that may be misidentified have a note giving a more likely molecular identity. The relative peak heights from the FTIR spectra will be used to qualitatively determine the effectiveness of the catalyst at removing certain moieties (O–H, N–H, C=O, and C=N) in the following sections. Although the intensity of absorbance will vary depending on the concentration of the bio-oil sample in dichloromethane, the relative intensities of different regions within the same sample will remain unchanged because the relative concentrations of the moieties are independent of solvent loading.

A catalyst free control experiment was not performed within this set of experiments, so the thermal contribution to denitrogenation and deoxygenation will be difficult to deconvolute, however, possible thermal or hydrothermal contributions have been suggested through the use of literature in Section 7.2.2.1.

All figures and tables depicting GC-MS and FTIR spectra have been placed in Appendix A and B

7.2.1 Biocrude Analysis

GC-MS results in Figure A.1 show that the biocrude contains many hydrocarbons along with oxygen and nitrogen-containing compounds. Even with the gentle separation method described in Section 4.4.1.6, the GC was unable to obtain clean separation for many of the compounds. This incomplete separation led to difficulty in

Bond type	Range (cm^{-1})
X–H	3500 – 3000
C–H, alkenyl	3100 – 3000
C–H, alkyl	3000 – 2850
C=O	1760 – 1665
C=C	1680 – 1650
N–H bend	1650 – 1580

Table 7.2: General ranges of IR absorbances by functional group (X=O or N)

identifying many compounds through MS, however some compounds were able to be positively identified. Figure A.1 shows that most products elute from the GC at retention times of 30 minutes to 105 minutes. The identified compounds associated with these times include nitrogen-containing compounds, oxygen-containing compounds, alkanes, alkenes, and aromatics. The linear hydrocarbons range from dodecane (C_{12}) at 41 min to tricosene (C_{23}) at 82 minutes.

The GC-MS analysis has revealed some of molecules in the biocrude, but the identified compounds comprise less than 28% of the total peak area. Other methods are needed to analyze the biocrude more completely. FTIR of the biocrude oil gives insight as to which functional groups are present in the biocrude. FTIR shows absorbances as listed in Table 7.2.

The FTIR spectrum, Figure B.1 shows absorbances in the following distinct regions: from 3500 cm^{-1} – 3000 cm^{-1}, 3000 cm^{-1} – 2800 cm^{-1}, 1700 cm^{-1} – 1500 cm^{-1}, and 1450 cm^{-1} and below. These absorbances give evidence for X–H bonds, where X is defined as O or N, pointing to the presence of O–H or N–H moieties. The spectrum also shows evidence for C=O and C=C moieties. These combined point to the existence of oxygen or nitrogen which are undesirable from a fuels stand-

point. The strong absorptions from 3000 – 2850 cm^{-1} indicate that much of the hydrogen present is bonded to alkyl carbons as opposed to alkenyl carbons where little to no signal is visible (3100 – 3000 cm^{-1}).

7.2.2 Upgraded Bio-oil

7.2.2.1 No Catalyst

Noncatalytic upgrading of algal HTL biocrude is capable of yielding a bio-oil with improved physical and chemical properties compared to the original biocrude oil.

Roussis et al. thermally treated HTL biocrude that was prepared at 260 °C. They treated the biocrude at 350, 400, and 450 °C for 1 hour, and they measured the boiling point range, elemental composition, and the types of functional groups present in the resulting bio-oil. The nitrogen content of the oil remained unchanged at 4.2% through the temperature range tested. The sulfur content decreased from 0.4 to 0.1% from 400 – 450 °C, and the oxygen content reached a minimum of 0.2 % at 400 °C. The biocrude shows the largest mass fraction of products boiling from 630 – 1020 °F. The bio-oils treated at 350 and 450 °C also show the largest mass fraction of the products boiling in the same range, but it is evident that that boiling point range of the products has shifted from higher boiling point compounds to lower boiling point compounds. The boiling point distribution shows a larger fraction of the bio-oil that boil below 630 °F, and the bio-oil from the 450 °C treatment has the major mass fraction boiling from 260 – 400 °F. The functional groups that are most abundant in the biocrude are amides, fatty acids, and sterols. The thermally

treated bio-oils show the major compounds to be saturated hydrocarbons. Increasing temperature yields a larger fraction of aromatics, smaller fraction of amides, and the nitriles show a maximum at the 400 °C treatment. The purely thermal treatment reduces the sulfur and oxygen content of the biocrude, shifts the boiling point range to lower temperatures, and increases the hydrocarbon fraction of the resulting bio-oil without catalyst present [125].

Duan et al. performed upgrading experiments at 400 °C for 4 hours on HTL biocrudes synthesized at 320 °C. One particular experiment used no catalyst but with added H_2. The total acid number was reduced from 257 to 50. The O, N and S content were reduced from 6.5, 4.9, and 0.7% to 4.3, 2.2%, and below detection, respectively. The heating value also increased from 40.1 MJ/kg to 42.6 MJ/kg. The area percent in the total ion chromatograms also show an increase in saturated hydrocarbons as well as a decrease in the fatty acid content, and in general, the upgraded oil components have shorter elution times than the components present in the biocrude. Duan et al. shows that noncatalytic upgrading in H_2 can yield bio-oils with lower acidity and decreased O, N, and S content.

Faeth et al. studied fast HTL of algae where the biocrude was produced at shorter reaction times in comparison to the longer reaction times more commonly studied in literature. They studied times from as short as 1 minute. Although their studies are not strictly hydrothermal upgrading as biocrude, one might consider the chemistry to be similar to a noncatalytic upgrading reaction. The biocrude created at higher temperatures or longer times than the conditions used to synthesize the oil in this dissertation, Chapter 4, could be considered to be "upgraded" bio-

oils. For example, a biocrude produced using a 40 minute reaction time could be considered as an upgraded bio-oil in comparison to biocrude produced in a 350 °C and 20 minute reaction, the conditions used to produce biocrude in this dissertation. Their N, S, and O analysis shows that the biocrude processed at 400 °C retained 87% of the nitrogen, sulfur content increased by 15%, and the oxygen content was reduced by 75% of the biocrude processed at 350 °C for 20 minutes. They also showed that HTL of algae at 400 °C from 30 to 40 min showed little change in the resulting biocrude N, S, and O content [126]. Their liquefaction studies, however, have the aqueous-phase present during reaction. Thus, their "workup" procedure differs from the workup procedures in this catalyst screening study.

The noncatalytic upgrading work available from literature suggests that even without catalysts, purely thermal or hydrothermal treatment is capable of reducing oxygen, nitrogen, and sulfur content from HTL biocrude as well as reducing the boiling point profile of the resulting oil.

7.2.2.2 Pt Catalysts

Reacting biocrude over Pt/TiO_2 without hydrogen, see Table A.2, produces a large amount of early eluting compounds. The carbon-chain lengths range from C_7 for toluene (13.3 min) to C_{23} for tricosane (81.9 min). Most of the identified compounds are alkanes with a significant minority as alkenes. Oxygen and nitrogen containing molecules such as phenols, ketones, and indoles were observed in lesser amounts. The FTIR spectrum, Figure B.2, indicates that there is a significant growth in X–H character in comparison to the raw biocrude with the large increase in signal above

3000 cm^{-1} where the intensity of the X–H peak is roughly the same as the C–H peak. The growth in the X–H peak is in agreement with the observed phenols and indoles indentified by MS.

With added hydrogen, see Figure A.2, the product profile completely shifts to 2 major products. The product identities are given in Table A.3. The first at 80 min was not identifiable with MS. The peak could possibly be a C_{23} alkene as it is situated near tricosane (81.9 min). The second major peak at 62.5 min was identified as dodecyl acrylate. Even in the presence of hydrogen, there are still oxygenated compounds in the upgraded bio-oil. The oxygenates include the dodecyl acrylate, phenol derivatives, and ketones. Nitrogen-containing compounds are also evident in the form of pyrrole derivatives and amides. The X–H peak is significantly reduced in the oil upgraded over Pt/TiO_2 with hydrogen such that there is no discernible signal in the FTIR spectrum. Pt/TiO_2 with H_2 also shows a large reduction in the region where C=O, C=C, and N–H moieties absorb in comparison to both products from Pt/TiO_2 without H_2 and the raw biocrude.

Pt/HY, Table A.4, gave products that eluted mostly from 35 to 70 min with a major pentadecane peak at 54.9 min. The major peak at 13.8 min is a triply unsaturated C_7 hydrocarbon, possibly cycloheptatriene or toluene. Most of the identified peaks were either alkanes or alkenes with lesser amounts of heteroatom-containing compounds such as carboxylic acids or indole derivatives. Many of these compounds would make high quality liquid fuels in terms of their carbon numbers.

Pt/HY with H_2, Table A.5, yielded heavier compounds than those seen without H_2. Some of the major products that eluted include branched hydrocarbons, *n*-

hexadecanoic acid, and hexadecanamide. The observed compounds range from C_7 to C_{23} with the majority falling between C_{15} to C_{23}. The biocrude oil lost some X–H character due to decreased FTIR signal strength at wavenumbers above 3000 cm^{-1}, Figure B.3. Biocrude treatment over Pt/HY noticeably reduced signal strength at 1650 cm^{-1}. This points to either loss of N–H, C=O, or C=C groups. The additional hydrogen reduced the absorption at 1650 cm^{-1} to an even greater extent. These two signal reductions taken together suggest the loss of acidity or N–H function in the treated bio-oil.

In general, the supported Pt catalysts yielded molecules that fall in the range for both gasoline and diesel in the absence of hydrogen. Comparing results from the TiO_2 and HY supports however, shows different products when biocrude is reacted without hydrogen present. Pt/TiO_2, Figure B.2, does not remove X–H or C=O as effectively as Pt/HY as is shown by the large increase in the FTIR signal strength from 3500 – 3000 cm^{-1} for Pt/TiO_2. Although the N and O may have been removed from the oil, these heteroatoms could possibly still be held within C–N and C–O where the absorbances fall below 1500 cm^{-1} which is in the fingerprint region, but the mass spectra did not indicate the presence of single-bonded N or O compounds that would not be detectable in the previously analyzed FTIR spectral regions. Although Pt/TiO_2 produces earlier eluting compounds that may appear to be suitable for gasoline, these likely contain more undesirable O and N atoms in comparison to the oil produced from Pt/HY. When hydrogen is introduced, the products for both TiO_2 and HY supports are shifted to heavier, later eluting products, and much of the FTIR signal from the O and N has been reduced. The

signal reduction suggests that Pt on either support effectively removes O and N in the presence of H_2, but Pt/TiO_2 is selective towards two compounds judging by the peak intensity in the chromatogram, whereas the HY support is less selective and gives a large range of late eluting molecules.

7.2.2.3 Pd Catalysts

Pd/HY upgrading results in a decrease of absorption activity at 1700 – 1500 and a possible decrease at 3500 – 3000 cm^{-1}, which corresponds to C=O, C=C, or N–H and a decrease of X–H signal strength relative to the signal at 3000 – 2800 cm^{-1}, Figure B.5. The decrease in signal strength for the X–H bond is evident due to the local maximum in the biocrude signal at 3250 cm^{-1}. The upgraded biocrude oils lack the local maximum in the signal at 3250 cm^{-1}. The FTIR spectra suggest a possible reduction in nitrogen or oxygen through the loss of signal that corresponds to N–H or C=O and C–H in both regions of the spectra, but the nitrogen or could have formed C–N or C–O bonds which would be difficult to deconvolute from other types of single bonds in the < 1500 cm^{-1} region of the spectra.

Unlike Pt/HY, the two chromatograms for Pd/HY with and without external H_2 show a similar product distribution. Figure A.5 shows that the majority of products elute within the 40 – 75 minute time range. Two different transformations can result in a shorter elution time. One is the removal of oxygen and nitrogen, and the other is removal of carbon. Both of these transformations lead to a lighter molecule with higher vapor pressures and therefore shorter elution times. The reduction of elution time could then indicate that there has been a reduction

of heteroatoms (i.e. oxygen and nitrogen) from the oil, or the larger molecules have been broken into smaller molecules that are better suited for fuel production. In both cases, the catalyst produced mostly alkanes, alkenes, and heterocyclic nitrogen-containing compounds. The major peaks identified at 55 minutes were pentadecene and pentadecane.

Pd/TiO_2, Figure B.4, shows a significant reduction in the strength of the absorbance in the range of 1700 – 1500 cm^{-1} where the maximum signal within that range as a percentage of the maximum signal from 3000 – 2800 cm^{-1} has decreased from 75% for the biocrude to 38% for both upgraded oils. This signal reduction means that Pd/TiO_2 significantly reduces the amount of C=O, N–H, or C=C both with and without hydrogen. There is also a reduction in the X–H strength particularly for the reaction with hydrogen. The reduction of this signal also happens with Pd/HY, but the reduction happens at a lesser extent. Oils treated with both catalysts reduce the signal above 3000 cm^{-1}, but Pd/TiO_2 with H_2 shows the greatest reduction of the signal.

Additionally, the GC-MS chromatogram, Figure A.4, shows that both with and without hydrogen, the majority of products elutes between 10 – 70 min whereas with the untreated biocrude, the majority of projducts elutes between 40 and 100 minutes. Oxygen is shown to be present in phenol derivatives, and nitrogen is present in indole derivatives. The reactions with and without hydrogen performed similarly in terms of reduction of N–H, C=C, and C=O moieties and the profile of compounds eluting from GC, but using hydrogen further reduced the signal strength from the carbonyl and N–H moieties and yielded some heavier hydrocar-

bons.

7.2.2.4 Ru Catalysts

FTIR spectra in Figure B.6 shows that the Ru/MgO catalysts are effective for reducing X–H and C=O, C=C, or N–H signal in treated bio-oil. Most of the reduction happens with the moieties which are active in the 1650 cm^{-1} range, and this is more pronounced when external H_2 is added to the reactor. However, this data suggests that even with H_2 addition, carbonyl-containing or amide-containing compounds will still be present in the bio-oil. Ru/TiO_2 treated bio-oil, see Figure B.7, shows a greater reduction in the signal in the same region. The treatment with Ru/TiO_2 gives a greater reduction with H_2 compared to without.

GC-MS, Figure A.6, again shows qualitatively similar chromatograms for reactions both with and without hydrogen. Ru notably has shifted many of the products to lower molecular weight products based on the lower elution times. Bio-oil treated with Ru/TiO_2 with no H_2 shows a greater abundance of products from 10 – 35 min in comparison to oil treated with Ru/MgO. The identified products in both oils show many smaller molecular weight products such as toluene and benzene. Many of the identified compounds are olefins and aromatics. We also see evidence of heterocyclic nitrogen compounds. Adding H_2 as a reagent does not seem to have a major impact on the profile of product elution times for oil treated with Ru catalysts supported on MgO or TiO_2.

Both Ru/MgO and Ru/TiO_2 effectively treated biocrude in terms of producing lighter compounds and reducing C=O and X–H function. The effect of adding

external H_2 had a minor effect compared to that observed with the Pt and Pd catalysts, but the FTIR spectra showed that external H_2 yielded no observable change in the spectra for Ru/MgO between with and without hydrogen. The FTIR spectra show that without H_2, there is a lower intensity C=O peak in comparison to the treatment with H_2. The Ru supported on TiO_2 support produced more early eluting compounds from biocrude than Ru supported on MgO.

7.2.2.5 Ni Catalysts

Figure A.13 shows that Ni/TiO_2 without added H_2 generates molecules from biocrude eluting mostly from 60 – 70 min which correspond to alkenes and alkanes ranging from 16 – 19 carbons. When H_2 is added to the biocrude oil as a reactant, the resulting bio-oil still contains many of the same types of products, but the overall intensity is lower.

Figure A.14 shows C_{15} – C_{20} alkanes when biocrude is reacted over Ni/TiO_2–SiO_2. However, when H_2 is introduced as a reactant, the resulting products from biocrude have very low abundances in comparison to the other chromatograms.

The chromatograms for the bio-oils treated with Ni-based catalyst contain relatively few compounds in comparison to the other catalysts tested here. The low number of compounds has allowed for the MS identification of most of the eluting compounds, and between 85% to 100% of the identified compounds are alkanes and alkenes. The compounds that identify as containing O or N are nitriles, ketones, and organic acids. See Tables A.24, A.25, A.26, and A.27 for the identified compounds. The oil resolvable by GC-MS shows a reduced heteroatom content in

comparison to the biocrude, but the intensity of peaks from GC-MS show that in comparison to the non-Ni catalysts, much of the carbon is lost. When H_2 is introduced, the intensities of the peaks within the chromatograms is even lower. Ni is likely gasifying the biocrude at these conditions. Although the compounds that eluted from GC showed low heteroatom content, GC can only analyze a fraction of the compounds present.

FTIR is unavailable for the oil treated with Ni containing catalysts.

7.2.2.6 Hexaaluminate Catalysts

Biocrude treated with $LaPtAl_{12}O_{19}$, Figure B.8, shows an increase in the signal strength at 1700 cm^{-1} while the signal strength at 1600 cm^{-1} decreases. C=O transitioning from a conjugated carbonyl to an isolated carbonyl could explain the change in spectra. When adding external H_2, the treated bio-oil shows a decreased signal at 1650 cm^{-1}, possibly an unconjugated C=O, C=C, or N–H, while the signal at 1700 cm^{-1} remains unchanged. FTIR suggests that some N–H or conjugated C=O groups are removed. The two chromatograms for $LaPtAl_{12}O_{19}$, Figure A.8, show similar compounds in the same range of molecular weights. The majority of the compounds elute between 40 and 75 minutes which correspond to $C_{12} - C_{20}$ linear alkanes with some heavier compounds eluting afterwards. The products from GC-MS are an improvement upon biocrude from a fuels perspective because the heavier compounds eluting after 75 minutes have been reduced in comparison to the biocrude. Furthermore, the compounds that remain elute at regular intervals suggesting that they may be alkanes of different carbon numbers. The MS

identification shows mostly alkenes, alkanes, aromatic compounds, indoles, and fatty acids for both reactions with and without H_2 present.

The FTIR spectra of biocrude treated with $LaPdAl_{11}O_{19}$, Figure B.9, show a significant increase in C=O (1700 cm^{-1}) such that the intensity of the C=O signal is roughly 5 times stronger than the signal for alkyl C–H stretches. Compared to the other metal catalysts tested in this dissertation, the increase in the C=O signal strength is the largest increase. There also appears to be a decrease in X–H stretching for the bio-oil treated with H_2 as there is no observed peak from 3500 – 3000 cm^{-1}. GC-MS shows a shift towards lighter compounds such that the majority of compounds elute prior to 75 minutes, but heavier compounds are still present. The chromatograms without and with H_2 as a reactant are qualitatively similar. When comparing the identified compounds from mass spectrometry, Tables A.16 and A.17, we see that in the reaction with no hydrogen, there is a greater representation of alkenes and aromatic compounds. There are alkanes, but to a lesser extent than the alkenes. In contrast, the reaction with H_2 shows many alkanes have been identified with alkenes being a minority. However, many compounds remain identified in samples both with and without H_2 treatment.

$LaRuAl_{12}O_{19}$ increases the carbonyl oxygen signal above 1700 cm^{-1} with respect to the biocrude in the treated bio-oil when reacted in the absence of hydrogen as shown in the FTIR spectra, Figure B.10. In the presence of hydrogen, the signal above 1700 cm^{-1} is unaffected, and the signal from 1700 – 1500 cm^{-1} which corresponds to N–H, C=O, or C=C moieties is reduced from the original biocrude signal. The GC-MS chromatograms for both with and without hydrogen in Figure

A.10 show similar product distributions in terms of molecular mass and by way of retention times. As corroborated by the FTIR signal at 3050 cm^{-1} for the treatment without H_2, GC-MS suggests the absence of external hydrogen produced more unsaturated hydrocarbons while the presence of hydrogen produced more alkanes.

Biocrude treated with $LaNi_3Al_9O_{19}$ showed most compounds reside between 50 – 80 minutes in the chromatogram, Figure A.15. Interestingly, when external H_2 is added to the reaction, the resulting bio-oil shows a very low signal intensity for the compounds that do elute. One possible reason may be gasification of the products. FTIR spectra are not available for this particular bio-oil.

In summary for La-based hexaaluminates, biocrude reactions with these catalysts without external H_2 general show large increases in carbonyl signal strength above 1700 cm^{-1}. In order of decreasing signal strength relative to the alkyl-H from 3000 – 2800 cm^{-1}, Pd > Ru > Pt where a stronger signal is undesirable. A new signal is generated with all three catalysts in the hydrogen free condition. A signal is apparent at 3050 cm^{-1} which indicates the generation of alkenyl hydrogens. This catalyst likely dehydrogenates compounds within the biocrude to generate the alkene function. With a H_2 atmosphere, the La-based hexaaluminates did show some reduction of the carbonyl containing moieties, but the degree of reduction is smaller in comparison what the other catalysts tested within this dissertation have generated. No evidence of alkene function is generated with H_2 present.

FTIR spectra for $BaPdAl_{11}O_{19}$ both with and without hydrogen have similar upgrading activity in terms of removing N–H, O–H, C=O, and C=C moieties, Figure B.12. There is a decrease at 1650 cm^{-1} which demonstrates the removal of

N–H or C=O from the biocrude oil. The GC-MS also shows many heavy products eluting after 75 minutes still present in the bio-oil after upgrading. The identified peaks, Table A.22, show mostly hydrocarbons, heterocyclic nitrogen, organic acids, and ketones for the reaction without H_2. With H_2, similar products were identified with amides and nitriles in addition to those seen without H_2, but without ketones. Many products still remain unidentified by GC-MS.

Biocrude treated with $BaPtAl_{12}O_{19}$ and no H_2 shows decreased N–H, C=C, or C=O which is apparent from the decrease in activity from the raw biocrude around 1600 cm^{-1}. Adding external H_2 shows a slight decrease on the functional groups previously listed when compared to the reaction without external H_2, Figure B.11. GC-MS shows a similar product profile for the liquid phase products for $BaPtAl_{12}O_{19}$ in the absence of external hydrogen, but the abundance is approximately 4 times what is observed with the added H_2. The lower yield of products with H_2 could possibly stem from gasification of products. There is also a shift from heavier products to lighter products in comparison to the products in the biocrude. The identified products in Table A.20 show mostly alkanes, alkenes, aromatics, and hexadecanoic acid. Similarly, the identified products with H_2 in Table A.21 show mostly alkanes and alkenes. The identified products from the $BaPtAl_{12}O_{19}$ show many linear hydrocarbons ranging from C_{12} – C_{23} which are characterized by high cetane numbers. The identified products from biocrude treatment with the $BaPtAl_{12}O_{19}$ catalyst would make high quality diesel fuel based on chain-length and cetane number suitable for blending into lower cetane petroleum hydrocarbons.

$BaNi_3Al_9O_{19}$ treatment of biocrude without H_2, Figure A.16, shows products eluting mostly from 40 – 80 min. In the presence of hydrogen, the products are shifted to longer residence times than without hydrogen. The addition of H_2 produces several major products, Table A.30, which are identified as alkanes, alkenes, and esters. The abundance of products eluting from GC are lower without hydrogen than with hydrogen, and both with and without hydrogen generated fewer products and lower abundances than the other non-Ni catalysts tested in this dissertation. FTIR spectra are not available for this catalyst.

Overall, the Ba hexaaluminates reduced more of the carbonyl moieties in the biocrude in comparison to La, and Ba did not promote the generation of alkenes. Comparing the La and Ba hexaaluminate catalysts, the Pt-containing catalysts performed better than Pd in terms of reducing carbonyl compounds.

7.2.3 Limitations of the Experimental Methods

The results presented here do not show compounds that would evaporate with the drying of the dichloromethane solvent. The biocrude oil was separated using dichloromethane, and that dichloromethane was subsequently dried to determine the mass. The biocrude was then redissolved in dichloromethane for the experimental convenience of transferring the oil. The dichloromethane was again dried prior to catalyst loading and reaction. These processing steps require repeated solvent evaporation and lead to the evaporation of lighter hydrocarbons. In addition to the loss of light compounds, gas chromatography is only capable of analyzing

compounds that are volatile. Heavier compounds will not be able to elute from the column, and thus will not be detected. During processing of these biocrude and upgraded bio-oil samples, the GC injection port liner became noticeably darkened after repeated injections, and the guard column needed periodic cutting to maintain performance. Heavier compounds not suitable for eluting from the column were the likely culprits for the darkened liner and the performance degradation.

7.3 Conclusion

All the catalysts produced lighter molecular weight compounds, but they all also produced heavier compounds which eluted later than C_{20} hydrocarbons (elution time of 73 minutes on these chromatograms). In general, the addition of H_2 produced heavier molecules than reactions without external hydrogen. Catalysts that produced molecules in the gasoline to diesel fuel range include Ru/TiO_2, Pt/TiO_2 without hydrogen, Pd/TiO_2, Pd/HY, Pt/HY, Ru/MgO, $LaPtAl_{11}O_{19}$, and $LaPdAl_{11}O_{19}$.

The La hexaaluminates were not as active as the noble metal catalysts for the reduction of C=O and N–H containing compounds. The lack of this activity is evidenced by the high signal strength in the 1700 – 1500 cm^{-1} after reaction with the La-based catalysts.

Ni based catalysts, including the hexaaluminates, generated fewer products from biocrude without added H_2 both in terms of quantity and abundance based on the chromatograms. Ni is known to be a gasification catalyst [127, 128], and at the 400 °C reaction temperature here, Ni is likely gasifying the biocrude rather

than producing liquid range products. The addition of H_2 here may be facilitating the production of gaseous hydrocarbons through hydrogenolysis of C–C bonds.

The supports examined here include HY zeolite, TiO_2, TiO_2–SiO_2, and MgO. The FTIR spectra reveal that the monometallic catalysts supported on TiO_2 gave the largest reduction in C=O and N–H from the crude oil. TiO_2–SiO_2 treated bio-oil was not available for this particular characterization.

Overall, the best catalyst metal was Pt in terms of generating bio-oil from biocrude with molecules in the appropriate carbon length range for gasoline and diesel, and in the reduction of the C=O and X–H observed in the resulting oil. TiO_2 support performed better than HY zeolite and MgO for reducing FTIR signals for O and N from the biocrude. Long-term activity maintenance of these catalysts still remains to be tested.

Biocrude treated in the absence of any catalyst still produced compounds that elute earlier than compounds in the original biocrude with a small reduction in O and N content. However, this reduction in O and N is small, approximately 13% and 25% respectively based on work done by Faeth et al. [126]. Without the noncatalytic control experiment, deconvolution of the thermal component and the catalytic component is difficult. However, the chromatograms between different catalysts are unique whereas one would expect with no catalyst activity, the chromatograms for different catalysts would appear to be the same because the thermal treatment would be solely responsible for the chemistry. Because the appearance of the chromatograms changes from sample to sample, the catalysts all likely have some activity.

7.4 Acknowledgements

We thank Ching Shen Chan for performing much of the experimental work presented here. We also thank the Landau lab for synthesizing and characterizing all the catalysts presented here. The University of Michigan provided funding for the project.

CHAPTER 8

Conclusions, Future Work, and Outlook

The dissertation demonstrated that Pt/C catalysts deactivate over a period of 24 h in a continuous flow reactor with a first-order rate constant of $0.063 \pm 0.006\ h^{-1}$. The catalyst deactivated to the point of having lost more than half the original activity after 24 h. Analysis of Pt/TiO_2 revealed that a combination of coking and molecular poisoning were responsible for deactivation. The poison is suspected to be an unsaturated hydrocarbon as determined from treatment of Pt/TiO_2 after reaction in H_2. The coke may have formed through oligomerization and polymerization of the poisons formed on the surface. Pt/C still managed to retain its high selectivity towards the decarboxylation product as it deactivated.

The rapid deactivation of the Pt/C catalyst will be an important consideration should hydrothermal decarboxylation of fatty acids or biocrude upgrading be scaled up for a production process. Design of a deactivation-resistant catalyst or selection of support materials that are resistant to catalyst regeneration steps such as controlled oxidation will be required for the longevity of a process.

With unsaturated fatty acids, Pt catalysts exhibited low selectivity as previously indicated in literature, but this dissertation shows that Pt can be improved through

alloying with Sn. The $PtSn_x/C$ catalysts yielded 2 – 3 times more heptadecane from oleic and linoleic acids (1 hour at 350 °C) than did monometallic Pt/C. Even after the improvement with Sn, however, the $PtSn_x$ catalysts still exhibited decreasing selectivity to decarboxylation products with increasing degrees of fatty acid unsaturation. One interesting note was that the decarboxylation products underwent hydrogenation and resulted in the saturated alkane.

The catalysts can be improved by increasing resistance to deactivation from unsaturated hydrocarbons. This will be imperative for a commercial process both for a process dealing with algae and a process with traditional seed oils because the feed and the products will include unsaturated compounds. $PtSn_x$ does show improved handling of these unsaturated compounds, but the reactions with fatty acids with more olefin character still yield undesirable products. Developing a catalyst that can give the direct decarboxylation product of alkenes as opposed to a saturated alkane would likely lead to higher selectivities because hydrogen is not needed for the reaction. Additionally, the ability of a catalyst to be unaffected by C=C double bonds could lead to improved catalyst longevity as the Pt/C catalyst was likely deactivated through an unsaturated hydrocarbon, and the catalysts previously discussed for unsaturated fatty acid decarboxylation are adversely affected by the unsaturation. The $PtSn_x/C$ catalysts used here were still adversely affected by unsaturation, and a process using these catalysts may still require external hydrogen to achieve the desired yields of decarboyxlation products from unsaturated fatty acids. A catalyst completely insensitive to unsaturation, from an economics and environmental perspective, would be a boon because hydrogen is

an expensive reagent, and at this point is a non-renewable resource.

In addition to deactivation through molecular poisoning and coking, the hydrothermal environment is particularly harsh and causes extensive catalyst deactivation. Designing a catalyst support that is resistant to degradation and loss of surface area is another important factor in maintaining catalyst activity. TiO_2, TiO_2–SiO_2, and La and Ba hexaaluminates are examples of promising catalyst supports that have shown ability to resist degradation in hydrothermal environments [93, 122]. These supports coupled with active metals such as Pt and Pd have shown the ability to upgrade biocrude oil in terms of X–H and C=O removal and isomerization of straight chain hydrocarbons. However, the removal of these functional groups and moieties is incomplete as evidenced by FTIR, and the possibility remains that these N and O heteroatoms remain in the bio-oil as C–N and C–O compounds that are difficult to detect through FTIR. Moreover, GC-MS showed that there are isomerized alkanes within the upgraded bio-oil but there are also still straight chain alkanes and alkenes that remain. The support stability remains to be seen in further studies, and the resulting oil still needs further upgrading both in terms of removal of heteroatom-containing functional groups and hydrocarbon isomerization.

Future catalysis work for converting algal biomass to liquid fuels involves the development of catalysts that are capable of deoxygenating both saturated and unsaturated fatty acids without the need for an external hydrogen input. These fatty acids are the source of much of the high quality bio-derived fuel. While fatty acids are important, oil from the protein content will be an important considera-

tion. Some of the nitrogen content from algae HTL becomes an amide or is bound within a heterocyclic compound. Nitrogen fertilizer is also an expensive input, and recycling of nitrogen is currently studied [129]. A catalyst that is capable of denitrogenating these biocrude compounds to produce a bio-available nitrogen as the end product of the denitrogenation would be valuable economically and environmentally. Recycling nitrogen is an economic benefit because the reuse of nitrogen as fertilizer reduces the need to purchase fertilizer for algae growth. The environmental benefit is twofold. First, the reduction in fertilizer need reduces the fossil fuel demand for the process because nitrogen fertilizers are made from fossil energy. Second, nitrogen does not have to be released into the environment and contribute to hypoxia of bodies of water [6]. The fate of sulfur from HTL also needs to be considered. Sulfur will be an important consideration for the longevity of a catalyst as it is a common poison. Even though the concentration of sulfur is typically low, the concentrations are sufficient to cause catalyst deactivation [85].

Most of the work in this field has investigated noble metal catalysts such as Pt, Pd, and Ru, but these metals are expensive and limited resources. The development of a catalyst made of more abundant and low cost materials would make the development of the process more attractive from a cost perspective.

Processing of algae to liquid fuels still has many challenges to overcome. The catalyst design is just one important part of the solution, but these challenges are not insurmountable. Two widely used tools that evaluate overall process feasibility are life-cycle analysis and technoeconomic analysis. Amer et al. examined the economic feasibility of algae biofuels [130]. They compared the end cost of produc-

ing fatty acid methyl esters (FAMEs) on a per kilogram basis. Their best case scenary using open raceway ponds was capable of producing FAMEs at $4/kg which corresponds to rough $13 per gallon and is expected to decrease with improving technology [130]. Brentner et al. analyzed the possible algal-biodiesel plant using flat plate photobioreactors and supercritical methanol esterification [131]. They found that this process gives fatty acid methyl esters for biofuel at a slightly negative EROI, but they stated that with advances in technology, this would likely become positive[131]. A pilot-scale life cycle study for algal biofuel production via HTL projected that the process can produce algal-derived diesel and gasoline with EROIs of greater than 2.5 at full-scale[8]. The EROI is less than that of gasoline at 3.5 [8], but this particular process was analyzed using centrifugation, an energy intensive step, as one of the dewatering steps[8]. An actual production process would more likely use a lower energy dewatering process such as filtration. The EROI in this study will likely increase with a dewatering step that requires a lower energy input. Technoeconomics suggest that algal biofuels may be able to compete with fossil fuels with improving technology, and from an environmental perspective, algal fuels can offer EROI greater than unity [3, 8, 130–134]. Overall, algae is a promising candidate suitable for processing into liquid hydrocarbon fuels.

APPENDIX A

Mass Spectrometry Results for Biocrude and its Upgraded Derivatives

The GC-MS plots presented here have dots above identified peaks. Every 5th identified peak is numbered, and the numbering corresponds to the peak number in the tables of identified compounds for that particular run. Compounds denoted with the same superscript within a sample are possibly isomers of each other or some other structurally similar compound. The fatty acids identified multiple times that also elute within a minute of each other may be the same compound because of a tailing effect in their separation on non-polar GC columns. Compounds in parentheses denote a possible alternate identity.

Peak	Time (min)	Area %	Library Match	Quality
1	36.87	1.28	1-Ethyl-2-pyrrolidinone	93
2	38.26	0.81	2,5-Pyrrolidinedione, 1-ethyl-	83
3	41.42	2.20	Dodecane	94
4	45.88	0.51	1-Tridecene	98
5	49.20	0.41	Naphthalene, 1,2-dihydro-1,1,6-trimethyl-	97
6	49.31	1.23	Naphthalene, 1,2,3,4-tetrahydro-1,1,6-trimethyl-	95
7	54.67	1.70	1-Pentadecene	99
8	54.83	1.31	1H-Indole, 1-ethyl-	86

Peak	Time (min)	Area %	Library Match	Quality
9	54.97	0.69	Pentadecane	87
10	62.72	0.75	Heptadecane	96
11	66.67	1.34	Hexadecane, 2,6,10,14-tetramethyl-	90
12[1]	67.26	0.72	2-Hexadecene, 3,7,11,15-tetramethyl-, [R-[R*,R*-(E)]]-	96
13[1]	67.47	2.42	2-Hexadecene, 3,7,11,15-tetramethyl-, [R-[R*,R*-(E)]]-	83
14[1]	67.54	1.75	2-Hexadecene, 3,7,11,15-tetramethyl-, [R-[R*,R*-(E)]]-	94
15[1]	67.95	2.97	2-Hexadecene, 3,7,11,15-tetramethyl-, [R-[R*,R*-(E)]]-	91
16	72.29	0.68	Tetradecanamide	94
17	81.74	0.50	9-Tricosene, (Z)-	98
18	89.58	0.68	Pyrrolidine, 1-(1-oxooctadecyl)-	87
19	96.30	3.26	Cholest-4-ene	94
20	96.61	2.44	Cholest-5-ene	96

Table A.1: Identified Products from Biocrude.

Peak	Time (min)	Area %	Library Match	Quality
1	13.15	0.81	Heptane, 2-methyl-	87
2	13.34	6.21	Toluene	83
3	16.72	0.82	Bicyclo[3.1.0]hexane, 1,5-dimethyl-	87
4	18.97	0.39	Methyl ethyl cyclopentene	86
5	20.81	3.99	Ethylbenzene	83
6	23.18	0.72	Benzene, 1,3-dimethyl-	90
7	23.65	0.73	Nonane	87
8[1]	30.06	0.93	Benzene, 1,3,5-trimethyl-	83
9	30.71	0.25	2-Decene, (E)-	86
10[1]	31.85	0.25	Benzene, 1,3,5-trimethyl-	94
11	32.89	1.39	2-Cyclopenten-1-one, 2,3-dimethyl-	90
12	34.26	0.89	2-Cyclopenten-1-one, 2,3,4-trimethyl-	91
13[2]	35.19	1.58	Phenol, 4-methyl-	94
14[2]	35.28	1.40	Phenol, 4-methyl-	94
15	35.63	1.09	1-Phenyl-1-butene	87
16	36.17	0.82	Undecane	87
17	38.55	0.16	Benzene, 2-butenyl-	81
18[3]	38.79	0.40	1H-Indene, 2,3-dihydro-1,2-dimethyl-	93
19	39.79	0.47	Naphthalene, 1,2,3,4-tetrahydro-	93

Peak	Time (min)	Area %	Library Match	Quality
20	40.11	1.19	Phenol, 4-ethyl-	90
21	41.42	2.80	Dodecane	93
22[3]	41.63	0.76	1H-Indene, 2,3-dihydro-1,2-dimethyl-	81
23	42.12	1.18	Undecane, 2,6-dimethyl-	97
24	44.21	0.46	1H-Indene, 2,3-dihydro-1,2-dimethyl-	90
25	45.24	0.44	(1-Methylenebut-2-enyl)benzene	81
26	45.83	0.35	1H-Indene, 2,3-dihydro-4,7-dimethyl-	93
27	46.08	0.50	1-Tridecene	84
28	46.25	1.46	Tridecane	97
29	47.61	0.49	Benzene, (1-methyl-1-butenyl)-	89
30	49.33	1.42	Naphthalene, 1,2,3,4-tetrahydro-1,1,6-trimethyl-	93
31	50.13	0.18	5-Benzocyclooctenol, 5,6,7,8-tetrahydro-, (E)-	90
32	50.42	0.63	5-Tetradecene, (E)-	93
33	50.75	1.64	Tetradecane	95
34	50.97	0.59	2-Tetradecene, (E)-	95
35	51.54	0.37	Naphthalene, 2,3-dimethyl-	83
36	52.34	0.82	Naphthalene, 1,6-dimethyl-	97
37	54.66	1.18	1-Pentadecene	95
38	54.97	2.99	Pentadecane	97
39	55.17	2.80	1H-Indole, 2,3-dimethyl-	90
40	57.26	0.68	n-Nonylcyclohexane	90
41	58.21	0.41	1H-Indole, 2,3,5-trimethyl-	81
42	58.96	0.84	Hexadecane	96
43	59.16	1.02	2,3,7-Trimethylindole	96
44	62.73	1.35	Heptadecane	98
45	65.95	0.51	Cyclohexadecane, 1,2-diethyl-	94
46	66.31	0.40	Octadecane	93
47	66.67	1.40	Hexadecane, 2,6,10,14-tetramethyl-	99
48	67.48	0.66	Cyclohexadecane, 1,2-diethyl-	89
49	67.54	0.25	2-Hexadecene, 3,7,11,15-tetramethyl-, [R-[R*,R*-(E)]]-	91
50	67.96	0.89	2-Hexadecene, 3,7,11,15-tetramethyl-, [R-[R*,R*-(E)]]-	90
51	69.71	0.54	Nonadecane	83
52	75.40	0.54	Naphthalene, tris(1-methylethyl)-	83
53	76.07	0.29	Pentadecane (C_{19}+ alkane)	89
54	81.89	0.37	Tricosane	97

Peak	Time (min)	Area %	Library Match	Quality

Table A.2: Identified Products from Pt/TiO_2

Peak	Time (min)	Area %	Library Match	Quality
1	13.32	1.48	Toluene	91
2	20.79	0.69	Ethylbenzene	81
3	29.60	0.56	Phenol	87
4	33.93	0.36	Phenol, 2-methyl-	95
5	35.06	6.01	Phenol, 4-methyl-	94
6	36.83	0.34	1-Ethyl-2-pyrrolidinone	81
7	39.02	4.34	Phenol, 2,3-dimethyl-	94
8	39.41	0.59	Phenol, 2,5-dimethyl-	91
9	39.99	0.62	Phenol, 4-ethyl-	93
10	40.07	1.86	Phenol, 3-ethyl-	87
11	49.32	0.52	Naphthalene, 1,2,3,4-tetrahydro-1,1,6-trimethyl-	92
12	52.32	0.17	Naphthalene, 2,6-dimethyl-	95
13	54.97	0.65	Pentadecane	97
14	55.17	0.59	1H-Indole, 2,3-dimethyl-	94
15	59.13	0.29	1H-Indole, 2,3,5-trimethyl-	90
16	62.53	7.59	Dodecyl acrylate	91
17	62.73	0.52	Heptadecane	97
18	66.68	0.56	Eicosane ($C_{18} - C_{22}$ alkane)	96
19	67.48	0.35	Cyclohexadecane, 1,2-diethyl-	80
20	71.24	0.19	Acridine, 9,10-dihydro-9,9-dimethyl-	93
21	77.78	1.44	Bis(2-ethylhexyl) maleate	91
22	78.65	0.69	Hexadecanamide	90
23	81.88	0.34	Tricosane	90
24	83.78	0.71	Benzyl butyl phthalate	87
25	85.26	0.27	Triphenyl phosphate	96
26	88.74	1.71	Bis(2-ethylhexyl) phthalate	87
27	92.21	0.48	Eicosane (C_{23}+ alkane)	95
28	94.56	0.64	Docosane (C_{23}+ alkane)	95
29	95.45	2.42	Squalene	93
30	96.62	0.42	Cholestane	92
31	97.84	0.34	Cyclopropanenonanoic acid, 2-[(2-butylcyclopropyl)methyl]-, methyl ester	91

Table A.3: Identified Products from Pt/TiO_2 with H_2

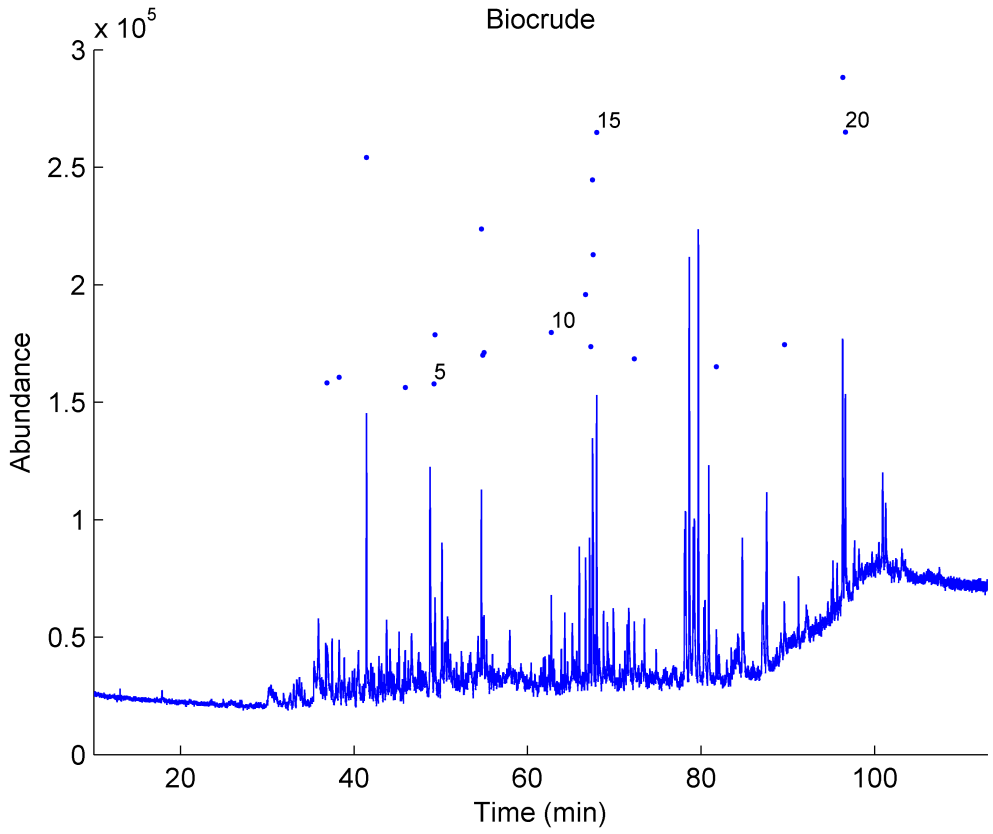

Figure A.1: Biocrude chromatogram from liquefaction at 350 °C for 15 min

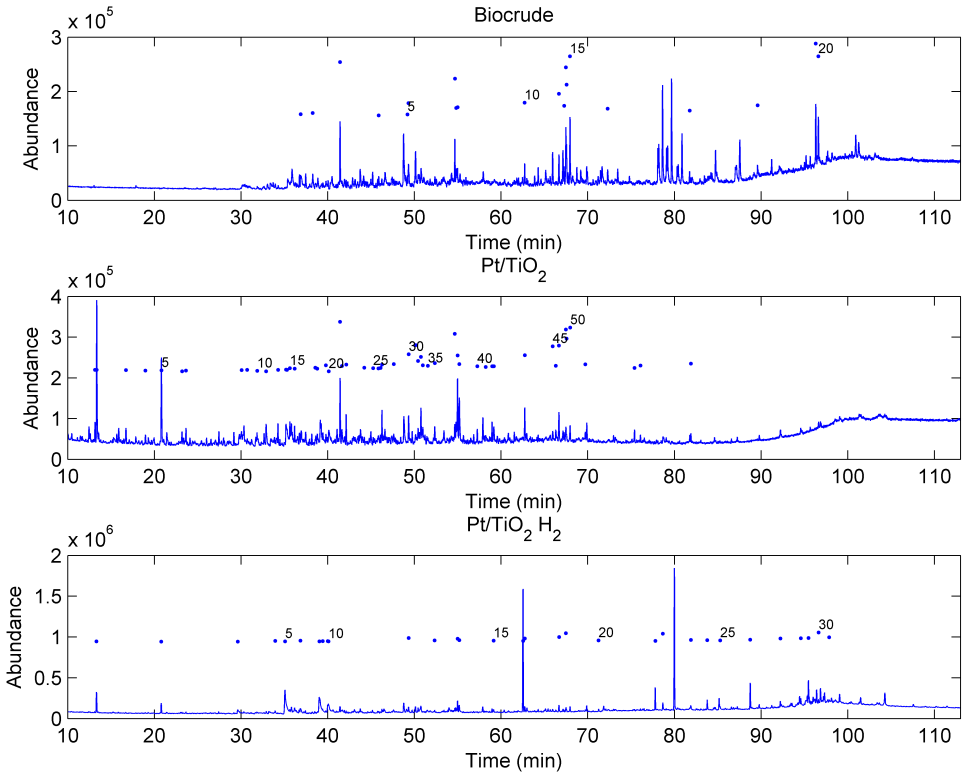

Figure A.2: Chromatograms of Pt/TiO_2 upgraded bio-oil at 400 °C for 60 min

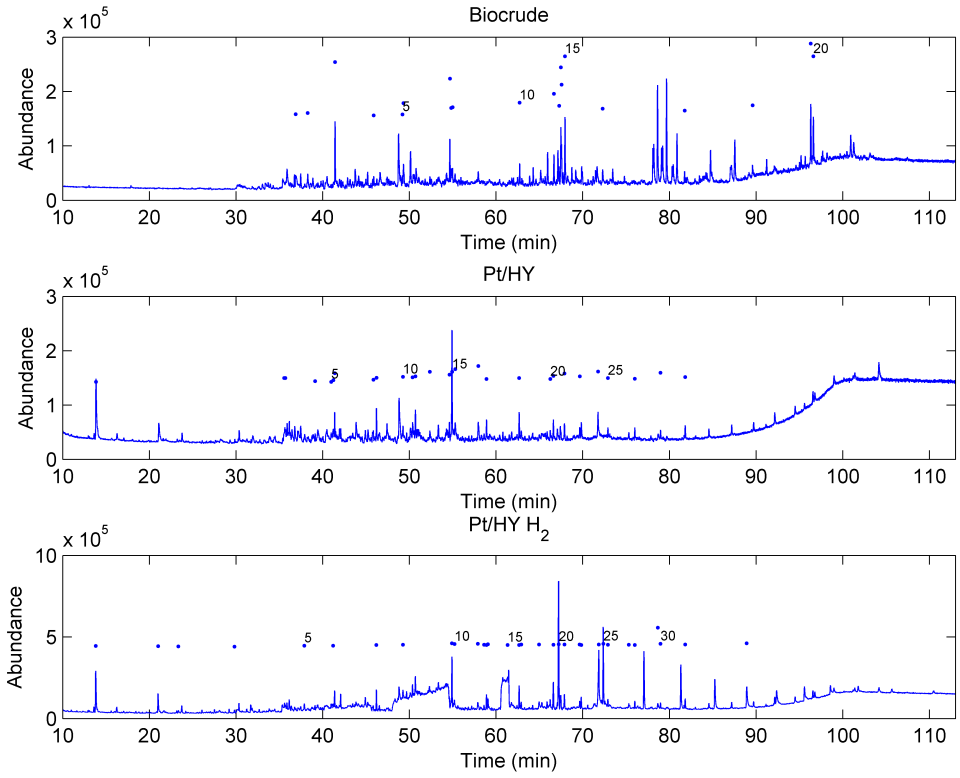

Figure A.3: Chromatograms of Pt/HY upgraded bio-oil at 400 °C for 60 min

Peak	Time (min)	Area %	Library Match	Quality
1	13.84	7.73	1,3,5-Cycloheptatriene	81
2[1]	35.54	0.75	Phenol, 4-methyl-	87
3[1]	35.69	0.68	Phenol, 4-methyl-	86
4	39.12	0.47	Benzene, (1-methyl-1-propenyl)-, (E)-	87
5	40.97	0.93	Cyclododecane	95
6	41.20	1.15	1H-Pyrrole, 2-ethyl-3,4,5-trimethyl-	90
7	41.37	2.20	Dodecane	93
8	45.83	0.82	1-Tridecene	96
9	46.19	2.05	Tridecane	97
10	49.26	1.85	Naphthalene, 1,2,3,4-tetrahydro-1,1,6-trimethyl-	96
11	50.36	1.55	1-Tetradecene	98
12	50.69	2.01	Tetradecane	97
13	52.35	0.56	Naphthalene, 2,7-dimethyl-	94
14	54.61	1.43	1-Pentadecene	96
15	54.91	8.57	Pentadecane	96
16	55.27	1.27	1H-Indole, 2,3-dimethyl-	95
17	57.94	2.56	1H-Indole, 5,6,7-trimethyl-	87
18	58.89	1.36	Hexadecane	97
19	62.66	1.89	Heptadecane	97
20	66.24	0.58	Octadecane	90
21	66.61	1.06	Hexadecane, 2,6,10,14-tetramethyl-	90
22	67.89	1.36	2-Hexadecene, 3,7,11,15-tetramethyl-, [R-[R*,R*-(E)]]-	93
23	69.64	0.84	Nonadecane	92
24	71.75	2.55	n-Hexadecanoic acid	95
25	72.90	0.77	Eicosane	92
26	76.00	0.77	Octadecane (Heneicosane)	95
27	78.97	0.62	Docosane	96
28	81.82	0.86	Eicosane (Tricosane)	96

Table A.4: Identified Products from Pt/HY

Peak	Time (min)	Area %	Library Match	Quality
1	13.80	2.71	Toluene	83
2	21.00	1.14	Ethylbenzene	87
3	23.32	0.19	Benzene, 1,3-dimethyl-	91
4	29.81	0.19	1-Decene	91
5	37.87	0.65	1H-Pyrrole, 2,3,4,5-tetramethyl-	93
6	41.19	0.25	1H-Pyrrole, 2-ethyl-3,4,5-trimethyl-	86

Peak	Time (min)	Area %	Library Match	Quality
7	46.19	0.91	Tridecane	97
8	49.25	1.60	Naphthalene, 1,2,3,4-tetrahydro-1,1,6-trimethyl-	84
9	54.90	2.79	Pentadecane	94
10	55.19	1.17	2-Methyl-5-(butin-1-yl)pyridine	81
11	57.88	0.86	1-Methoxy-5-trimethylsilyloxy-3-phenylpentane	86
12	58.61	0.35	1-Hexadecene	91
13	58.89	0.81	Hexadecane	97
14	59.06	0.79	Diethyl Phthalate	94
15	61.32	2.77	Dibutanoylmorphine	86
16	61.44	2.41	Cyclooctasiloxane, hexadecamethyl-	91
17	62.65	1.08	Heptadecane	97
18	62.89	0.46	Pentadecane, 2,6,10,14-tetramethyl-	97
19	64.95	0.47	Tetradecanoic acid	91
20	66.60	1.56	Hexadecane, 2,6,10,14-tetramethyl-	99
21	67.21	7.42	4-(3,4-Dimethoxybenzylidene)-1-(4-nitrophenyl)-3-phenyl-2-pyrazolin-5-one	80
22	67.87	0.95	2-Hexadecene, 3,7,11,15-tetramethyl-, [R-[R*,R*-(E)]]-	92
23	69.64	0.72	Nonadecane	97
24	69.81	0.77	Hexadecanenitrile	90
25	71.85	6.04	n-Hexadecanoic acid	99
26	72.36	4.44	4-Nitro-4'-chlorodiphenylsulphoxide	93
27	72.89	0.38	Eicosane	98
28	75.31	0.27	Naphthalene, tris(1-methylethyl)-	83
29	76.00	0.38	Heneicosane	98
30	78.65	0.39	Hexadecanamide	98
31	78.96	0.27	Docosane	98
32	81.81	0.44	Tricosane	98
33	88.91	2.14	4-Nitro-4'-chlorodiphenylsulphoxide	91

Table A.5: Identified Products from Pt/HY with H_2

Peak	Time (min)	Area %	Library Match	Quality
1	13.16	0.70	Heptane, 2-methyl-	90
2	13.35	5.74	Toluene	83
3	16.72	0.60	Cyclopentene, 1,2,3-trimethyl-	81

Peak	Time (min)	Area %	Library Match	Quality
4	18.97	0.36	Methyl ethyl cyclopentene	92
5	20.82	3.61	Ethylbenzene	91
6[1]	21.44	0.87	p-Xylene	92
7[1]	23.19	0.70	p-Xylene	93
8	23.65	0.79	Nonane	81
9	29.82	0.62	Phenol	81
10	30.71	0.27	4-Decene	91
11	31.85	0.58	Benzene, 1-ethyl-3-methyl-	83
12	32.90	1.06	2-Cyclopenten-1-one, 2,3-dimethyl-	90
13	35.25	1.20	Phenol, 4-methyl-	95
14	35.63	1.05	1-Phenyl-1-butene	90
15	36.17	0.81	Undecane	91
16	39.79	0.57	Naphthalene, 1,2,3,4-tetrahydro-	93
17	40.14	0.53	Phenol, 2-ethyl-	90
18	40.18	0.48	Phenol, 4-ethyl-	90
19	41.42	2.68	Dodecane	94
20	41.64	1.16	Benzene, (3-methyl-2-butenyl)-	87
21	42.12	1.21	Undecane, 2,6-dimethyl-	95
22	45.83	0.34	1H-Indene, 2,3-dihydro-4,7-dimethyl-	93
23	46.25	1.52	Tridecane	96
24	49.33	1.68	Naphthalene, 1,2,3,4-tetrahydro-1,1,6-trimethyl-	96
25	50.42	1.10	1-Tetradecene	98
26	50.75	2.27	Tetradecane	91
27	50.97	1.26	2-Tetradecene, (E)-	89
28	51.44	0.35	3-Tetradecene, (Z)-	94
29	52.34	0.61	Naphthalene, 2,6-dimethyl-	94
30	54.97	2.91	Pentadecane	96
31	55.18	2.68	1H-Indole, 2,5-dimethyl-	93
32	55.65	0.34	1-Pentadecene	97
33	56.84	0.41	1H-Indole, 1,2,3-trimethyl-	91
34	57.25	0.54	n-Nonylcyclohexane	93
35	58.96	0.79	Hexadecane	94
36	59.16	0.90	1H-Indole, 2,3,5-trimethyl-	94
37	62.73	1.35	Heptadecane	97
38	66.67	1.41	Hexadecane, 2,6,10,14-tetramethyl-	99
39[2]	67.48	0.83	2-Hexadecene, 3,7,11,15-tetramethyl-, [R-[R*,R*-(E)]]-	83
40[2]	67.95	0.92	2-Hexadecene, 3,7,11,15-tetramethyl-, [R-[R*,R*-(E)]]-	96
41	69.72	0.52	Nonadecane	95

Peak	Time (min)	Area %	Library Match	Quality
42	69.89	1.02	Hexadecanenitrile	93
43	72.97	0.28	Tetradecane (Eicosane)	91
44	75.40	0.54	Naphthalene, tris(1-methylethyl)-	86
45	76.08	0.27	Heneicosane	90

Table A.6: Identified Products from Pd/TiO_2

Peak	Time (min)	Area %	Library Match	Quality
1	13.15	0.49	Heptane, 2-methyl-	87
2	13.35	6.62	Toluene	91
3	20.82	3.14	Ethylbenzene	91
4	23.21	0.52	Benzene, 1,3-dimethyl-	93
5	23.64	0.65	Nonane	95
6	27.47	0.48	Benzene, propyl-	90
7	30.34	0.59	Decane	92
8	31.87	0.30	Benzene, 1,3,5-trimethyl-	87
9[1]	35.27	1.76	Phenol, 4-methyl-	93
10[1]	35.46	0.33	Phenol, 4-methyl-	90
11	40.23	0.69	Phenol, 4-ethyl-	90
12	40.27	0.56	Phenol, 2-ethyl-	87
13	41.01	0.52	1-Dodecene	93
14	42.12	1.09	Undecane, 2,6-dimethyl-	94
15	45.88	0.66	1-Tridecene	95
16	46.25	1.35	Tridecane	95
17	49.31	1.09	Naphthalene, 1,2,3,4-tetrahydro-1,1,6-trimethyl-	95
18	49.73	0.55	Dodecane, 2,6,10-trimethyl-	81
19	50.41	1.22	Cyclododecane	94
20	50.75	1.51	Tetradecane	97
21	52.36	0.82	Naphthalene, 2,7-dimethyl-	97
22	54.66	1.62	1-Pentadecene	99
23	54.83	1.64	Benzenamine, N-methyl-N-2-propynyl-	86
24	54.97	3.52	Pentadecane	97
25	55.24	2.41	Indolizine, 2,3-dimethyl-	87
26	57.93	1.23	Indolizine, 2-methyl-6-ethyl-	80
27	58.95	0.95	Hexadecane	97
28	62.48	0.58	1-Tridecene	87
29	62.72	2.06	Heptadecane	97
30	65.94	1.46	1-Hexadecanol, 3,7,11,15-tetramethyl-	86
31	66.30	0.81	Octadecane	97
32	66.67	3.06	Hexadecane, 2,6,10,14-tetramethyl-	99

Peak	Time (min)	Area %	Library Match	Quality
33[2]	67.54	0.95	2-Hexadecene, 3,7,11,15-tetramethyl-, [R-[R*,R*-(E)]]-	95
34[2]	67.95	2.27	2-Hexadecene, 3,7,11,15-tetramethyl-, [R-[R*,R*-(E)]]-	94
35	69.71	0.48	Nonadecane	98
36	69.88	0.83	Hexadecanenitrile	90
37	72.96	0.64	Tetradecane (Eicosane)	92
38	76.06	0.52	Octadecane (Heneicosane)	96
39	78.67	0.46	Hexadecanamide	94
40	79.03	0.34	Heptadecane (Docosane)	92
41	81.88	0.82	Tricosane	98
42	84.61	0.45	Eicosane (Tetracosane)	95
43	87.24	0.59	Nonadecane (C_{25}+)	91
44	92.21	0.81	Octadecane (C_{25}+)	95
45[3]	95.66	0.82	Cholestane	91
46	96.30	0.88	Cholest-4-ene	92
47[3]	96.61	1.84	Cholestane	97

Table A.7: Identified Products from Pd/TiO_2 with H_2

Peak	Time (min)	Area %	Library Match	Quality
1	13.83	3.52	1,3,5-Cycloheptatriene	81
2	21.06	1.35	Ethylbenzene	81
3	23.76	0.54	Nonane	81
4	35.53	0.28	Phenol, 4-methyl-	92
5	35.91	0.96	1H-Pyrrole, 2,3,4,5-tetramethyl-	91
6	36.14	0.94	Undecane	90
7	40.97	0.54	1-Dodecene	96
8	41.20	0.52	1H-Pyrrole, 2-ethyl-3,4,5-trimethyl-	91
9	41.37	1.44	Dodecane	93
10	42.07	1.00	Undecane, 2,6-dimethyl-	93
11	45.83	0.41	1-Tridecene	99
12	46.19	1.75	Tridecane	97
13	49.26	1.23	Naphthalene, 1,2,3,4-tetrahydro-1,1,6-trimethyl-	94
14	49.67	0.59	Dodecane, 2,6,10-trimethyl-	87
15	50.36	1.02	1-Tetradecene	98
16	50.68	1.86	Tetradecane	97
17	52.35	0.65	Naphthalene, 1,6-dimethyl-	95
18	54.39	0.91	1-Tridecene	95
19[1]	54.60	0.96	1-Pentadecene	99
20	54.91	8.05	Pentadecane	97
21[1]	55.10	1.14	1-Pentadecene	89

Peak	Time (min)	Area %	Library Match	Quality
22	55.26	1.19	1H-Indole, 2,3-dimethyl-	90
23	58.89	1.40	Hexadecane	98
24	62.66	2.43	Heptadecane	98
25	62.89	0.95	Pentadecane, 2,6,10,14-tetramethyl-	87
26	66.24	0.80	Octadecane	98
27	66.61	3.12	Hexadecane, 2,6,10,14-tetramethyl-	99
28[2]	67.41	0.78	2-Hexadecene, 3,7,11,15-tetramethyl-, [R-[R*,R*-(E)]]-	91
29[2]	67.47	0.39	2-Hexadecene, 3,7,11,15-tetramethyl-, [R-[R*,R*-(E)]]-	93
30[2]	67.88	0.98	2-Hexadecene, 3,7,11,15-tetramethyl-, [R-[R*,R*-(E)]]-	93
31	69.64	0.78	Nonadecane	97
32	69.81	1.43	Hexadecanenitrile	90
33	71.82	4.17	n-Hexadecanoic acid	99
34	71.95	0.10	Lumiflavine	83
35	72.90	0.64	Eicosane	98
36	76.00	0.67	Heneicosane	98
37	78.66	0.90	Octadecanamide	95
38	78.96	0.59	Octadecane (Docosane)	96
39	81.81	0.96	Tricosane	98
40	84.55	0.56	Tetracosane	96
41	87.17	0.67	Eicosane (Pentacosane)	95

Table A.8: Identified Products from Pd/HY

Peak	Time (min)	Area %	Library Match	Quality
1	13.83	4.96	Toluene	83
2	36.14	0.77	Undecane	89
3	40.97	0.65	1-Dodecene	90
4	41.22	0.75	1H-Pyrrole, 2-ethyl-3,4,5-trimethyl-	91
5	41.38	1.46	Dodecane	93
6	42.07	1.67	Undecane, 2,6-dimethyl-	91
7	45.83	1.18	1-Tridecene	97
8	45.99	0.55	7-Tetradecene, (Z)-	84
9	46.20	1.67	Tridecane	95
10	49.26	1.77	Naphthalene, 1,2,3,4-tetrahydro-1,1,6-trimethyl-	95
11	50.36	1.87	1-Tetradecene	98
12	50.69	2.15	Tetradecane	97
13	52.36	1.07	Naphthalene, 2,7-dimethyl-	93

Peak	Time (min)	Area %	Library Match	Quality
14	54.61	1.22	1-Pentadecene	98
15	54.90	5.90	Pentadecane	96
16	55.31	0.50	2-Methyl-5-(butin-1-yl)pyridine	93
17	58.89	1.06	Hexadecane	98
18	62.66	2.58	Heptadecane	98
19	65.88	1.13	2-Hexadecene, 3,7,11,15-tetramethyl-, [R-[R*,R*-(E)]]-	89
20	66.24	0.76	Octadecane	96
21	66.61	3.51	Hexadecane, 2,6,10,14-tetramethyl-	99
22[1]	67.40	1.69	2-Hexadecene, 3,7,11,15-tetramethyl-, [R-[R*,R*-(E)]]-	83
23[1]	67.47	1.01	2-Hexadecene, 3,7,11,15-tetramethyl-, [R-[R*,R*-(E)]]-	97
24[1]	67.88	2.22	2-Hexadecene, 3,7,11,15-tetramethyl-, [R-[R*,R*-(E)]]-	96
25	69.65	1.07	Nonadecane	95
26[2]	71.80	5.62	n-Hexadecanoic acid	99
27[2]	71.98	0.05	n-Hexadecanoic acid	83
28	72.89	0.55	Eicosane	99
29	76.00	0.72	Octadecane (Heneicosane)	96
30	78.67	0.66	Octadecanamide	87
31	78.96	0.52	Docosane	95
32	81.81	1.03	Tricosane	99

Table A.9: Identified Products from Pd/HY with H_2

Peak	Time (min)	Area %	Library Match	Quality
1	36.07	1.13	1-Phenyl-1-butene	86
2	36.49	1.07	Undecane	83
3	41.68	3.43	Dodecane	93
4	42.37	1.24	Undecane, 2,6-dimethyl-	94
5	46.49	2.54	Tridecane	95
6	46.82	0.55	Cyclopentane, propyl-	86
7	49.57	2.43	Naphthalene, 1,2,3,4-tetrahydro-1,1,6-trimethyl-	95
8	50.65	1.33	2-Tetradecene, (E)-	96
9	50.97	2.73	Tetradecane	96
10	52.78	0.51	Naphthalene, 2,3-dimethyl-	95
11	54.88	0.98	1-Pentadecene	95
12	55.18	4.05	Pentadecane	97
13	55.86	1.62	1H-Indole, 2,3-dimethyl-	91
14	57.45	0.48	Cyclohexane, octyl-	90
15	58.43	0.93	1H-Indole, 5,6,7-trimethyl-	87

Peak	Time (min)	Area %	Library Match	Quality
16	59.16	1.30	Hexadecane	98
17	62.92	2.52	Heptadecane	97
18	66.49	1.09	Octadecane	93
19	66.85	3.99	Hexadecane, 2,6,10,14-tetramethyl-	99
20	68.13	1.72	2-Hexadecene, 3,7,11,15-tetramethyl-, [R-[R*,R*-(E)]]-	93
21	69.89	1.10	Nonadecane	90
22	73.13	0.71	Eicosane	93
23	76.23	0.83	Heneicosane	96
24	82.04	1.19	Tricosane	86

Table A.10: Identified Products from Ru/MgO

Peak	Time (min)	Area %	Library Match	Quality
1	41.69	4.53	Dodecane	93
2	42.37	1.79	Undecane, 2,6-dimethyl-	93
3	46.17	1.56	1H-Indene, 2,3-dihydro-1,2-dimethyl-	83
4	46.49	3.04	Tridecane	94
5	49.57	3.23	Naphthalene, 1,2,3,4-tetrahydro-1,1,6-trimethyl-	96
6	50.65	1.22	1-Tetradecene	86
7	50.97	2.45	Tetradecane	87
8	52.81	0.68	Naphthalene, 1,3-dimethyl-	96
9	52.82	0.29	Naphthalene, 1,7-dimethyl-	95
10	54.89	0.83	1-Pentadecene	95
11	55.18	4.32	Pentadecane	97
12	55.87	1.66	2-Methyl-5-(butin-1-yl)pyridine	89
13	57.46	0.89	n-Nonylcyclohexane	81
14	59.16	1.64	Hexadecane	96
15	62.92	2.82	Heptadecane	98
16	66.85	4.21	Hexadecane, 2,6,10,14-tetramethyl-	99
17[1]	67.44	1.03	2-Hexadecene, 3,7,11,15-tetramethyl-, [R-[R*,R*-(E)]]-	94
18[1]	67.72	1.33	2-Hexadecene, 3,7,11,15-tetramethyl-, [R-[R*,R*-(E)]]-	93
19[1]	68.13	3.14	2-Hexadecene, 3,7,11,15-tetramethyl-, [R-[R*,R*-(E)]]-	93
20	69.89	1.17	Nonadecane	97
21	73.13	0.83	Eicosane	90
22	75.58	1.18	Naphthalene, tris(1-methylethyl)-	91

Peak	Time (min)	Area %	Library Match	Quality
23	76.23	0.98	Heneicosane	91

Table A.11: Identified Products from Ru/MgO with H_2

Peak	Time (min)	Area %	Library Match	Quality
1	12.47	0.64	Cyclopropane, 1-methyl-1-isopropenyl-	87
2	13.16	0.68	Heptane, 2-methyl-	91
3	13.36	6.81	Toluene	91
4	15.89	0.63	Octane	90
5	16.73	0.66	Bicyclo[3.1.0]hexane, 1,5-dimethyl-	90
6	18.98	0.39	Methyl ethyl cyclopentene	91
7	20.82	4.56	Ethylbenzene	91
8	21.46	0.26	Benzene, 1,3-dimethyl-	81
9	23.21	0.63	Benzene, 1,2-dimethyl-	87
10	23.65	0.76	Nonane	91
11	29.20	0.48	Benzene, 1-ethyl-2-methyl-	91
12	29.83	0.38	Phenol	80
13	30.34	1.10	Decane	87
14	31.85	0.44	Benzene, 1,3,5-trimethyl-	97
15	32.93	0.61	2-Cyclopenten-1-one, 2,3-dimethyl-	87
16	34.11	0.28	Phenol, 2-methyl-	87
17	35.31	1.83	Phenol, 4-methyl-	93
18	35.63	1.00	Benzene, (2-methyl-1-propenyl)-	87
19	35.82	1.43	2-Cyclopenten-1-one, 2,3,4-trimethyl-	93
20	40.17	1.01	Phenol, 4-ethyl-	87
21	42.12	1.11	Undecane, 2,6-dimethyl-	95
22	44.22	0.61	1H-Indene, 2,3-dihydro-4,7-dimethyl-	81
23	46.07	0.55	3-Tridecene, (Z)-	86
24	46.25	1.28	Tridecane	95
25	46.48	0.43	2-Tridecene, (Z)-	89
26	49.32	1.40	Naphthalene, 1,2,3,4-tetrahydro-1,1,6-trimethyl-	97
27[1]	50.41	0.56	1-Tetradecene	97
28[1]	50.57	0.39	1-Tetradecene	91
29	50.75	1.41	Tetradecane	96
30	50.97	0.60	2-Tetradecene, (E)-	93
31	52.36	0.45	Naphthalene, 1,6-dimethyl-	95
32[2]	54.47	0.47	1-Pentadecene	87
33[2]	54.66	1.29	1-Pentadecene	98

Peak	Time (min)	Area %	Library Match	Quality
34	54.80	0.86	Cyclopropane, nonyl-	87
35	54.97	2.43	Pentadecane	96
36	55.18	2.62	1H-Indole, 2,3-dimethyl-	81
37	57.25	0.70	n-Nonylcyclohexane	94
38	58.23	0.67	1H-Indole, 1,2,3-trimethyl-	81
39	58.95	0.97	Hexadecane	97
40	59.16	1.30	2,3,7-Trimethylindole	96
41	59.58	0.14	1,1'-Biphenyl, 2-methyl-	80
42	62.47	0.65	1-Heptadecene	95
43	62.72	1.67	Heptadecane	97
44	66.30	0.68	Octadecane	86
45	66.67	1.68	Hexadecane, 2,6,10,14-tetramethyl-	99
46[2]	67.14	1.14	2-Hexadecene, 3,7,11,15-tetramethyl-, [R-[R*,R*-(E)]]-	89
47[2]	67.54	0.67	2-Hexadecene, 3,7,11,15-tetramethyl-, [R-[R*,R*-(E)]]-	96
48[2]	67.95	1.58	2-Hexadecene, 3,7,11,15-tetramethyl-, [R-[R*,R*-(E)]]-	94
49	69.72	0.42	Tridecane (Nonadecane)	92
50	69.87	0.99	Hexadecanenitrile	90
51	72.97	0.47	Tetradecane (Eicosane)	92
52	75.38	0.75	Naphthalene, tris(1-methylethyl)-	83
53	76.06	0.39	Heneicosane	96
54	76.51	0.51	2(3H)-Furanone, 5-dodecyldihydro-	86
55	79.03	0.28	Pentadecane (Docosane)	90
56	81.76	0.32	1,2,3,4,5,6,7,8-Octahydrotriphenylene	93
57	81.88	0.49	Tricosane	96

Table A.12: Identified Products from Ru/TiO_2

Peak	Time (min)	Area %	Library Match	Quality
1	13.14	0.59	Heptane, 2-methyl-	91
2	13.33	5.94	Toluene	91
3	13.56	0.32	Cyclohexene, 4-methyl-	80
4	15.17	0.25	Cyclooctane	93
5	15.87	0.69	Octane	90
6	16.71	0.33	1,3-Dimethyl-1-cyclohexene	80
7	17.84	0.27	Cyclotrisiloxane, hexamethyl-	83
8	19.28	0.19	Cyclopentanone, 2-methyl-	81
9	20.79	2.77	Ethylbenzene	91
10[1]	21.42	0.43	p-Xylene	94

Peak	Time (min)	Area %	Library Match	Quality
11	23.01	0.26	1-Nonene	95
12[1]	23.16	0.62	p-Xylene	94
13	23.63	0.68	Nonane	87
14	26.00	0.33	Octane, 2,6-dimethyl-	80
15	29.15	0.46	Benzene, 1-ethyl-2-methyl-	94
16	29.71	0.43	Phenol	86
17	30.32	0.91	Decane	93
18	31.83	0.33	Benzene, 1,2,4-trimethyl-	94
19	32.93	0.31	2-Cyclopenten-1-one, 2,3-dimethyl-	83
20	34.04	0.52	Phenol, 2-methyl-	93
21	35.14	1.87	Phenol, 3-methyl-	93
22[2]	35.29	0.48	Phenol, 4-methyl-	81
23[2]	35.36	0.34	Phenol, 4-methyl-	91
24	35.80	0.52	2-Cyclopenten-1-one, 2,3,4-trimethyl-	93
25	36.16	0.78	Undecane	87
26	39.22	0.51	Phenol, 2,3-dimethyl-	80
27	39.78	0.22	Naphthalene, 1,2,3,4-tetrahydro-	92
28	40.09	1.08	Phenol, 4-ethyl-	90
29	41.42	1.75	Dodecane	93
30	42.11	1.07	Undecane, 2,6-dimethyl-	96
31	45.88	0.68	1-Tridecene	97
32	46.25	1.71	Tridecane	95
33	48.40	0.18	Heptylcyclohexane	83
34	49.31	1.27	Naphthalene, 1,2,3,4-tetrahydro-1,1,6-trimethyl-	95
35	49.73	0.53	Dodecane, 2,6,10-trimethyl-	87
36	50.41	0.87	Cyclopropane, nonyl-	95
37	50.74	1.73	Tetradecane	91
38	51.51	0.32	Naphthalene, 2,6-dimethyl-	93
39	52.33	0.73	Naphthalene, 2,7-dimethyl-	95
40	54.66	2.22	Cycloheptasiloxane, tetradecamethyl-	86
41	54.97	2.85	Pentadecane	97
42	55.18	1.78	1H-Indole, 2,5-dimethyl-	90
43	58.21	0.26	Dinordesoxy-3,9-dimethyleseroline	83
44	58.95	0.75	Hexadecane	97
45	59.15	0.58	2,3,7-Trimethylindole	96
46	60.38	0.23	1H-Indole, 2,3-dihydro-1,3,3-trimethyl-2-methylene-	89
47	61.50	1.61	Cyclooctasiloxane, hexadecamethyl-	90

Peak	Time (min)	Area %	Library Match	Quality
48	62.47	0.53	1-Heptadecene	95
49	62.72	1.61	Heptadecane	98
50	66.30	0.39	Octadecane	97
51	66.67	2.30	Hexadecane, 2,6,10,14-tetramethyl-	99
52	67.47	0.80	Cyclohexadecane, 1,2-diethyl-	91
53[2]	67.54	0.36	2-Hexadecene, 3,7,11,15-tetramethyl-, [R-[R*,R*-(E)]]-	83
54[2]	67.95	1.16	2-Hexadecene, 3,7,11,15-tetramethyl-, [R-[R*,R*-(E)]]-	94
55	69.70	0.54	Nonadecane	98
56	69.87	1.00	Hexadecanenitrile	87
57	72.96	0.46	Eicosane	97
58	75.38	0.35	9H-Thioxanthen-9-one, 2-(1-methylethyl)-	81
59	76.07	0.45	Heneicosane	99
60	79.03	0.32	Docosane	96
61	81.88	0.58	Eicosane (Tricosane)	96
62	84.62	0.25	Eicosane (Tetracosane)	91
63	87.25	0.38	Eicosane (Pentacosane)	96
64	92.22	0.55	Eicosane (C_{26}+)	95
65	95.66	0.41	Coprostane	91
66	96.62	0.94	Cholestane	97

Table A.13: Identified Products from Ru/TiO_2 with H_2

Peak	Time (min)	Area %	Library Match	Quality
1	41.69	1.83	Dodecane	93
2	46.14	0.91	1-Tridecene	91
3	46.49	1.75	Tridecane	95
4	49.57	1.72	Naphthalene, 1,2,3,4-tetrahydro-1,1,6-trimethyl-	96
5	49.94	1.52	Dodecane, 2,6,10-trimethyl-	87
6	50.63	1.50	2-Tetradecene, (E)-	96
7	50.96	2.18	Tetradecane	95
8	54.87	0.92	1-Pentadecene	98
9	55.17	3.18	Pentadecane	97
10	55.95	0.23	1H-Indole, 2,3-dimethyl-	81
11	58.87	0.55	Cyclohexadecane	83
12	59.15	1.21	Hexadecane	98
13	62.65	0.52	1-Hexadecene	93
14	62.90	2.04	Heptadecane	97
15	63.13	1.67	Pentadecane, 2,6,10,14-tetramethyl-	86

Peak	Time (min)	Area %	Library Match	Quality
16	66.48	0.78	Octadecane	93
17	66.84	4.56	Hexadecane, 2,6,10,14-tetramethyl-	99
18	67.64	0.96	1-Eicosene	83
19[1]	67.71	0.51	2-Hexadecene, 3,7,11,15-tetramethyl-, [R-[R*,R*-(E)]]-	94
20[1]	68.12	1.32	2-Hexadecene, 3,7,11,15-tetramethyl-, [R-[R*,R*-(E)]]-	81
21	69.88	0.94	Nonadecane	97
22	72.01	7.47	n-Hexadecanoic acid	99
23	73.12	0.67	Eicosane	96
24	76.22	0.77	Heneicosane	97
25	79.18	1.00	Docosane	96
26	82.03	1.31	Tricosane	95

Table A.14: Identified Products from $LaPtAl_{12}O_{19}$

Peak	Time (min)	Area %	Library Match	Quality
1	41.68	1.64	Dodecane	95
2	42.36	0.51	Undecane, 2,6-dimethyl-	93
3	46.13	0.69	1-Tridecene	95
4	46.48	0.84	Tridecane	95
5	49.56	1.74	Naphthalene, 1,2,3,4-tetrahydro-1,1,6-trimethyl-	95
6	50.63	0.93	2-Tetradecene, (E)-	98
7	50.96	0.98	Tetradecane	96
8	52.77	0.49	Naphthalene, 1,5-dimethyl-	91
9	54.87	1.66	1-Pentadecene	99
10	55.16	2.80	Pentadecane	97
11	58.43	0.06	1H-Indole, 5,6,7-trimethyl-	83
12	58.87	0.30	1-Hexadecene	96
13	59.15	0.59	Hexadecane	98
14	62.65	0.39	1-Heptadecene	93
15	62.90	1.68	Heptadecane	98
16	63.13	0.89	Hexadecane, 2,6,10-trimethyl-	80
17	66.11	1.87	2-Tetradecene, (E)-	89
18	66.47	0.71	Dodecane (Octadecane)	91
19	66.84	2.85	Hexadecane, 2,6,10,14-tetramethyl-	99
20[1]	67.71	1.46	2-Hexadecene, 3,7,11,15-tetramethyl-, [R-[R*,R*-(E)]]-	95
21[1]	68.12	3.23	2-Hexadecene, 3,7,11,15-tetramethyl-, [R-[R*,R*-(E)]]-	95
22	69.67	0.42	Cyclotetradecane	91

Peak	Time (min)	Area %	Library Match	Quality
23	69.87	0.81	Tridecane (Nonadecane)	93
24	71.53	0.71	Hexadecenoic acid, Z-11-	97
25[2]	72.04	7.58	n-Hexadecanoic acid	99
26[2]	72.32	0.50	n-Hexadecanoic acid	90
27	73.13	0.41	Eicosane	93
28	79.19	0.48	Docosane	89
29	81.89	0.39	1-Nonadecene	93
30	82.03	0.66	Eicosane (Tricosane)	97

Table A.15: Identified Products from $LaPtAl_{12}O_{19}$ with H_2

Peak	Time (min)	Area %	Library Match	Quality
1	13.60	0.58	Heptane, 2-methyl-	89
2	13.80	4.09	Toluene	87
3	21.01	2.93	Ethylbenzene	87
4	23.36	0.38	p-Xylene	92
5	23.74	0.89	Nonane	87
6	29.24	0.53	Benzene, 1-ethyl-2-methyl-	93
7	30.34	0.84	Decane	81
8	35.54	0.68	Phenol, 4-methyl-	93
9	35.61	1.24	Benzene, (2-methyl-1-propenyl)-	81
10	36.14	1.07	Undecane	87
11	36.45	0.40	Cyclopropane, 1-pentyl-2-propyl-	91
12	38.53	0.25	1H-Indene, 2,3-dihydro-5-methyl-	81
13	38.76	0.25	1H-Indene, 2,3-dihydro-1,2-dimethyl-	89
14	39.76	0.35	Naphthalene, 1,2,3,4-tetrahydro-	97
15[1]	40.29	0.26	Phenol, 4-ethyl-	87
16[1]	40.33	0.20	Phenol, 4-ethyl-	81
17[1]	40.37	0.20	Phenol, 4-ethyl-	80
18	40.97	0.23	1-Dodecene	87
19	41.37	1.94	Dodecane	94
20	41.60	0.39	1H-Indene, 2,3-dihydro-1,6-dimethyl-	91
21	41.65	0.23	2-Dodecene, (E)-	89
22	42.07	1.14	Undecane, 2,6-dimethyl-	95
23	45.79	0.50	Benzene, (3-methyl-2-butenyl)-	94
24	46.01	0.48	4-Nonene, 5-butyl-	83
25	46.19	1.89	Tridecane	97
26	46.32	0.40	Naphthalene, 1,2,3,4-tetrahydro-6-methyl-	83
27	46.43	0.47	2-Tridecene, (E)-	95
28	47.32	0.33	Naphthalene, 2-methyl-	81

Peak	Time (min)	Area %	Library Match	Quality
29	49.26	1.38	Naphthalene, 1,2,3,4-tetrahydro-1,1,6-trimethyl-	95
30	50.36	1.02	2-Tetradecene, (E)-	98
31[2]	50.52	0.38	3-Tetradecene, (E)-	84
32	50.69	1.57	Tetradecane	97
33	50.91	0.97	5-Tetradecene, (E)-	86
34[2]	51.38	0.26	3-Tetradecene, (E)-	89
35	52.33	1.32	Naphthalene, 2,7-dimethyl-	95
36	54.60	0.61	1-Pentadecene	96
37	54.91	4.86	Pentadecane	97
38	55.23	1.80	2-Methyl-5-(butin-1-yl)pyridine	90
39	57.19	0.48	n-Nonylcyclohexane	93
40	58.28	0.42	3-(2-Methyl-propenyl)-1H-indene	86
41	58.89	1.20	Hexadecane	96
42[3]	59.21	0.31	1H-Indole, 1,2,3-trimethyl-	94
43[3]	59.24	0.40	1H-Indole, 1,2,3-trimethyl-	95
44	62.66	1.69	Heptadecane	98
45	66.24	0.76	Octadecane	97
46	66.60	2.60	Hexadecane, 2,6,10,14-tetramethyl-	99
47	69.64	0.56	Nonadecane	98
48	69.83	1.05	Hexadecanenitrile	90
49	71.80	3.51	n-Hexadecanoic acid	99
50	72.90	0.55	Eicosane	96
51[4]	75.31	0.71	Naphthalene, tris(1-methylethyl)-	91
52	75.99	0.50	Heneicosane	98
53[4]	77.85	0.39	Naphthalene, tris(1-methylethyl)-	90
54	78.67	0.98	Hexadecanamide	90
55	78.96	0.37	Docosane	96
56	81.81	0.70	Eicosane (Tricosane)	95
57	83.00	0.26	1,4-Dimethyl-5-phenyl-naphthalene	83
58	84.54	0.29	Eicosane (Tetracosane)	96

Table A.16: Identified Products from $LaPdAl_{11}O_{19}$

Peak	Time (min)	Area %	Library Match	Quality
1	13.84		Toluene	81
2	35.71	0.90	Phenol, 4-methyl-	91
3	41.38	2.25	Dodecane	93
4	42.08	1.11	Undecane, 2,6-dimethyl-	95
5	46.20	1.86	Tridecane	95
6	49.27	1.98	Naphthalene, 1,2,3,4-tetrahydro-1,1,6-trimethyl-	95

Peak	Time (min)	Area %	Library Match	Quality
7	50.36	1.72	1-Tetradecene	98
8	50.70	1.72	Tetradecane	96
9	52.39	1.23	Naphthalene, 2,7-dimethyl-	95
10	54.61	0.73	1-Pentadecene	99
11	54.91	6.20	Eicosane (Pentadecane)	97
12	55.32	1.20	2-Methyl-5-(butin-1-yl)pyridine	90
13	58.89	1.08	Hexadecane	96
14	62.67	2.09	Heptadecane	96
15	62.90	1.55	Pentadecane, 2,6,10,14-tetramethyl-	87
16	66.24	0.81	Octadecane	93
17	66.61	4.82	Hexadecane, 2,6,10,14-tetramethyl-	99
18	67.89	1.74	2-Hexadecene, 3,7,11,15-tetramethyl-, [R-[R*,R*-(E)]]-	96
19	69.65	1.05	Nonadecane	93
20	71.80	6.35	n-Hexadecanoic acid	98
21	72.90	0.53	Eicosane	96
22	75.32	0.77	9H-Thioxanthen-9-one, 2-(1-methylethyl)-	83
23	76.00	0.63	Heptadecane, 2,6,10,15-tetramethyl-	91
24	78.70	1.09	Octadecanamide	86
25	78.97	0.55	Docosane	96
26	81.81	1.01	Tricosane	99

Table A.17: Identified Products from $LaPdAl_{11}O_{19}$ with H_2

Peak	Time (min)	Area %	Library Match	Quality
1	21.09		Ethylbenzene	81
2	35.65	0.27	Benzene, (2-methyl-1-propenyl)-	87
3	41.39	1.59	Dodecane	95
4	46.21	1.45	Tridecane	96
5	49.15	0.67	Naphthalene, 1,2-dihydro-1,5,8-trimethyl-	93
6	49.27	1.14	Naphthalene, 1,2,3,4-tetrahydro-1,1,6-trimethyl-	96
7	50.37	0.33	2-Tetradecene, (E)-	97
8	50.70	1.27	Tetradecane	97
9[1]	54.61	2.09	1-Pentadecene	99
10[1]	54.74	0.77	1-Pentadecene	98
11	54.91	5.93	Pentadecane	95
12[1]	55.12	1.91	1-Pentadecene	83
13	55.38	0.52	1H-Indole, 2,5-dimethyl-	87

Peak	Time (min)	Area %	Library Match	Quality
14	58.89	1.09	Hexadecane	97
15	62.41	0.76	1-Heptadecene	93
16	62.67	2.14	Heptadecane	97
17	65.88	1.26	2-Hexadecene, 3,7,11,15-tetramethyl-, [R-[R*,R*-(E)]]-	83
18	66.61	2.48	Hexadecane, 2,6,10,14-tetramethyl-	99
19	67.07	1.93	1-Eicosene	83
20[1]	67.20	0.90	2-Hexadecene, 3,7,11,15-tetramethyl-, [R-[R*,R*-(E)]]-	95
21[1]	67.48	1.33	2-Hexadecene, 3,7,11,15-tetramethyl-, [R-[R*,R*-(E)]]-	99
22[1]	67.89	3.50	2-Hexadecene, 3,7,11,15-tetramethyl-, [R-[R*,R*-(E)]]-	96
23	69.65	1.04	Nonadecane	95
24	69.83	3.86	Hexadecanenitrile	90
25	70.57	0.32	Hexadecanoic acid, methyl ester	94
26	71.79	3.29	n-Hexadecanoic acid	98
27	72.90	0.53	Heptadecane (Eicosane)	87
28	76.00	0.62	Octadecane (Heneicosane)	95
29	78.97	0.64	Nonadecane (Docosane)	96
30	81.82	0.95	Nonadecane (Tricosane)	98

Table A.18: Identified Products from $LaRuAl_{12}O_{19}$

Peak	Time (min)	Area %	Library Match	Quality
1	13.88		1,3,5-Cycloheptatriene	81
2	41.39	1.97	Dodecane	95
3	45.84	0.78	1-Tridecene	94
4	46.21	1.53	Tridecane	97
5	49.27	2.01	Naphthalene, 1,2,3,4-tetrahydro-1,1,6-trimethyl-	94
6	50.37	0.98	1-Decanethiol	95
7	50.70	1.76	Tetradecane	96
8	52.44	0.36	Naphthalene, 2,7-dimethyl-	93
9	54.61	1.07	1-Pentadecene	97
10	54.92	7.29	Pentadecane	97
11	55.38	1.20	1H-Indole, 2,3-dimethyl-	91
12	58.90	1.22	Hexadecane	97
13	62.67	2.07	Heptadecane	98
14	66.25	1.03	Octadecane	96
15	66.61	3.31	Hexadecane, 2,6,10,14-tetramethyl-	99

Peak	Time (min)	Area %	Library Match	Quality
16[1]	67.41	1.49	2-Hexadecene, 3,7,11,15-tetramethyl-, [R-[R*,R*-(E)]]-	94
17[1]	67.89	1.57	2-Hexadecene, 3,7,11,15-tetramethyl-, [R-[R*,R*-(E)]]-	91
18	69.65	1.22	Nonadecane	98
19	69.85	2.19	Hexadecanenitrile	81
20	71.77	3.88	n-Hexadecanoic acid	98
21	72.90	0.80	Eicosane	96
22	76.00	0.95	Heptadecane, 2,6,10,15-tetramethyl-	96
23	78.97	0.64	Docosane	95
24	81.81	1.28	Octadecane (Tricosane)	96

Table A.19: Identified Products from $LaRuAl_{12}O_{19}$ with H_2

Peak	Time (min)	Area %	Library Match	Quality
1	36.49	0.33	Undecane	93
2	41.28	0.37	1-Dodecene	95
3	41.68	1.66	Dodecane	93
4	42.37	0.35	Undecane, 2,6-dimethyl-	90
5	46.12	0.84	1-Tridecene	90
6	46.48	1.22	Tridecane	97
7	46.81	0.33	Cyclotetradecane	83
8	49.45	0.49	Naphthalene, 1,2-dihydro-1,1,6-trimethyl-	91
9	49.56	1.01	Naphthalene, 1,2,3,4-tetrahydro-1,1,6-trimethyl-	96
10	49.94	0.66	Dodecane, 2,6,10-trimethyl-	81
11	50.63	0.58	1-Tetradecene	98
12	50.96	0.82	Tetradecane	96
13	52.77	0.40	Naphthalene, 1,5-dimethyl-	95
14	54.87	1.35	1-Pentadecene	99
15	55.17	3.65	Pentadecane	96
16	58.88	0.23	1-Hexadecene	98
17	59.14	0.83	Hexadecane	97
18	62.66	0.22	1-Hexadecene	99
19	62.90	1.70	Heptadecane	98
20	63.14	0.70	Pentadecane, 2,6,10,14-tetramethyl-	86
21	64.05	0.22	Cycloundecane, 1,1,2-trimethyl-	90
22	66.48	0.72	Octadecane	95
23	66.85	1.79	Hexadecane, 2,6,10,14-tetramethyl-	97

Peak	Time (min)	Area %	Library Match	Quality
24[1]	67.43	0.77	2-Hexadecene, 3,7,11,15-tetramethyl-, [R-[R*,R*-(E)]]-	99
25[1]	67.71	1.28	2-Hexadecene, 3,7,11,15-tetramethyl-, [R-[R*,R*-(E)]]-	94
26[1]	68.12	2.75	2-Hexadecene, 3,7,11,15-tetramethyl-, [R-[R*,R*-(E)]]-	93
27	69.68	0.21	1-Hexadecene	95
28	69.88	0.58	Nonadecane	95
29	72.02	0.82	n-Hexadecanoic acid	89
30	73.13	0.51	Eicosane	99
31	76.22	0.58	Heneicosane	98
32	79.19	0.65	Heptadecane (Docosane)	96
33	81.90	0.43	11-Tricosene	95
34	82.03	0.89	Eicosane (Tricosane)	98
35	84.77	0.53	Eicosane (Tetracosane)	97
36	87.39	0.78	Eicosane (Pentacosane)	96

Table A.20: Identified Products from $BaPtAl_{12}O_{19}$

Peak	Time (min)	Area %	Library Match	Quality
1	46.50	2.30	Tridecane	94
2	49.58	2.04	Naphthalene, 1,2,3,4-tetrahydro-1,1,6-trimethyl-	96
3	50.66	1.29	1-Tetradecene	96
4	50.98	1.52	Tetradecane	94
5	54.89	1.25	1-Pentadecene	96
6	55.19	5.05	Pentadecane	97
7	59.17	1.56	Hexadecane	96
8	62.92	2.20	Heptadecane	96
9	66.49	1.19	Octadecane	97
10	66.85	2.05	Hexadecane, 2,6,10,14-tetramethyl-	90
11	69.89	1.25	Nonadecane	94
12	73.14	1.05	Eicosane	98
13	76.24	1.02	Heneicosane	96
14	78.87	6.35	Hexadecanoic acid, butyl ester	96
15	79.20	1.32	Docosane	96
16	82.04	1.60	Nonadecane (Tricosane)	84

Table A.21: Identified Products from $BaPtAl_{12}O_{19}$ with H_2

Peak	Time (min)	Area %	Library Match	Quality
1	14.28	2.86	Toluene	81

Peak	Time (min)	Area %	Library Match	Quality
2	36.02	0.50	Benzene, (2-methyl-1-propenyl)-	81
3	36.64	0.02	Phenol, 4-methyl-	93
4	39.49	0.51	1-Phenyl-1-butene	90
5	40.11	0.26	Naphthalene, 1,2,3,4-tetrahydro-	95
6	40.96	0.16	Phenol, 3-ethyl-	87
7	41.27	0.35	1-Dodecene	89
8	41.66	1.43	Dodecane	94
9	43.31	0.27	1H-Indene, 2,3-dihydro-4,7-dimethyl-	86
10	46.11	1.05	1-Tridecene	95
11	46.47	1.39	Tridecane	96
12	48.03	0.28	Benzene, (3-methyl-2-butenyl)-	90
13	49.55	1.30	Naphthalene, 1,2,3,4-tetrahydro-1,1,6-trimethyl-	95
14	49.94	0.78	Dodecane, 2,6,10-trimethyl-	86
15	50.63	0.72	1-Tetradecene	98
16	50.95	1.22	Tetradecane	97
17	52.68	0.81	Naphthalene, 2,7-dimethyl-	93
18	54.87	0.53	1-Pentadecene	95
19	55.16	3.44	Pentadecane	96
20	55.68	0.56	1H-Indole, 2,3-dimethyl-	87
21	56.53	0.25	1(2H)-Naphthalenone, 3,4-dihydro-4,6,7-trimethyl-	83
22	56.71	0.19	Benzene, 3,5-dimethyl-1-(phenylmethyl)-	90
23	57.44	0.39	Heptylcyclohexane	89
24	59.14	0.97	Hexadecane	98
25	62.65	0.31	1-Hexadecene	97
26	62.90	1.50	Heptadecane	98
27	63.14	1.04	Pentadecane, 2,6,10,14-tetramethyl-	97
28	63.64	0.20	4H-Pyrrolo[3,2,1-ij]quinolin-4-one, 1,2,5,6-tetrahydro-6-methyl-	83
29	66.48	0.55	Octadecane	95
30	66.84	3.68	Hexadecane, 2,6,10,14-tetramethyl-	99
31	67.64	0.68	5-Tetradecene, (E)-	89
32[1]	67.70	0.30	2-Hexadecene, 3,7,11,15-tetramethyl-, [R-[R*,R*-(E)]]-	95
33[1]	68.13	1.04	2-Hexadecene, 3,7,11,15-tetramethyl-, [R-[R*,R*-(E)]]-	97
34	69.88	0.49	Nonadecane	95
35	70.07	0.77	Hexadecanenitrile	90
36	70.80	0.15	Germacyclopentane, 1-propyl-	86

Peak	Time (min)	Area %	Library Match	Quality
37[2]	72.08	6.33	n-Hexadecanoic acid	99
38[2]	72.31	0.18	n-Hexadecanoic acid	91
39[2]	72.43	0.02	n-Hexadecanoic acid	86
40	73.12	0.37	Eicosane	97
41	76.22	0.47	Heneicosane	98
42	78.93	0.89	Hexadecanamide	97
43	79.19	0.39	Docosane	96
44	82.03	0.87	Eicosane (Tricosane)	99
45	84.77	0.32	Eicosane, 2-methyl-	83

Table A.22: Identified Products from $BaPdAl_{11}O_{19}$

Peak	Time (min)	Area %	Library Match	Quality
1	21.62	0.30	Ethylbenzene	87
2	41.67	2.00	Dodecane	94
3	46.48	1.80	Tridecane	91
4	49.56	1.82	Naphthalene, 1,2,3,4-tetrahydro-1,1,6-trimethyl-	93
5	50.63	1.07	2-Tetradecene, (E)-	98
6	50.96	1.58	Tetradecane	94
7	51.51	0.02	1H-Indole, 4-methyl-	93
8	52.75	0.92	Naphthalene, 2,7-dimethyl-	91
9	54.87	0.95	1-Pentadecene	99
10	55.16	4.10	Pentadecane	96
11	55.38	1.15	Benzonitrile, 2,4,6-trimethyl-	92
12[1]	55.76	0.60	1H-Indole, 2,3-dimethyl-	93
13[1]	55.79	0.40	1H-Indole, 2,3-dimethyl-	90
14	55.85	1.04	1H-Indole, 1,2-dimethyl-	93
15	58.88	0.45	1-Tridecene	90
16	59.14	1.17	Hexadecane	97
17	62.90	1.79	Heptadecane	98
18	66.48	0.73	Octadecane	95
19	66.84	2.97	Hexadecane, 2,6,10,14-tetramethyl-	99
20[2]	67.64	0.77	2-Hexadecene, 3,7,11,15-tetramethyl-, [R-[R*,R*-(E)]]-	93
21[2]	67.71	0.38	2-Hexadecene, 3,7,11,15-tetramethyl-, [R-[R*,R*-(E)]]-	95
22[2]	68.12	0.99	2-Hexadecene, 3,7,11,15-tetramethyl-, [R-[R*,R*-(E)]]-	83
23	69.88	0.73	Nonadecane	95
24	70.09	0.95	Hexadecanenitrile	90
25[3]	72.03	5.52	n-Hexadecanoic acid	96
26[3]	72.32	0.38	n-Hexadecanoic acid	92

Peak	Time (min)	Area %	Library Match	Quality
27	73.12	0.91	Eicosane	96
28	76.22	0.61	Heneicosane	98
29	78.97	0.20	9-Octadecenamide, (Z)-	90
30	79.19	0.59	Docosane	96
31	82.04	1.04	Eicosane (Tricosane)	97

Table A.23: Identified Products from $BaPdAl_{11}O_{19}$ with H_2

Peak	Time (min)	Area %	Library Match	Quality
1	63.0405	1.3601	Heptadecane	97
2	66.8855	2.1964	Hexadecane, 2,6,10,14-tetramethyl-	99
3	67.7644	2.6725	2-Hexadecene, 3,7,11,15-tetramethyl-, [R-[R*,R*-(E)]]-	96
4	76.2429	0.6055	Heptadecane, 2,6,10,15-tetramethyl-	90
5	82.0395	0.8934	Tricosane	86

Table A.24: Identified Products from Ni/TiO_2

Peak	Time (min)	Area %	Library Match	Quality
1	55.4993	5.2392	Pentadecane	97
2	59.396	2.2094	Hexadecane	96
3	63.073	2.744	Heptadecane	97
4[1]	63.2346	0.9051	Hexadecane, 2,6,10,14-tetramethyl-	80
6	66.6273	1.8277	Octadecane	92
7[1]	66.9116	3.1214	Hexadecane, 2,6,10,14-tetramethyl-	87
9[2]	67.7129	1.6471	2-Hexadecene, 3,7,11,15-tetramethyl-, [R-[R*,R*-(E)]]-	93
10[2]	67.7905	1.1162	2-Hexadecene, 3,7,11,15-tetramethyl-, [R-[R*,R*-(E)]]-	90
11[2]	68.2105	1.6839	2-Hexadecene, 3,7,11,15-tetramethyl-, [R-[R*,R*-(E)]]-	97
12	69.9876	2.992	Nonadecane	96
13	70.3495	9.8443	2-Heptadecanone	94
14	70.5951	4.3312	Hexadecanenitrile	81
15	73.1735	1.5866	Eicosane	96
17	76.2689	2.0074	Heneicosane	93
18	76.689	2.1216	2-Pentadecanone	89
20	79.2157	1.7294	Docosane	98
21	82.0461	2.8176	Tricosane	98

Peak	Time (min)	Area %	Library Match	Quality

Table A.25: Identified Products from Ni/TiO_2 with H_2

Peak	Time (min)	Area %	Library Match	Quality
1	55.4476	2.0966	Pentadecane	91
2	63.0149	2.9802	Heptadecane	98
3	66.8728	4.4774	Hexadecane, 2,6,10,14-tetramethyl-	91
4[1]	67.3381	4.8124	2-Hexadecene, 3,7,11,15-tetramethyl-, [R-[R*,R*-(E)]]-	83
5[1]	67.4674	2.7575	2-Hexadecene, 3,7,11,15-tetramethyl-, [R-[R*,R*-(E)]]-	94
6[1]	67.6742	7.8906	2-Hexadecene, 3,7,11,15-tetramethyl-, [R-[R*,R*-(E)]]-	86
7[1]	67.7517	4.8109	2-Hexadecene, 3,7,11,15-tetramethyl-, [R-[R*,R*-(E)]]-	91
8[1]	68.1653	8.7863	2-Hexadecene, 3,7,11,15-tetramethyl-, [R-[R*,R*-(E)]]-	91
9	72.6178	0.3501	n-Hexadecanoic acid	90
10	76.2302	1.2747	Heptadecane, 2,6,10,15-tetramethyl-	89

Table A.26: Identified Products from $Ni/TiO_2–SiO_2$

Peak	Time (min)	Area %	Library Match	Quality
1	63.1246	0.7566	Heptadecane	94
2	68.2491	0.7602	2-Hexadecene, 3,7,11,15-tetramethyl-, [R-[R*,R*-(E)]]-	91
3	73.2121	0.5299	Eicosane	95
4	79.2155	0.6206	Eicosane (Docosane)	90
5	82.046	0.8686	Tricosane	97

Table A.27: Identified Products from $Ni/TiO_2–SiO_2$ with H_2

Peak	Time (min)	Area %	Library Match	Quality
1	46.788	2.2101	Tridecane	91
2	49.877	1.0406	Naphthalene, 1,2,3,4-tetrahydro-1,1,6-trimethyl-	97
3	50.0708	0.941	Dodecane, 2,6,11-trimethyl-	83
4	51.1177	3.4904	Tetradecane	94
5	55.2342	13.9143	Pentadecane	97
6	59.2472	2.5677	Hexadecane	98
7	62.9759	5.5576	Heptadecane	98

Peak	Time (min)	Area %	Library Match	Quality
8	66.5689	1.952	Octadecane	93
9	66.8727	5.9157	Hexadecane, 2,6,10,14-tetramethyl-	99
10[1]	67.7774	0.5148	2-Hexadecene, 3,7,11,15-tetramethyl-, [R-[R*,R*-(E)]]-	83
11[1]	68.1845	1.0237	2-Hexadecene, 3,7,11,15-tetramethyl-, [R-[R*,R*-(E)]]-	81
12	69.9616	1.5571	Nonadecane	98
13	70.3623	13.8966	Hexadecanenitrile	91
14	73.1669	1.0999	Eicosane	99
15	76.2688	1.2118	Heneicosane	97
16	76.8633	2.6598	Hexadecanenitrile	95
17	79.2285	1.273	Docosane	96
18	82.0589	2.1756	Tricosane	98

Table A.28: Identified Products from $LaNi_3Al_9O_{19}$

Peak	Time (min)	Area %	Library Match	Quality
1	55.4346	1.2956	Pentadecane	95
2	63.1247	0.6729	Heptadecane	95
3	73.2446	0.2221	Eicosane	91

Table A.29: Identified Products from $LaNi_3Al_9O_{19}$ with H_2

Peak	Time (min)	Area %	Library Match	Quality
1	49.974	1.1487	Naphthalene,1,2,3,4-tetrahydro-1,1,6-trimethyl 95	
2	51.2277	2.0206	Tetradecane	83
3	55.1244	1.3386	1-Pentadecene	98
4	55.3247	3.7793	Pentadecane	96
5	59.3313	1.0219	Hexadecane	91
6	63.0407	1.8332	Heptadecane	98
7	66.6143	1.1975	Octadecane	83
8	66.8986	3.3402	Hexadecane, 2,6,10,14-tetramethyl-	91
9	68.2104	1.0034	2-Hexadecene, 3,7,11,15-tetramethyl-, [R-[R*,R*-(E)]]-	86
10	76.2689	0.7175	Eicosane (Heneicosane)	89
11	79.2092	0.7763	Docosane	90
12	82.0461	0.8569	Tricosane	92

Table A.30: Identified Products from $BaNi_3Al_9O_{19}$

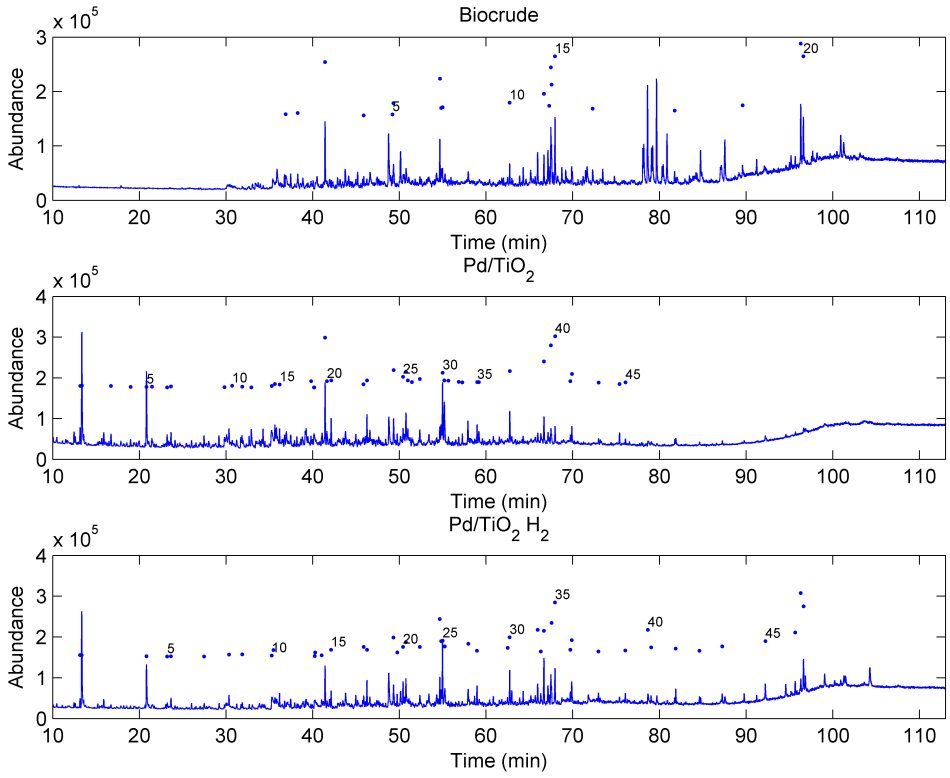

Figure A.4: Chromatograms of Pd/TiO_2 upgraded bio-oil at 400 °C for 60 min

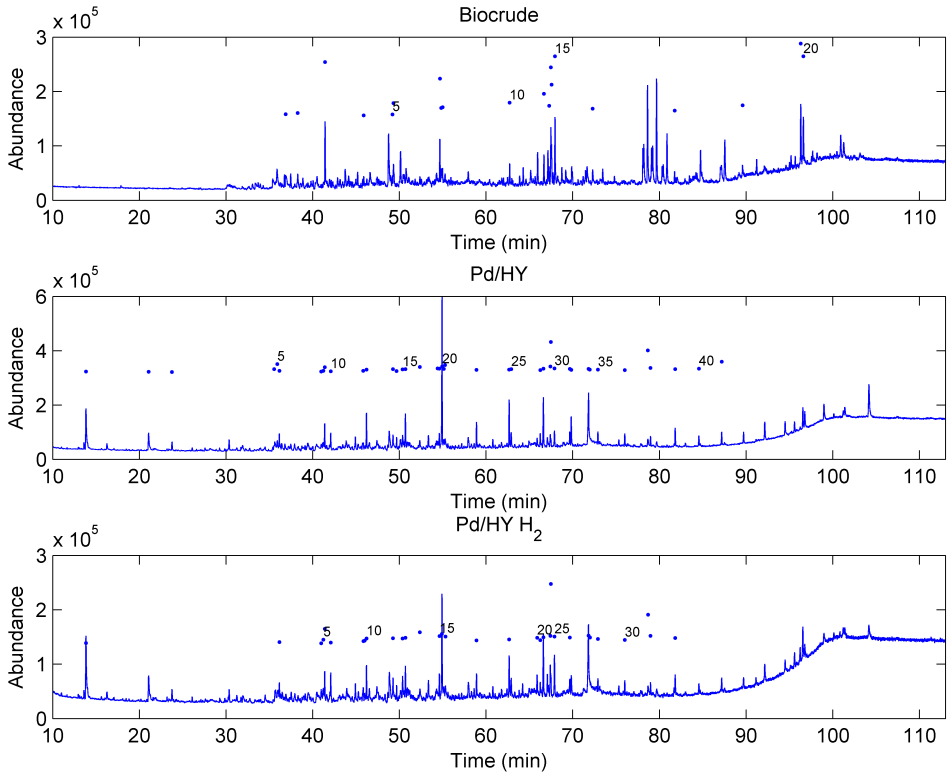

Figure A.5: Chromatograms of Pd/HY upgraded bio-oil at 400 °C for 60 min

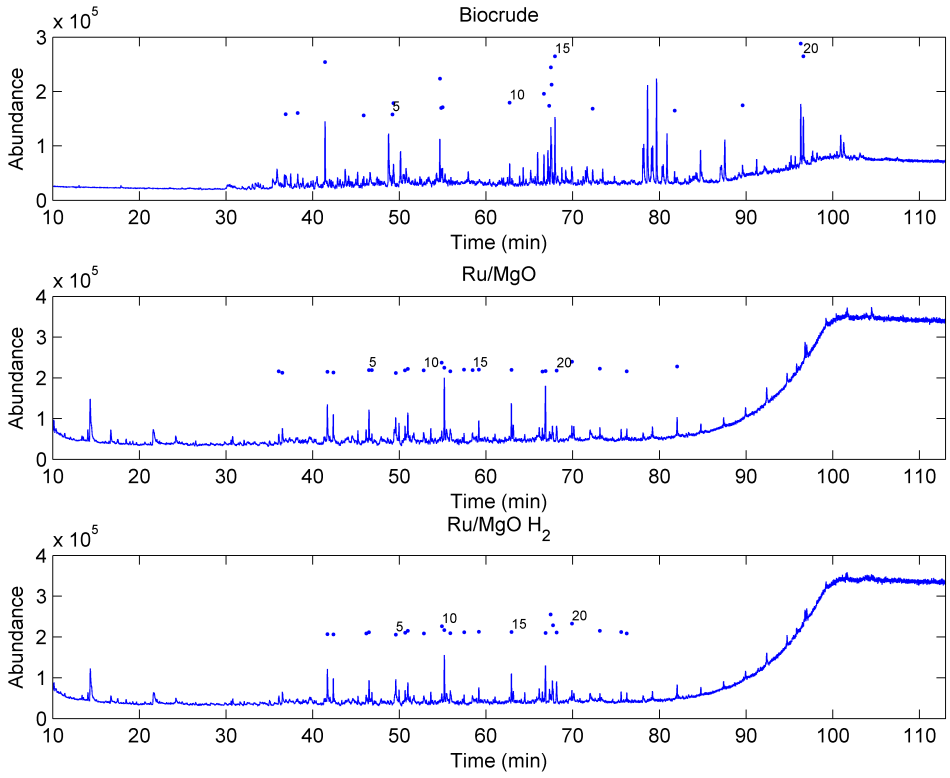

Figure A.6: Chromatograms of Ru/MgO upgraded bio-oil at 400 °C for 60 min

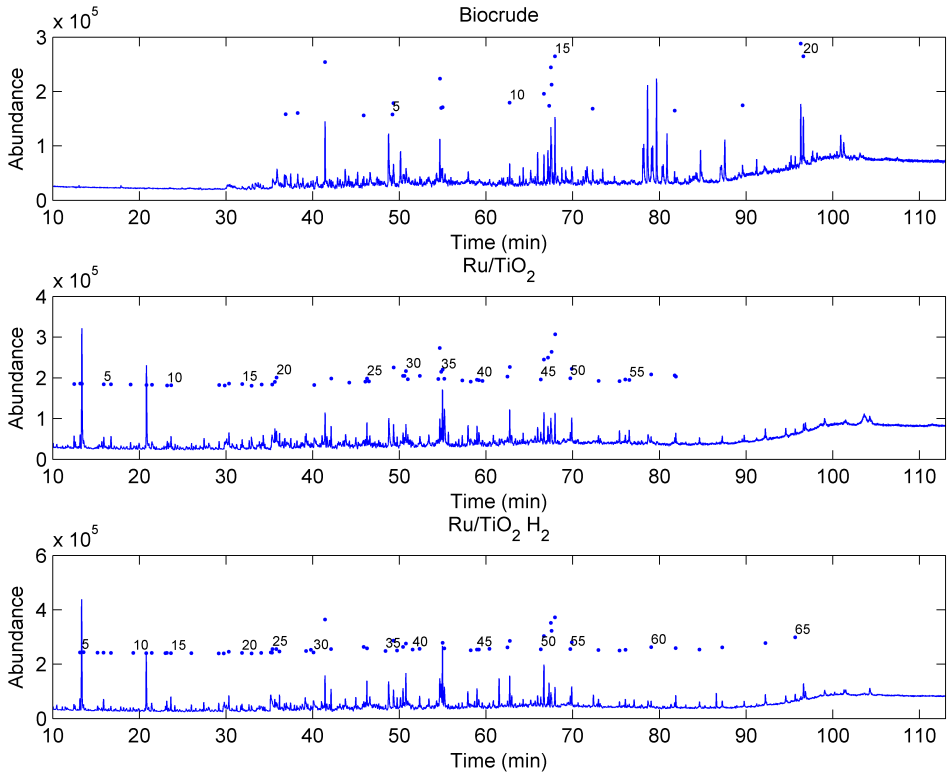

Figure A.7: Chromatograms of Ru/TiO_2 upgraded bio-oil at 400 °C for 60 min

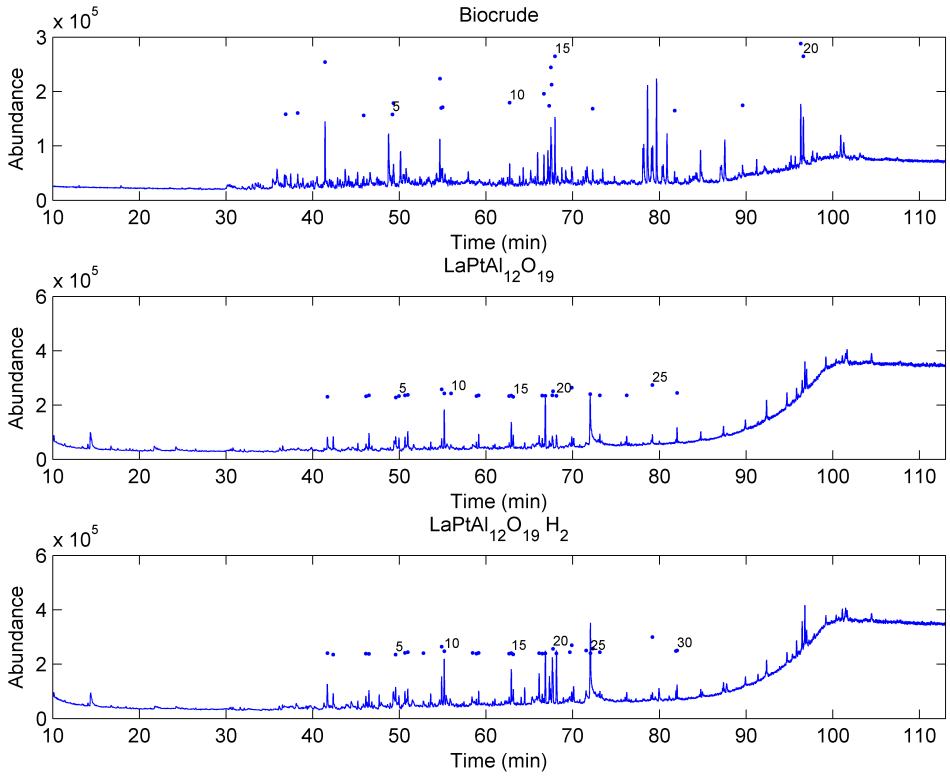

Figure A.8: Chromatograms of $LaPtAl_{12}O_{19}$ upgraded bio-oil at 400 °C for 60 min

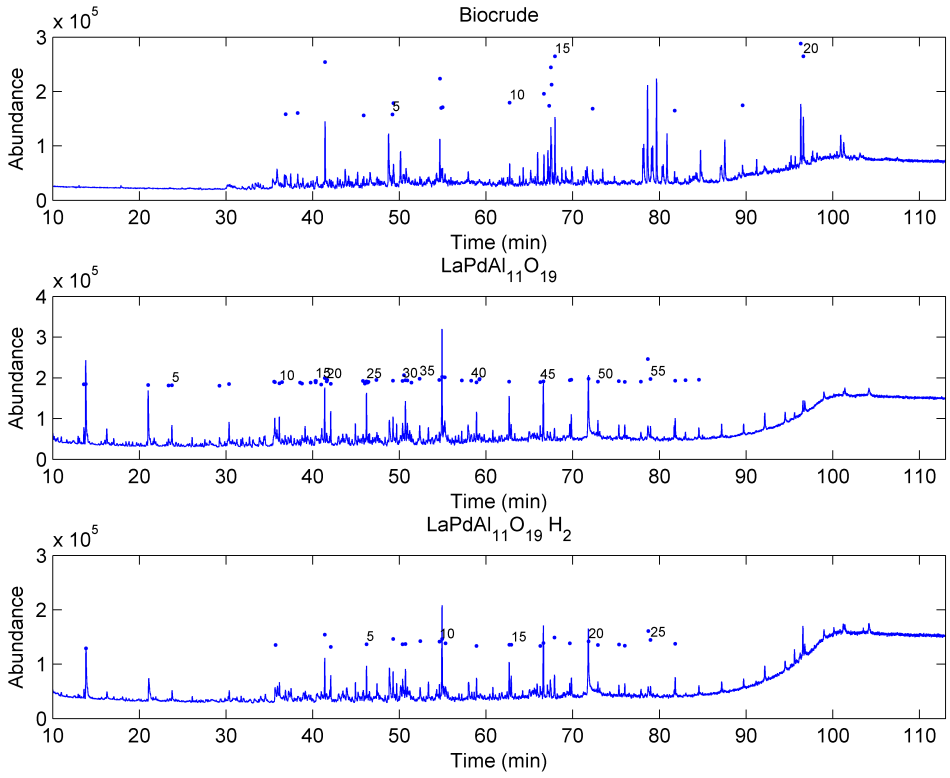

Figure A.9: Chromatograms of $LaPdAl_{11}O_{19}$ upgraded bio-oil at 400 °C for 60 min

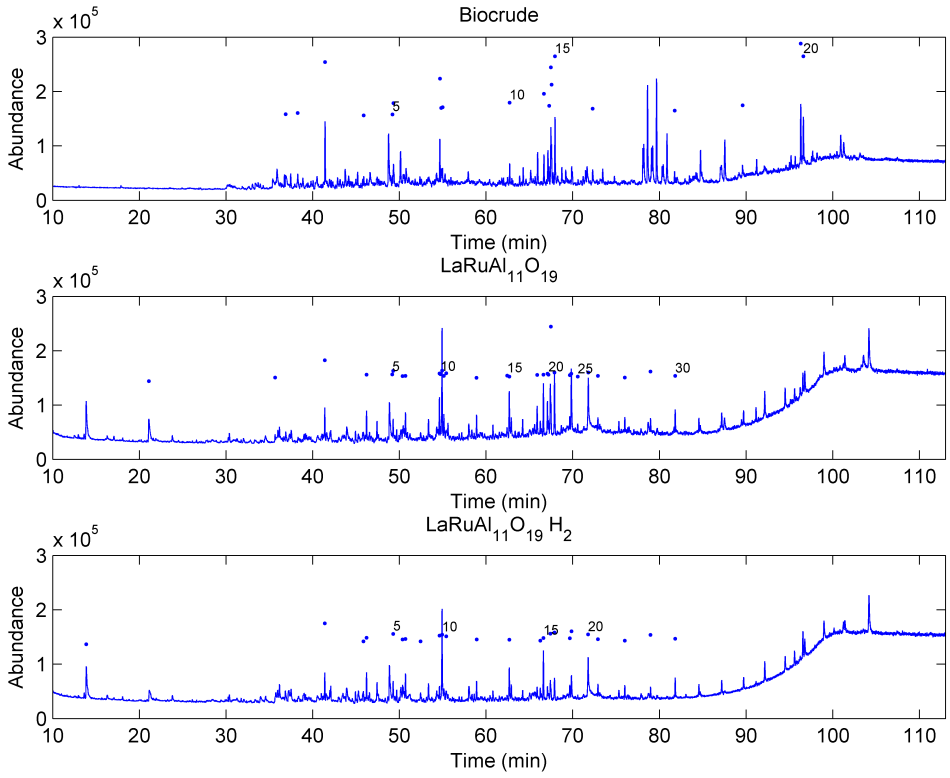

Figure A.10: Chromatograms of $LaRuAl_{12}O_{19}$ upgraded bio-oil at 400 °C for 60 min

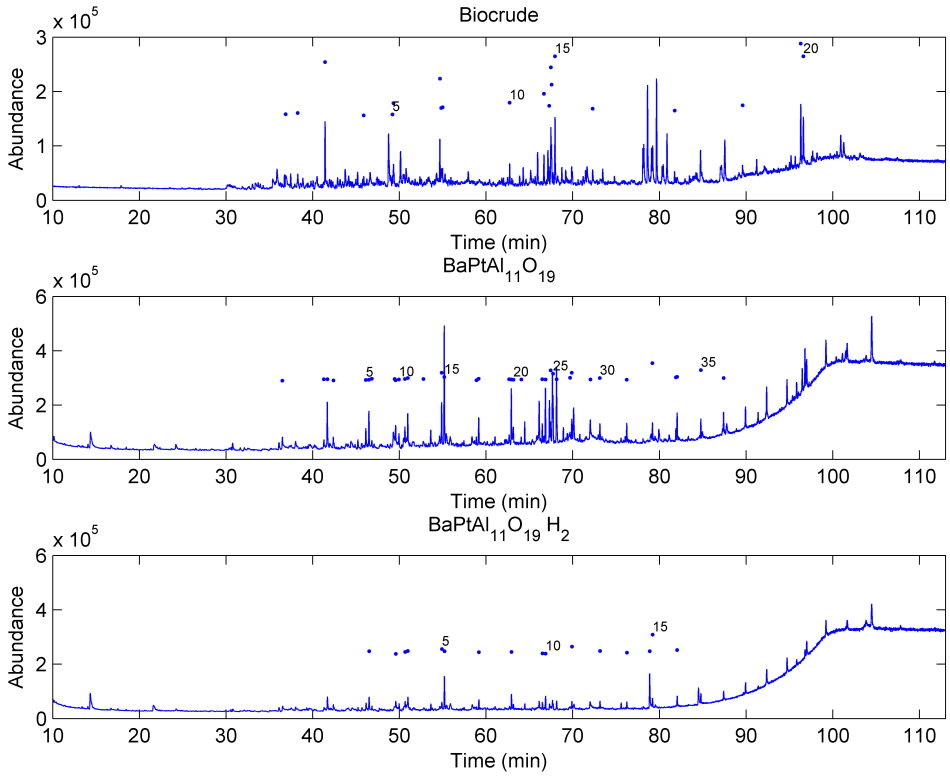

Figure A.11: Chromatograms of $BaPtAl_{12}O_{19}$ upgraded bio-oil at 400 °C for 60 min

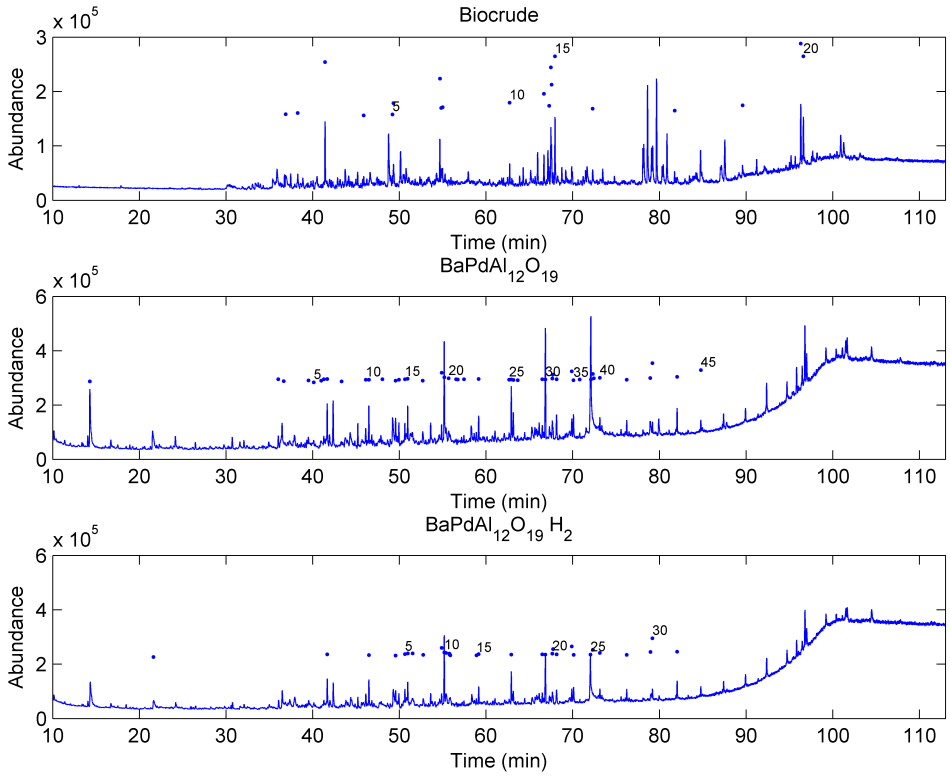

Figure A.12: Chromatograms of $BaPdAl_{11}O_{19}$ upgraded bio-oil at 400 °C for 60 min

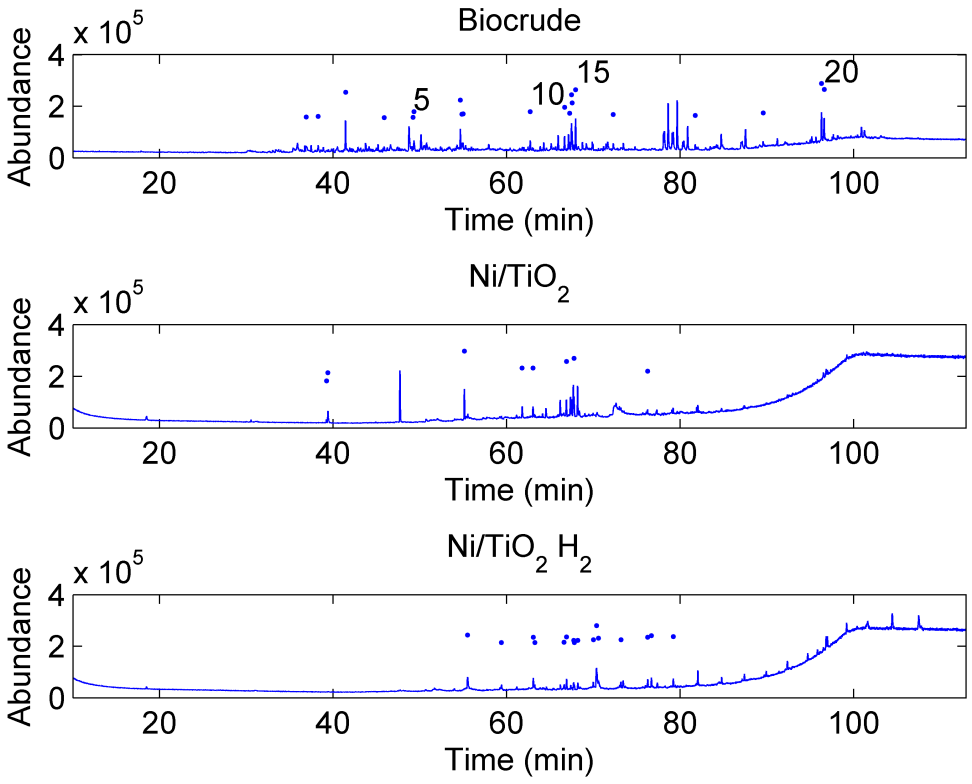

Figure A.13: Chromatograms of Ni/TiO_2 upgraded bio-oil at 400 °C for 60 min

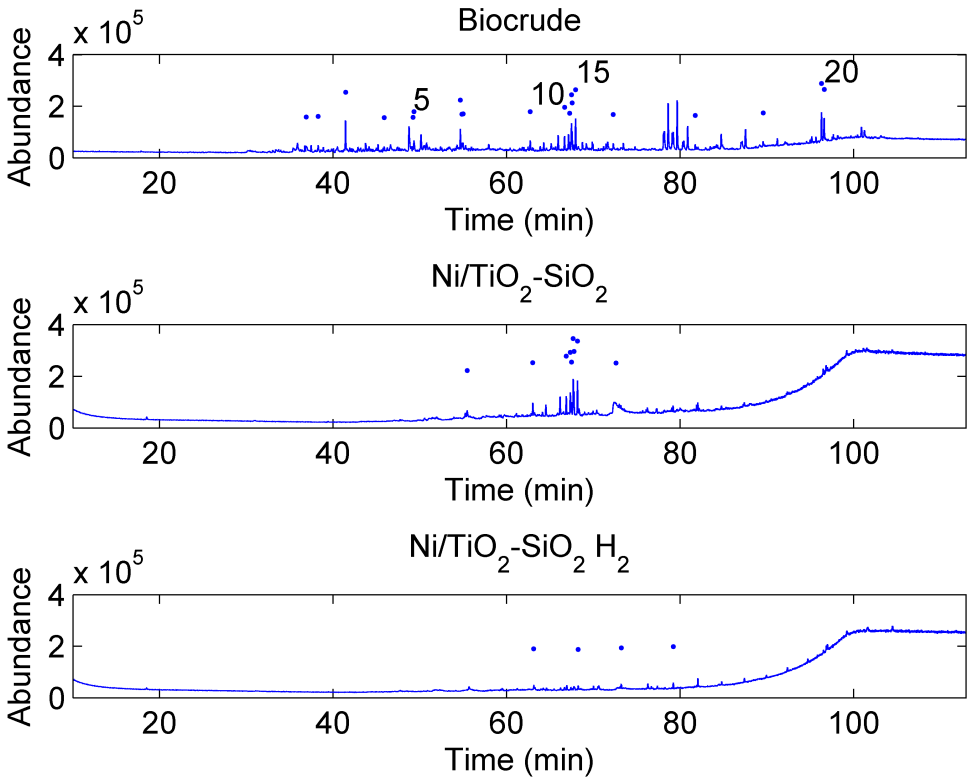

Figure A.14: Chromatograms of $Ni/TiO_2–SiO_2$ upgraded bio-oil at 400 °C for 60 min

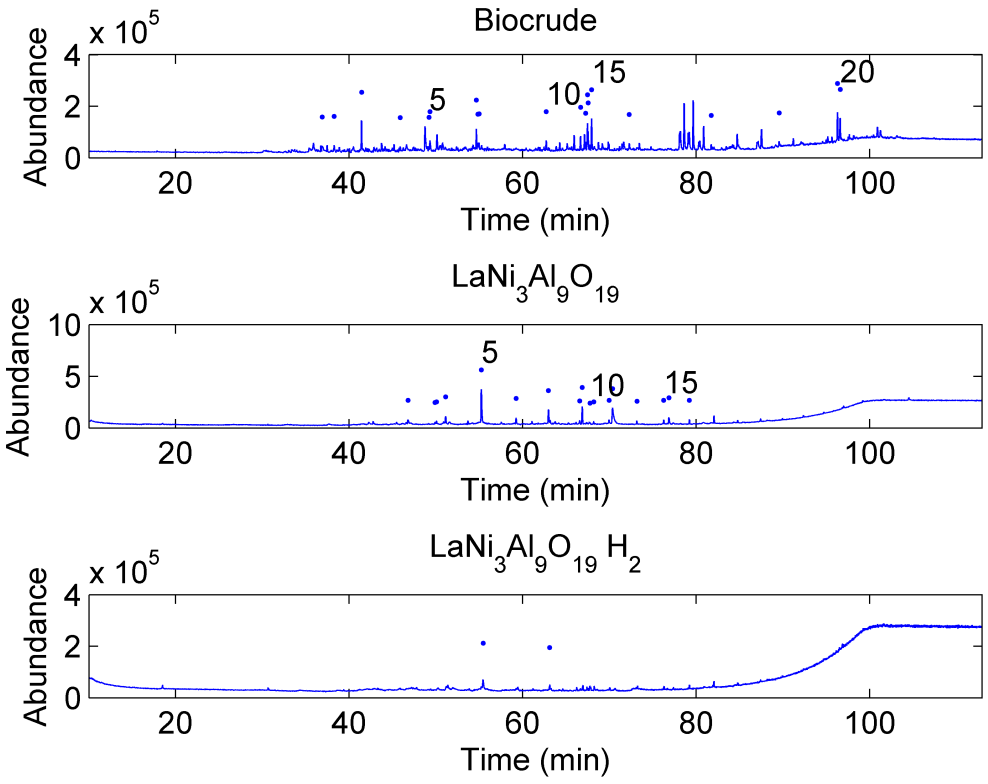

Figure A.15: Chromatograms of $LaNi_3Al_9O_{19}$ upgraded bio-oil at 400 °C for 60 min

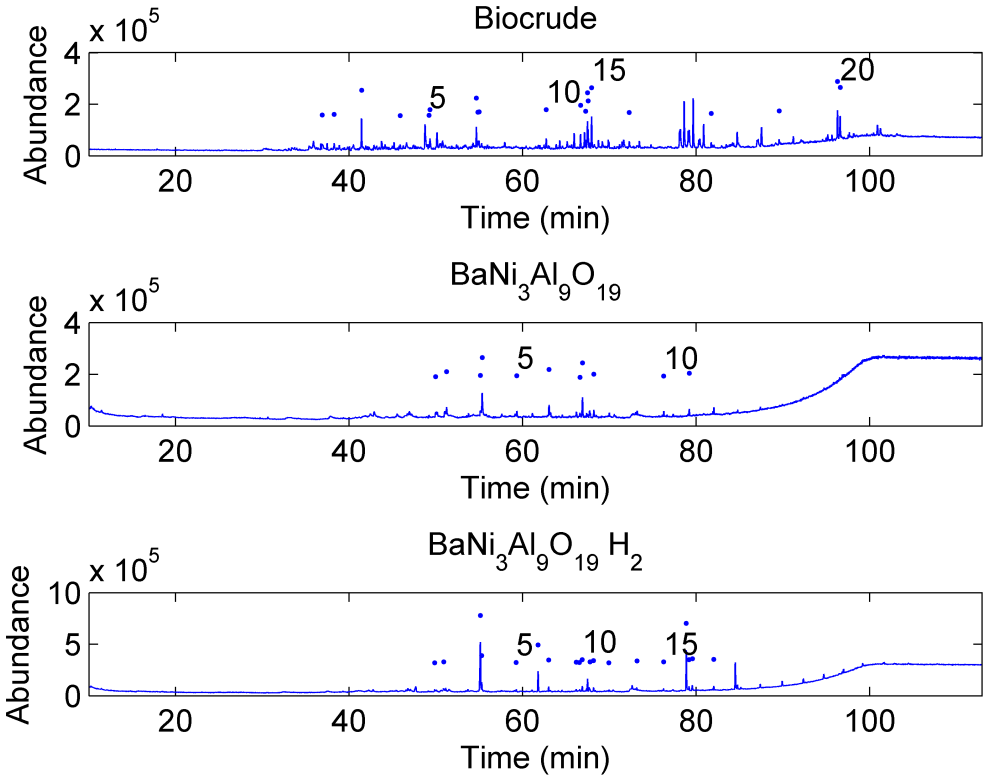

Figure A.16: Chromatograms of $BaNi_3Al_9O_{19}$ upgraded bio-oil at 400 °C for 60 min

Peak	Time (min)	Area %	Library Match	Quality
1	49.8642	0.812	Naphthalene,1,2,3,4-tetrahydro-1,1,6-trimethyl	93
2	50.8982	0.7374	2-Tetradecene, (E)-	95
3	55.2731	1.8356	Octadecane (Pentadecane)	96
4	59.2603	0.5389	Octadecane (Hexadecane)	94
5	62.9955	0.8953	Heptadecane	97
6[1]	66.162	0.5715	2-Hexadecene, 3,7,11,15-tetramethyl-, [R-[R*,R*-(E)]]-	81
7	66.5562	0.5528	Octadecane	95
8	66.8729	0.9453	Hexadecane, 2,6,10,14-tetramethyl-	99
9[1]	67.7582	0.4781	2-Hexadecene, 3,7,11,15-tetramethyl-, [R-[R*,R*-(E)]]-	90
10[1]	68.1718	0.6977	2-Hexadecene, 3,7,11,15-tetramethyl-, [R-[R*,R*-(E)]]-	90
11	69.9489	0.44	Nonadecane	90
12	73.1671	0.469	Eicosane	95
13	76.2431	0.3855	Heneicosane	95
14	78.8668	6.1056	Hexadecanoic acid, butyl ester	96
15	79.1834	0.7829	Nonadecane (Docosane)	93
16	79.5582	1.0883	1-Octadecene	96
17	82.0397	0.569	Tricosane	96
18	84.5148	4.6833	Octadecanoic acid, butyl ester	99

Table A.31: Identified Products from $BaNi_3Al_9O_{19}$ with H_2

APPENDIX B

Infrared Spectroscopy Results for Biocrude and its Upgraded Derivatives

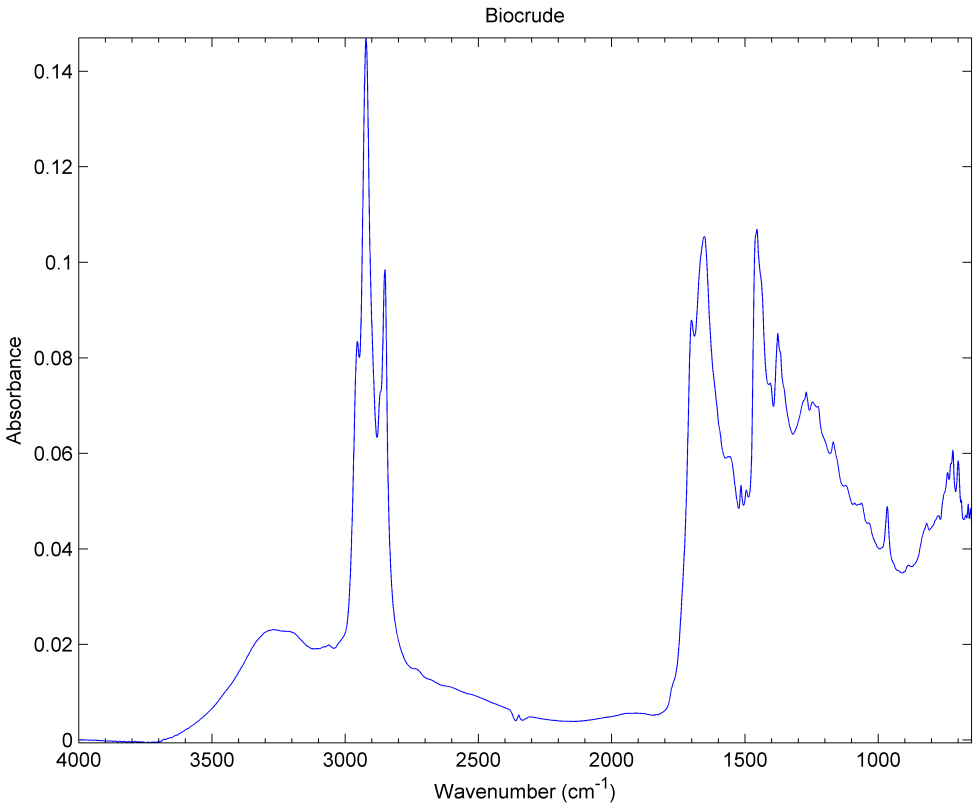

Figure B.1: Biocrude Fourier transform infrared spectrum from liquefaction at 400 °C for 60 min

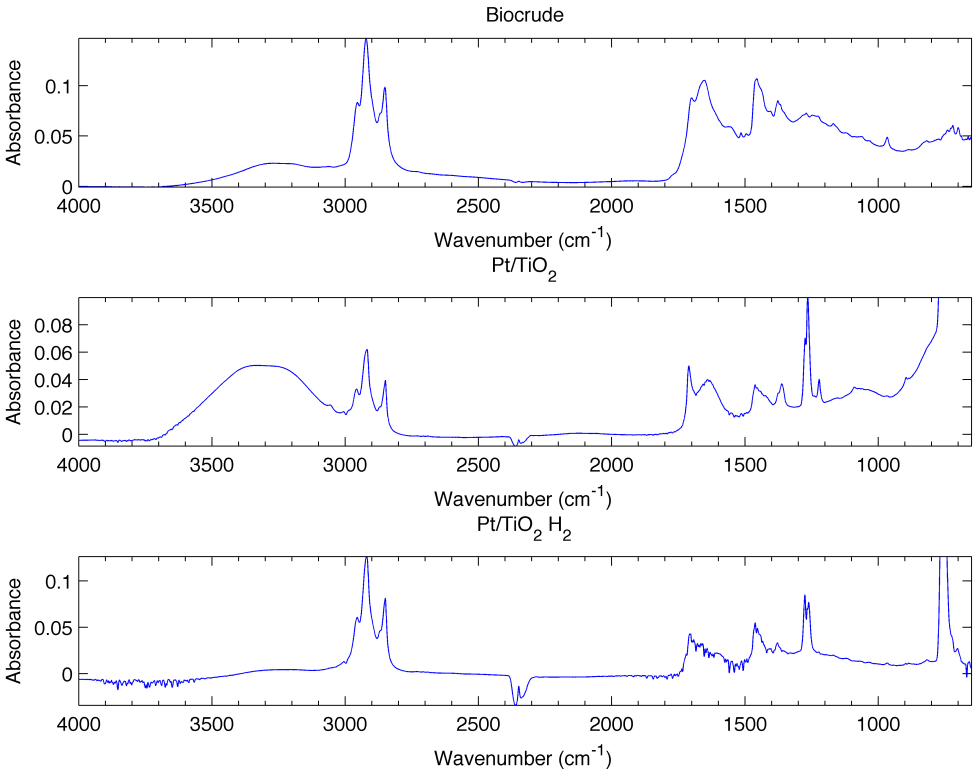

Figure B.2: Pt/TiO_2 Upgraded Bio-oil Fourier transform infrared spectrum at 400 °C for 60 min

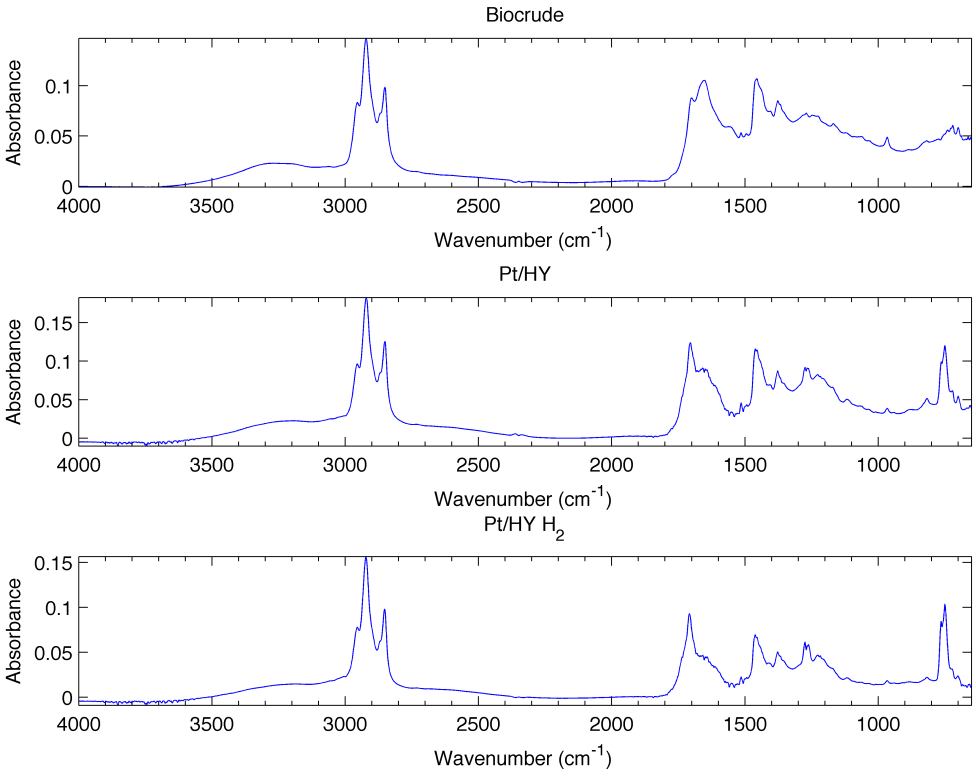

Figure B.3: Pt/HY Upgraded Bio-oil Fourier transform infrared spectrum at 400 °C for 60 min

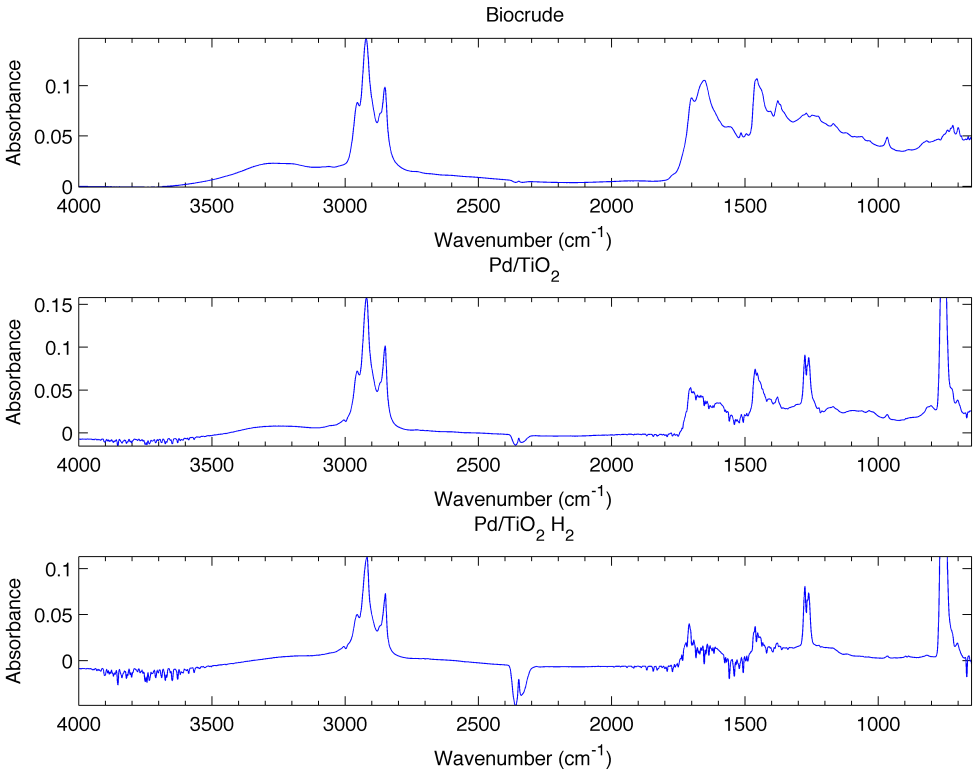

Figure B.4: $PdTiO_2$ Upgraded Bio-oil Fourier transform infrared spectrum at 400 °C for 60 min

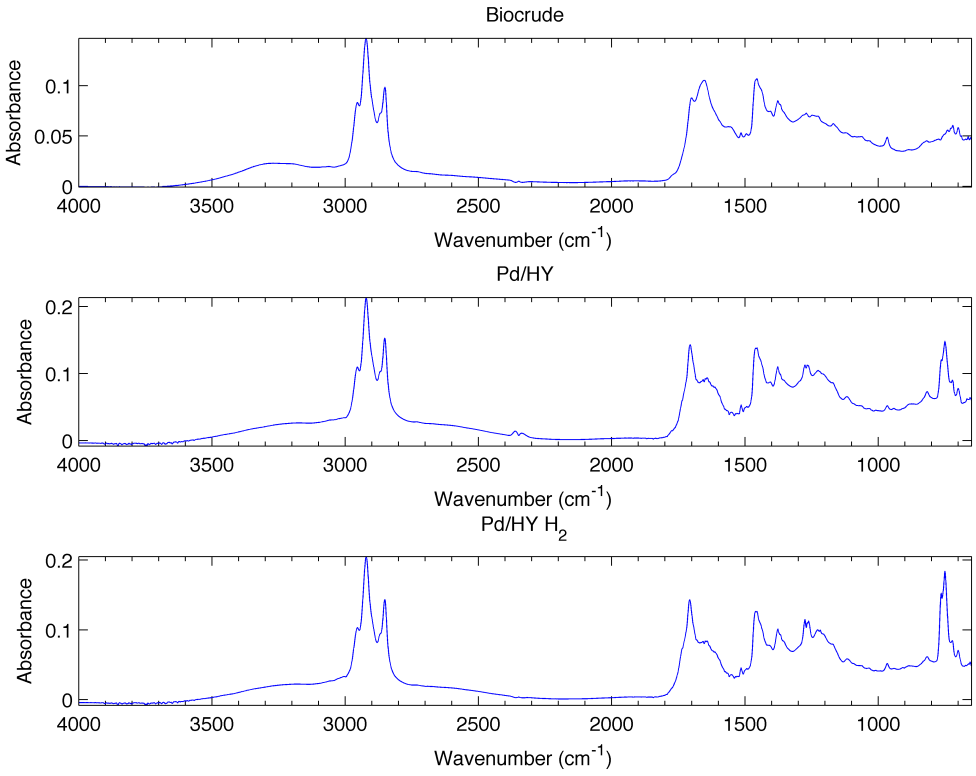

Figure B.5: Pd/HY Upgraded Bio-oil Fourier transform infrared spectrum at 400 °C for 60 min

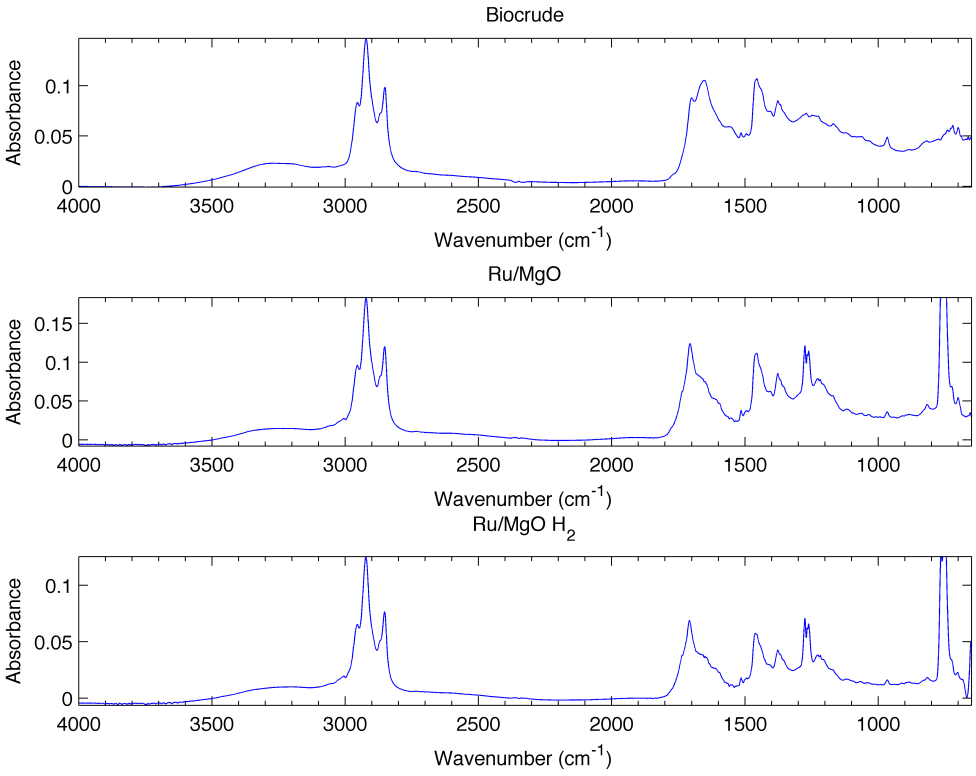

Figure B.6: Ru/MgO Upgraded Bio-oil Fourier transform infrared spectrum at 400 °C for 60 min

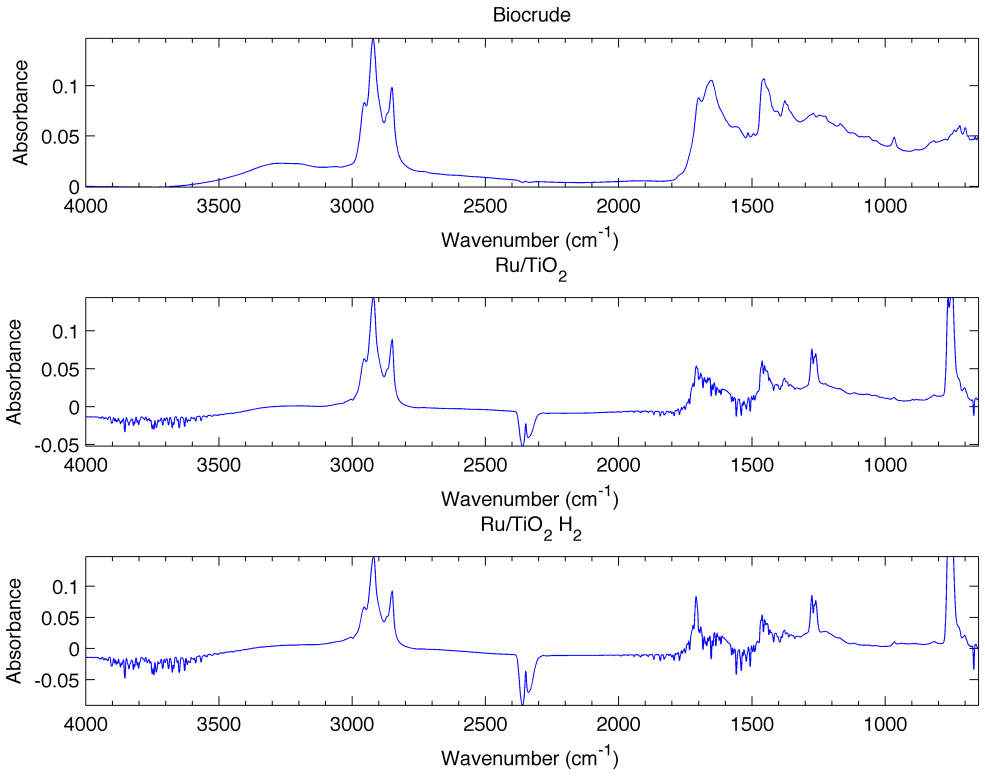

Figure B.7: $RuTiO_2$ Upgraded Bio-oil Fourier transform infrared spectrum at 400 °C for 60 min

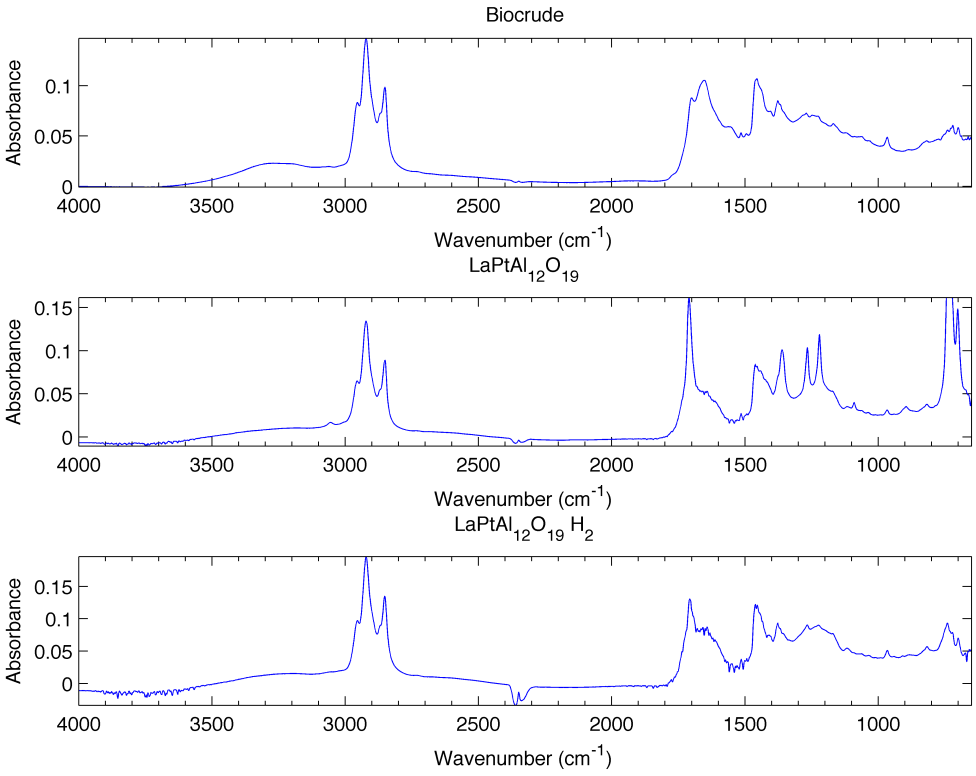

Figure B.8: $LaPtAl_{12}O_{19}$ Upgraded Bio-oil Fourier transform infrared spectrum at 400 °C for 60 min

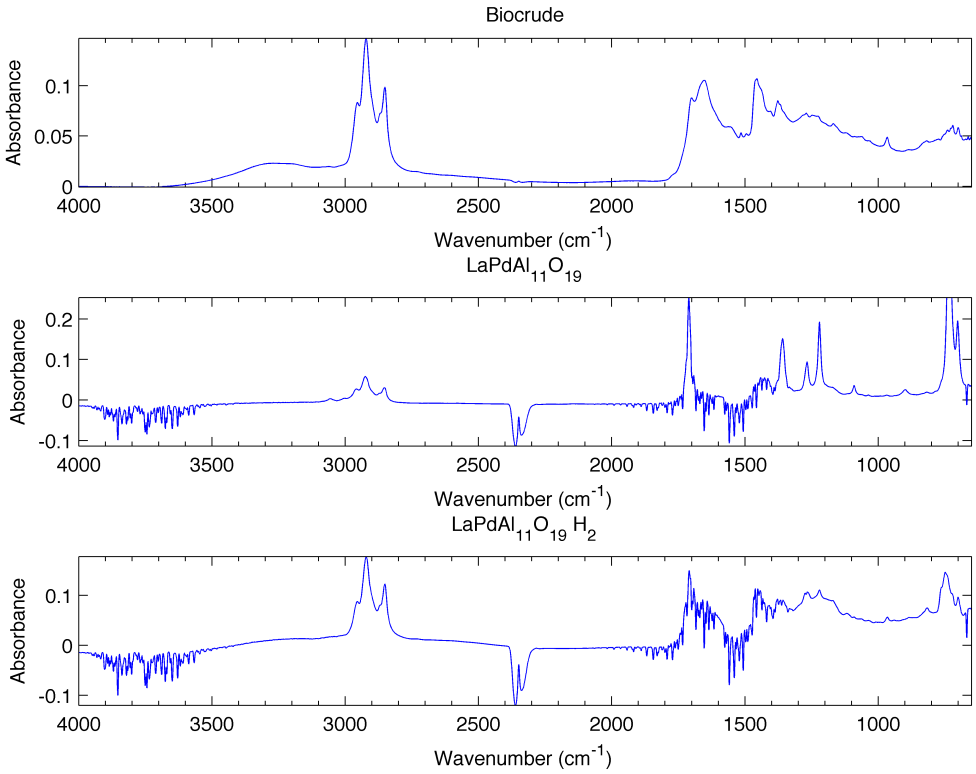

Figure B.9: $LaPdAl_{11}O_{19}$ Upgraded Bio-oil Fourier transform infrared spectrum at 400 °C for 60 min

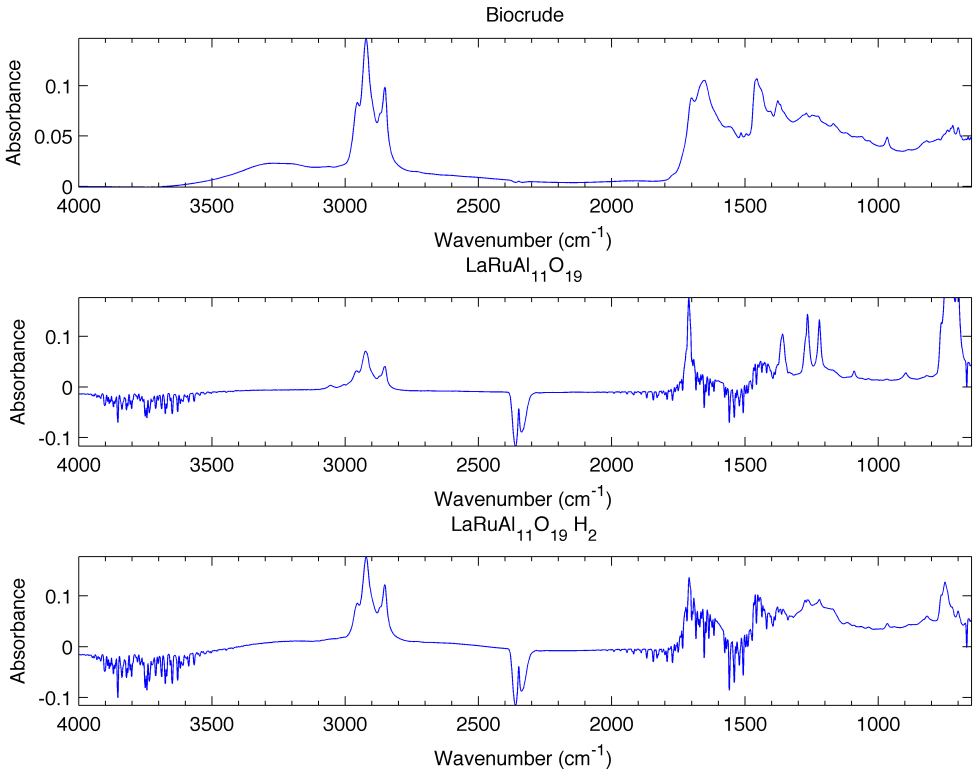

Figure B.10: $LaRuAl_{11}O_{19}$ Upgraded Bio-oil Fourier transform infrared spectrum at 400 °C for 60 min

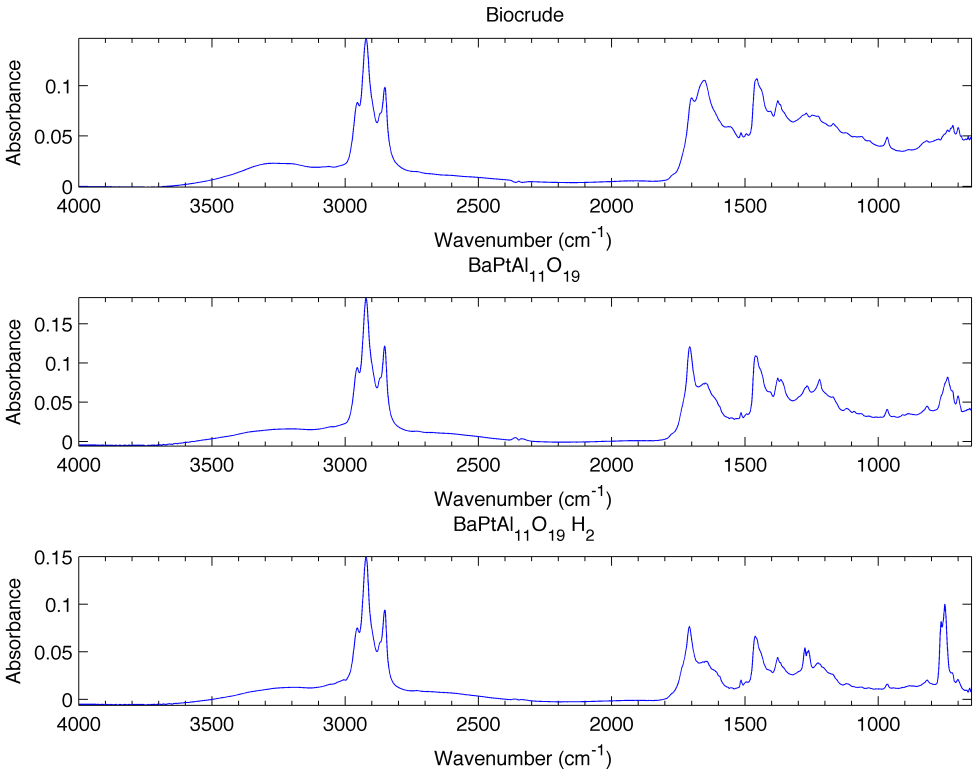

Figure B.11: $BaPtAl_{11}O_{19}$ Upgraded Bio-oil Fourier transform infrared spectrum at 400 °C for 60 min

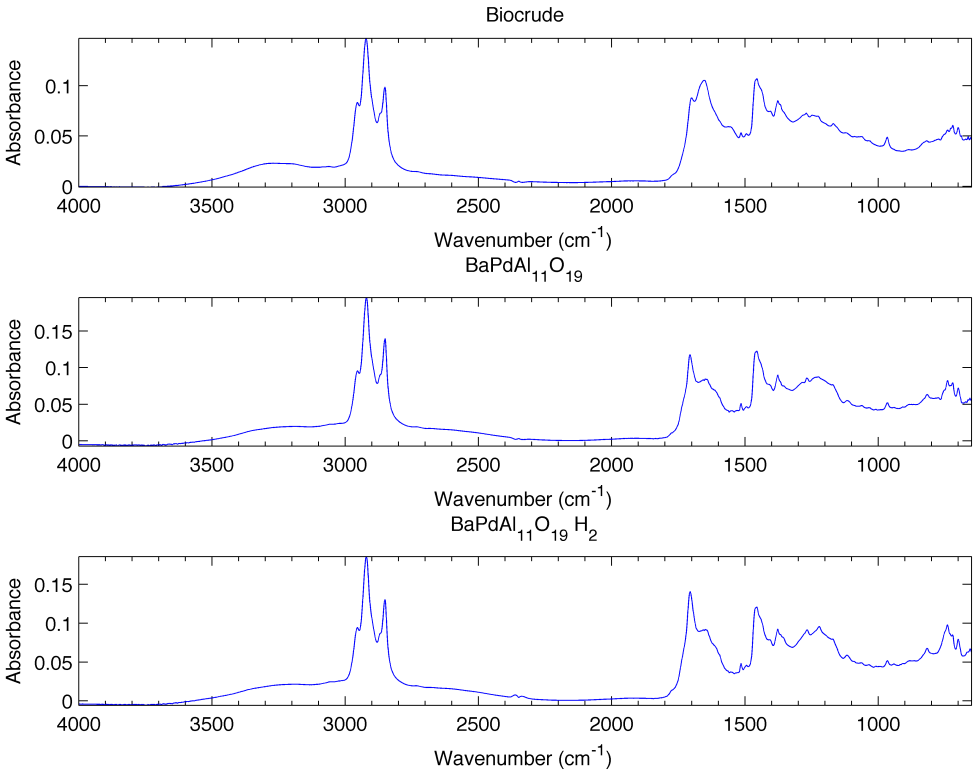

Figure B.12: $BaPdAl_{11}O_{19}$ Upgraded Bio-oil Fourier transform infrared spectrum at 400 °C for 60 min

BIBLIOGRAPHY

[1] "Annual Energy Outlook 2014 Early Release Overview," U.S. Energy Information Administration, Tech. Rep., 2014.

[2] "The Outlook for Energy: A View to 2040," ExxonMobil, Tech. Rep., 2014.

[3] C. A. S. Hall, S. Balogh, and D. J. Murphy, "What is the Minimum EROI that a Sustainable Society Must Have?" *Energies*, vol. 2, no. 1, pp. 25–47, 2009. [Online]. Available: http://www.mdpi.com/1996-1073/2/1/25

[4] D. Pimentel and T. W. Patzek, "Ethanol Production Using Corn, Switchgrass, and Wood; Biodiesel Production Using Soybean and Sunflower," *Natural Resources Research*, vol. 14, pp. 65–76, 2005. [Online]. Available: http://dx.doi.org/10.1007/s11053-005-4679-8

[5] A. E. Farrell, R. J. Plevin, B. T. Turner, A. D. Jones, M. O'Hare, and D. M. Kammen, "Ethanol Can Contribute to Energy and Environmental Goals," *Science*, vol. 311, no. 5760, pp. 506–508, 2006. [Online]. Available: http://www.sciencemag.org/content/311/5760/506.abstract

[6] N. N. Rabalais, R. E. Turner, and W. J. W. Jr., "Gulf of Mexico Hypoxia, a.k.a. "The Dead Zone"," *Annual Review of Ecology and Systematics*, vol. 33, pp. 235–263, 2002. [Online]. Available: http://www.jstor.org/stable/3069262

[7] T. Searchinger, R. Heimlich, R. A. Houghton, F. Dong, A. Elobeid, J. Fabiosa, S. Tokgoz, D. Hayes, and T.-H. Yu, "Use of u.s. croplands for biofuels increases greenhouse gases through emissions from land-use change," *Science*, vol. 319, no. 5867, pp. 1238–1240, 2008. [Online]. Available: http://www.sciencemag.org/content/319/5867/1238.abstract

[8] X. Liu, B. Saydah, P. Eranki, L. M. Colosi, B. G. Mitchell, J. Rhodes, and A. F. Clarens, "Pilot-scale data provide enhanced estimates of the life cycle energy and emissions profile of algae biofuels produced via hydrothermal liquefaction," *Bioresour. Technol.*, vol. 148, pp. 163–171, 2013. [Online]. Available: http://www.sciencedirect.com/science/article/pii/S0960852413013631

[9] D. M. Alonso, J. Q. Bond, and J. A. Dumesic, "Catalytic conversion of biomass to biofuels," *Green Chem.*, vol. 12, pp. 1493–1513, 2010. [Online]. Available: http://dx.doi.org/10.1039/C004654J

[10] E. Gies. (2014, November) For cellulosic ethanol makers, the road ahead is still uphill. Website. Yale, Environment 360. [Online]. Available: http://e360.yale.edu/feature/for_cellulosic_ethanol_makers_the_road_ahead_is_still_uphill/2821/

[11] K. Fletcher. (2014, June) POET-DSM, DuPont, Abengoa begin commissioning cellulosic plants. Website. Ethanol Producer Magazine. [Online]. Available: http://www.ethanolproducer.com/articles/11153/poet-dsm-dupont-abengoa-begin-commissioning-cellulosic-plants

[12] J. Lane. (2014, October) Update from DuPont on its Nevada project – labor shortages, new ethanol marketer deal. Website. Biofuels Digest. [Online]. Available: http://www.biofuelsdigest.com/bdigest/2014/10/28/

[13] (2014, May) How much gasoline does the United States consume? Website. U.S. Energy Information Administration. [Online]. Available: http://www.eia.gov/tools/faqs/faq.cfm?id=23&t=10

[14] K. Weyer, D. Bush, A. Darzins, and B. Willson, "Theoretical Maximum Algal Oil Production," *BioEnergy Research*, vol. 3, pp. 204–213, 2010. [Online]. Available: http://dx.doi.org/10.1007/s12155-009-9046-x

[15] A. Ben-Amotz, R. Fishler, and A. Schneller, "Chemical composition of dietary species of marine unicellular algae and rotifers with emphasis on fatty acids," *Mar. Biol.*, vol. 95, no. 1, pp. 31–36, 1987. [Online]. Available: http://dx.doi.org/10.1007/BF00447482

[16] P. Biller and A. Ross, "Potential yields and properties of oil from the hydrothermal liquefaction of microalgae with different biochemical content," *Bioresour. Technol.*, vol. 102, no. 1, pp. 215–225, 2011, special Issue: Biofuels - II: Algal Biofuels and Microbial Fuel Cells. [Online]. Available: http://www.sciencedirect.com/science/article/pii/S0960852410010096

[17] M. N. Campbell, "Biodiesel: Algae as a renewable source for liquid fuel," *Guelph Engineering Journal*, vol. 1, pp. 2 – 7, 2008.

[18] P. Kritzer and E. Dinjus, "An assessment of supercritical water oxidation (SCWO): Existing problems, possible solutions and new reactor concepts," *Chem. Eng. J.*, vol. 83, no. 3, pp. 207–214, 2001. [Online]. Available: http://www.sciencedirect.com/science/article/pii/S1385894700002552

[19] T. M. Yeh, J. G. Dickinson, A. Franck, S. Linic, L. T. Thompson, and P. E. Savage, "Hydrothermal catalytic production of fuels and chemicals from aquatic biomass," *J. Chem. Technol. Biotechnol.*, vol. 88, no. 1, pp. 13–24, 2013. [Online]. Available: http://dx.doi.org/10.1002/jctb.3933

[20] S. M. Heilmann, H. T. Davis, L. R. Jader, P. A. Lefebvre, M. J. Sadowsky, F. J. Schendel, M. G. von Keitz, and K. J. Valentas, "Hydrothermal carbonization

of microalgae," *Biomass and Bioenergy*, vol. 34, no. 6, pp. 875 – 882, 2010. [Online]. Available: http://www.sciencedirect.com/science/article/pii/S0961953410000462

[21] S. M. Heilmann, L. R. Jader, L. A. Harned, M. J. Sadowsky, F. J. Schendel, P. A. Lefebvre, M. G. von Keitz, and K. J. Valentas, "Hydrothermal carbonization of microalgae ii. fatty acid, char, and algal nutrient products," *Applied Energy*, vol. 88, no. 10, pp. 3286 – 3290, 2011, special Issue of Energy from algae: Current status and future trends. [Online]. Available: http://www.sciencedirect.com/science/article/pii/S0306261910005611

[22] R. B. Levine, C. O. S. Sierra, R. Hockstad, W. Obeid, P. G. Hatcher, and P. E. Savage, "The use of hydrothermal carbonization to recycle nutrients in algal biofuel production," *Environmental Progress & Sustainable Energy*, vol. 32, no. 4, pp. 962–975, 2013. [Online]. Available: http://dx.doi.org/10.1002/ep.11812

[23] T. M. Brown, P. Duan, and P. E. Savage, "Hydrothermal Liquefaction and Gasification of Nannochloropsis sp." *Energy & Fuels*, vol. 24, no. 6, pp. 3639–3646, 2011. [Online]. Available: http://pubs.acs.org/doi/abs/10.1021/ef100203u

[24] U. Jena and K. C. Das, "Comparative Evaluation of Thermochemical Liquefaction and Pyrolysis for Bio-Oil Production from Microalgae," *Energy & Fuels*, vol. 25, no. 11, pp. 5472–5482, 2011. [Online]. Available: http://pubs.acs.org/doi/abs/10.1021/ef201373m

[25] L. Garcia Alba, C. Torri, C. Samorì, J. van der Spek, D. Fabbri, S. R. A. Kersten, and D. W. F. W. Brilman, "Hydrothermal Treatment (HTT) of Microalgae: Evaluation of the Process As Conversion Method in an Algae Biorefinery Concept," *Energy & Fuels*, vol. 26, no. 1, pp. 642–657, 2012. [Online]. Available: http://pubs.acs.org/doi/abs/10.1021/ef201415s

[26] D. L. Barreiro, W. Prins, F. Ronsse, and W. Brilman, "Hydrothermal liquefaction (HTL) of microalgae for biofuel production: State of the art review and future prospects," *Biomass and Bioenergy*, vol. 53, pp. 113 – 127, 2013, 20th European Biomass Conference. [Online]. Available: http://www.sciencedirect.com/science/article/pii/S0961953412005272

[27] T. Minowa, S. Yokoyama, M. Kishimoto, and T. Okakura, "Oil production from algal cells of Dunaliella tertiolecta by direct thermochemical liquefaction," *Fuel*, vol. 74, no. 12, pp. 1735–1738, 1995. [Online]. Available: http://www.sciencedirect.com/science/article/pii/001623619580001X

[28] J. Akhtar and N. A. S. Amin, "A review on process conditions for optimum bio-oil yield in hydrothermal liquefaction of biomass," *Renewable and Sustainable Energy Reviews*, vol. 15, no. 3, pp. 1615–1624, 2011.

[Online]. Available: http://www.sciencedirect.com/science/article/pii/S1364032110004235

[29] P. J. Valdez, J. G. Dickinson, and P. E. Savage, "Characterization of Product Fractions from Hydrothermal Liquefaction of Nannochloropsis sp. and the Influence of Solvents," *Energy & Fuels*, vol. 25, no. 7, pp. 3235–3243, 2011. [Online]. Available: http://pubs.acs.org/doi/abs/10.1021/ef2004046

[30] P. J. Valdez, M. C. Nelson, H. Y. Wang, X. N. Lin, and P. E. Savage, "Hydrothermal liquefaction of nannochloropsis sp.: Systematic study of process variables and analysis of the product fractions," *Biomass and Bioenergy*, vol. 46, pp. 317 – 331, 2012, international Conference on Lignocellulosic ethanol. [Online]. Available: http://www.sciencedirect.com/science/article/pii/S0961953412003236

[31] Y. Dote, S. Inoue, T. Ogi, and S.-y. Yokoyama, "Distribution of nitrogen to oil products from liquefaction of amino acids," *Bioresour. Technol.*, vol. 64, no. 2, pp. 157–160, 1998. [Online]. Available: http://www.sciencedirect.com/science/article/pii/S0960852497000795

[32] Y. Dote, S. Inoue, T. Ogi, and S.-y. Yokoyama, "Studies on the direct liquefaction of protein-contained biomass: The distribution of nitrogen in the products," *Biomass and Bioenergy*, vol. 11, no. 6, pp. 491–498, 1996. [Online]. Available: http://www.sciencedirect.com/science/article/pii/S0961953496000451

[33] D. C. Elliott, T. R. Hart, A. J. Schmidt, G. G. Neuenschwander, L. J. Rotness, M. V. Olarte, A. H. Zacher, K. O. Albrecht, R. T. Hallen, and J. E. Holladay, "Process development for hydrothermal liquefaction of algae feedstocks in a continuous-flow reactor," *Algal Research*, vol. 2, no. 4, pp. 445 – 454, 2013. [Online]. Available: http://www.sciencedirect.com/science/article/pii/S2211926413000878

[34] J. G. Speight, *The Chemistry and Technology of Petroleum*, 3rd ed. Marcel Dekker, Inc., 1999.

[35] C. Torri, L. Garcia Alba, C. Samorì, D. Fabbri, and D. W. F. W. Brilman, "Hydrothermal Treatment (HTT) of Microalgae: Detailed Molecular Characterization of HTT Oil in View of HTT Mechanism Elucidation," *Energy & Fuels*, vol. 26, no. 1, pp. 658–671, 2012. [Online]. Available: http://pubs.acs.org/doi/abs/10.1021/ef201417e

[36] D. R. Vardon, B. Sharma, J. Scott, G. Yu, Z. Wang, L. Schideman, Y. Zhang, and T. J. Strathmann, "Chemical properties of biocrude oil from the hydrothermal liquefaction of Spirulina algae, swine manure, and digested anaerobic sludge," *Bioresource Technology*, vol. 102, no. 17, pp. 8295 – 8303, 2011. [Online]. Available: http://www.sciencedirect.com/science/article/pii/S0960852411008686

[37] D. Zhou, L. Zhang, S. Zhang, H. Fu, and J. Chen, "Hydrothermal Liquefaction of Macroalgae Enteromorpha prolifera to Bio-oil," *Energy & Fuels*, vol. 24, no. 7, pp. 4054–4061, 2010. [Online]. Available: http://pubs.acs.org/doi/abs/10.1021/ef100151h

[38] M. Snåre, I. Kubičková, P. Mäki-Arvela, K. Eränen, and D. Y. Murzin, "Heterogeneous Catalytic Deoxygenation of Stearic Acid for Production of Biodiesel," *Ind. Eng. Chem. Res.*, vol. 45, no. 16, pp. 5708–5715, 2006. [Online]. Available: http://pubs.acs.org/doi/abs/10.1021/ie060334i

[39] C. R. Fischer, A. A. Peterson, and J. W. Tester, "Production of C3 Hydrocarbons from Biomass via Hydrothermal Carboxylate Reforming," *Ind. Eng. Chem. Res.*, vol. 50, no. 8, pp. 4420–4424, 2011. [Online]. Available: http://pubs.acs.org/doi/abs/10.1021/ie1023386

[40] T. Kalnes, T. Marker, and D. R. Shonnard, "Green Diesel: A Second Generation Biofuel," *International Journal of Chemical Reactor Engineering*, vol. 5, pp. 1542–6580, 2007. [Online]. Available: http://dx.doi.org/10.2202/1542-6580.1554

[41] J. G. Immer and H. H. Lamb, "Fed-Batch Catalytic Deoxygenation of Free Fatty Acids," *Energy & Fuels*, vol. 24, no. 10, pp. 5291–5299, 2010. [Online]. Available: http://pubs.acs.org/doi/abs/10.1021/ef100576z

[42] J. Fu, F. Shi, L. T. Thompson, X. Lu, and P. E. Savage, "Activated Carbons for Hydrothermal Decarboxylation of Fatty Acids," *ACS Catal.*, vol. 1, no. 3, pp. 227–231, 2011. [Online]. Available: http://pubs.acs.org/doi/abs/10.1021/cs1001306

[43] J. Fu, X. Lu, and P. E. Savage, "Hydrothermal Decarboxylation and Hydrogenation of Fatty Acids over Pt/C," *ChemSusChem*, vol. 4, no. 4, pp. 481–486, 2011. [Online]. Available: http://dx.doi.org/10.1002/cssc.201000370

[44] F. Baldiraghi, M. D. Stanislao, G. Faraci, C. Perego, T. Marker, C. Gosling, P. Kokayeff, T. Kalnes, and R. Marinangeli, *Ecofining: New Process for Green Diesel Production from Vegetable Oil*. Wiley-VCH Verlag GmbH & Co. KGaA, 2009, pp. 427–438. [Online]. Available: http://dx.doi.org/10.1002/9783527629114.ch8

[45] P. Mäki-Arvela, M. Snåre, K. Eränen, J. Myllyoja, and D. Murzin, "Continuous decarboxylation of lauric acid over Pd/C catalyst," *Fuel*, vol. 87, no. 17–18, pp. 3543–3549, 2008. [Online]. Available: http://www.sciencedirect.com/science/article/pii/S0016236108002676

[46] I. Simakova, O. Simakova, M.-A. Päivi, and D. Y. Murzin, "Decarboxylation of fatty acids over Pd supported on mesoporous carbon," *Catal. Today*,

vol. 150, no. 1-2, pp. 28–31, 2010, carbon for Catalysis: CarboCat-III Symposium, Berlin, Germany, 2008. [Online]. Available: http://www.sciencedirect.com/science/article/pii/S0920586109004301

[47] M. Snåre, I. Kubicková, P. Mäki-Arvela, K. Eränen, J. W. Murzin, and D.Yu., "Production of diesel fuel from renewable feeds: Kinetics of ethyl stearate decarboxylation," *Chem. Eng. J.*, vol. 134, no. 1-3, pp. 29–34, 2007. [Online]. Available: http://www.sciencedirect.com/science/article/pii/S1385894707002197

[48] J. G. Immer, M. J. Kelly, and H. H. Lamb, "Catalytic reaction pathways in liquid-phase deoxygenation of C18 free fatty acids," *Appl. Catal., A*, vol. 375, no. 1, pp. 134–139, 2010. [Online]. Available: http://www.sciencedirect.com/science/article/pii/S0926860X09008710

[49] S. Lestari, P. Mäki-Arvela, H. Bernas, O. Simakova, R. Sjöholm, J. Beltramini, G. Q. M. Lu, J. Myllyoja, I. Simakova, and D. Y. Murzin, "Catalytic Deoxygenation of Stearic Acid in a Continuous Reactor over a Mesoporous Carbon-Supported Pd Catalyst," *Energy & Fuels*, vol. 23, no. 8, pp. 3842–3845, 2009. [Online]. Available: http://pubs.acs.org/doi/abs/10.1021/ef900110t

[50] J. Fu, X. Lu, and P. E. Savage, "Catalytic hydrothermal deoxygenation of palmitic acid," *Energy Environ. Sci.*, vol. 3, pp. 311–317, 2010. [Online]. Available: http://dx.doi.org/10.1039/B923198F

[51] M. Watanabe, H. Inomata, R. L. S. Jr., and K. Arai, "Catalytic decarboxylation of acetic acid with zirconia catalyst in supercritical water," *Appl. Catal., A*, vol. 219, no. 1–2, pp. 149 – 156, 2001. [Online]. Available: http://www.sciencedirect.com/science/article/pii/S0926860X01006779

[52] M. Watanabe, T. Iida, and H. Inomata, "Decomposition of a long chain saturated fatty acid with some additives in hot compressed water," *Energy Conversion and Management*, vol. 47, no. 18-19, pp. 3344 – 3350, 2006. [Online]. Available: http://www.sciencedirect.com/science/article/pii/S0196890406000410

[53] J. Lu, S. Behtash, and A. Heyden, "Theoretical Investigation of the Reaction Mechanism of the Decarboxylation and Decarbonylation of Propanoic Acid on Pd(111) Model Surfaces," *The Journal of Physical Chemistry C*, vol. 116, no. 27, pp. 14 328–14 341, 2012. [Online]. Available: http://pubs.acs.org/doi/abs/10.1021/jp301926t

[54] H. H. Lamb, L. Sremaniak, and J. L. Whitten, "Reaction pathways for butanoic acid decarboxylation on the (111) surface of a Pd nanoparticle," *Surf. Sci.*, vol. 607, pp. 130–137, 2013. [Online]. Available: http://www.sciencedirect.com/science/article/pii/S0039602812003160

[55] P. Duan and P. E. Savage, "Upgrading of crude algal bio-oil in supercritical water," *Bioresour. Technol.*, vol. 102, no. 2, pp. 1899–1906, 2011. [Online]. Available: http://www.sciencedirect.com/science/article/pii/S0960852410013659

[56] U. Poth, *Drying Oils and Related Products*. Wiley-VCH Verlag GmbH & Co. KGaA, 2000. [Online]. Available: http://dx.doi.org/10.1002/14356007.a09_055

[57] J. Asomaning, P. Mussone, and D. C. Bressler, "Thermal deoxygenation and pyrolysis of oleic acid," *J. Anal. Appl. Pyrolysis*, vol. 105, pp. 1 – 7, 2014. [Online]. Available: http://www.sciencedirect.com/science/article/pii/S0165237013002003

[58] S. Naik, V. V. Goud, P. K. Rout, and A. K. Dalai, "Production of first and second generation biofuels: A comprehensive review," *Renewable and Sustainable Energy Reviews*, vol. 14, no. 2, pp. 578 – 597, 2010. [Online]. Available: http://www.sciencedirect.com/science/article/pii/S1364032109002342

[59] M. Snåre, I. Kubicková, P. Mäki-Arvela, D. Chichova, K. Eränen, and D. Murzin, "Catalytic deoxygenation of unsaturated renewable feedstocks for production of diesel fuel hydrocarbons," *Fuel*, vol. 87, no. 6, pp. 933–945, 2008. [Online]. Available: http://www.sciencedirect.com/science/article/pii/S0016236107002840

[60] W.-C. Wang, N. Thapaliya, A. Campos, L. F. Stikeleather, and W. L. Roberts, "Hydrocarbon fuels from vegetable oils via hydrolysis and thermo-catalytic decarboxylation," *Fuel*, vol. 95, pp. 622 – 629, 2012. [Online]. Available: http://www.sciencedirect.com/science/article/pii/S0016236111008106

[61] E. Santillan-Jimenez and M. Crocker, "Catalytic deoxygenation of fatty acids and their derivatives to hydrocarbon fuels via decarboxylation/decarbonylation," *J. Chem. Technol. Biotechnol.*, vol. 87, no. 8, pp. 1041–1050, 2012. [Online]. Available: http://dx.doi.org/10.1002/jctb.3775

[62] E. L. Kunkes, D. A. Simonetti, R. M. West, J. C. Serrano-Ruiz, C. A. Gärtner, and J. A. Dumesic, "Catalytic Conversion of Biomass to Monofunctional Hydrocarbons and Targeted Liquid-Fuel Classes," *Science*, vol. 322, no. 5900, pp. 417–421, 2008. [Online]. Available: http://www.sciencemag.org/content/322/5900/417.abstract

[63] M. Chia, Y. J. Pagán-Torres, D. Hibbitts, Q. Tan, H. N. Pham, A. K. Datye, M. Neurock, R. J. Davis, and J. A. Dumesic, "Selective Hydrogenolysis of Polyols and Cyclic Ethers over Bifunctional Surface Sites on Rhodium–Rhenium Catalysts," *J. Am. Chem. Soc.*, 2011. [Online]. Available: http://pubs.acs.org/doi/abs/10.1021/ja2038358

[64] D. Wang, S. H. Hakim, D. Martin Alonso, and J. A. Dumesic, "A highly selective route to linear alpha olefins from biomass-derived lactones and unsaturated acids," *Chem. Commun.*, vol. 49, pp. 7040–7042, 2013. [Online]. Available: http://dx.doi.org/10.1039/C3CC43587C

[65] J. G. Dickinson, J. T. Poberezny, and P. E. Savage, "Deoxygenation of benzofuran in supercritical water over a platinum catalyst," *Applied Catalysis B: Environmental*, vol. 123–124, pp. 357–366, 2012. [Online]. Available: http://www.sciencedirect.com/science/article/pii/S0926337312002019

[66] H. Ohta, H. Kobayashi, K. Hara, and A. Fukuoka, "Hydrodeoxygenation of phenols as lignin models under acid-free conditions with carbon-supported platinum catalysts," *Chem. Commun.*, vol. 47, pp. 12 209–12 211, 2011. [Online]. Available: http://dx.doi.org/10.1039/C1CC14859A

[67] M. Badawi, J. Paul, S. Cristol, E. Payen, Y. Romero, F. Richard, S. Brunet, D. Lambert, X. Portier, A. Popov, E. Kondratieva, J. Goupil, J. E. Fallah, J. Gilson, L. Mariey, A. Travert, and F. Maug, "Effect of water on the stability of mo and como hydrodeoxygenation catalysts: A combined experimental and {DFT} study," *Journal of Catalysis*, vol. 282, no. 1, pp. 155 – 164, 2011. [Online]. Available: http://www.sciencedirect.com/science/article/pii/S0021951711001928

[68] J. G. Dickinson and P. E. Savage, "Stability and activity of pt and ni catalysts for hydrodeoxygenation in supercritical water," *Journal of Molecular Catalysis A: Chemical*, vol. 388389, pp. 56 – 65, 2014, special Issue on Biomass Catalysis. [Online]. Available: http://www.sciencedirect.com/science/article/pii/S1381116913002860

[69] C. Zhao and J. A. Lercher, "Selective Hydrodeoxygenation of Lignin-Derived Phenolic Monomers and Dimers to Cycloalkanes on Pd/C and HZSM-5 Catalysts," *ChemCatChem*, vol. 4, no. 1, pp. 64–68, 2012. [Online]. Available: http://dx.doi.org/10.1002/cctc.201100273

[70] C. Zhao, S. Kasakov, J. He, and J. A. Lercher, "Comparison of kinetics, activity and stability of Ni/HZSM-5 and Ni/Al_2O_3-HZSM-5 for phenol hydrodeoxygenation," *Journal of Catalysis*, vol. 296, pp. 12 – 23, 2012. [Online]. Available: http://www.sciencedirect.com/science/article/pii/S0021951712002746

[71] U. Jena, K. Das, and J. Kastner, "Effect of operating conditions of thermochemical liquefaction on biocrude production from Spirulina platensis," *Bioresour. Technol.*, vol. 102, no. 10, pp. 6221–6229, 2011. [Online]. Available: http://www.sciencedirect.com/science/article/pii/S0960852411002422

[72] P. Duan and P. E. Savage, "Catalytic hydrothermal hydrodenitrogenation of pyridine," *Applied Catalysis B: Environmental*, vol. 108-109, pp. 54–60,

2011. [Online]. Available: http://www.sciencedirect.com/science/article/pii/S0926337311003766

[73] P.-Q. Yuan, Z.-M. Cheng, X.-Y. Zhang, and W.-K. Yuan, "Catalytic denitrogenation of hydrocarbons through partial oxidation in supercritical water," *Fuel*, vol. 85, no. 3, pp. 367 – 373, 2006. [Online]. Available: http://www.sciencedirect.com/science/article/pii/S0016236105002395

[74] P. Yuan, Z. Cheng, W. Jiang, R. Zhang, and W. Yuan, "Catalytic desulfurization of residual oil through partial oxidation in supercritical water," *The Journal of Supercritical Fluids*, vol. 35, no. 1, pp. 70–75, 2005. [Online]. Available: http://www.sciencedirect.com/science/article/pii/S0896844604002785

[75] T. Adschiri, R. Shibata, T. Sato, M. Watanabe, and K. Arai, "Catalytic hydrodesulfurization of dibenzothiophene through partial oxidation and a water-gas shift reaction in supercritical water," *Ind. Eng. Chem. Res.*, vol. 37, no. 7, pp. 2634–2638, 1998. [Online]. Available: http://pubs.acs.org/doi/abs/10.1021/ie970751i

[76] K. Arai, T. Adschiri, and M. Watanabe, "Hydrogenation of Hydrocarbons through Partial Oxidation in Supercritical Water," *Industrial & Engineering Chemistry Research*, vol. 39, no. 12, pp. 4697–4701, 2000. [Online]. Available: http://dx.doi.org/10.1021/ie000326g

[77] P. Duan and P. E. Savage, "Catalytic hydrotreatment of crude algal bio-oil in supercritical water," *Applied Catalysis B: Environmental*, vol. 104, no. 1–2, pp. 136–143, 2011. [Online]. Available: http://www.sciencedirect.com/science/article/pii/S0926337311000907

[78] P. Duan and P. E. Savage, "Catalytic treatment of crude algal bio-oil in supercritical water: optimization studies," *Energy Environ. Sci.*, vol. 4, pp. 1447–1456, 2011. [Online]. Available: http://dx.doi.org/10.1039/C0EE00343C

[79] P. Duan, X. Bai, Y. Xu, A. Zhang, F. Wang, L. Zhang, and J. Miao, "Catalytic upgrading of crude algal oil using platinum/gamma alumina in supercritical water," *Fuel*, vol. 109, pp. 225 – 233, 2013. [Online]. Available: http://www.sciencedirect.com/science/article/pii/S0016236112010988

[80] P. Duan, Y. Xu, and X. Bai, "Upgrading of crude duckweed bio-oil in subcritical water," *Energy & Fuels*, vol. 27, no. 8, pp. 4729–4738, 2013. [Online]. Available: http://dx.doi.org/10.1021/ef4009168

[81] X. Bai, P. Duan, Y. Xu, A. Zhang, and P. E. Savage, "Hydrothermal catalytic processing of pretreated algal oil: A catalyst screening study," *Fuel*, vol. 120, pp. 141 – 149, 2014. [Online]. Available: http://www.sciencedirect.com/science/article/pii/S0016236113011496

[82] D. C. Elliott, "Catalytic hydrothermal gasification of biomass," *Biofuels, Bioprod. Biorefin.*, vol. 2, no. 3, pp. 254–265, 2008. [Online]. Available: http://dx.doi.org/10.1002/bbb.74

[83] A. A. Peterson, F. Vogel, R. P. Lachance, M. Froling, M. J. Antal, Jr., and J. W. Tester, "Thermochemical biofuel production in hydrothermal media: A review of sub- and supercritical water technologies," *Energy Environ. Sci.*, vol. 1, pp. 32–65, 2008. [Online]. Available: http://dx.doi.org/10.1039/B810100K

[84] M. Osada, N. Hiyoshi, O. Sato, K. Arai, and M. Shirai, "Effect of sulfur on catalytic gasification of lignin in supercritical water," *Energy Fuels*, vol. 21, no. 3, pp. 1400–1405, 2007. [Online]. Available: http://pubs.acs.org/doi/abs/10.1021/ef060636x

[85] Q. Guan, C. Wei, and P. E. Savage, "Hydrothermal Gasification of Nannochloropsis sp. with Ru/C," *Energy & Fuels*, vol. 26, no. 7, pp. 4575–4582, 2012. [Online]. Available: http://dx.doi.org/10.1021/ef3007992

[86] M. H. Waldner, F. Krumeich, and F. Vogel, "Synthetic natural gas by hydrothermal gasification of biomass: Selection procedure towards a stable catalyst and its sodium sulfate tolerance," *The Journal of Supercritical Fluids*, vol. 43, no. 1, pp. 91–105, 2007. [Online]. Available: http://www.sciencedirect.com/science/article/pii/S0896844607001441

[87] S. Stucki, F. Vogel, C. Ludwig, A. G. Haiduc, and M. Brandenberger, "Catalytic gasification of algae in supercritical water for biofuel production and carbon capture," *Energy Environ. Sci.*, vol. 2, pp. 535–541, 2009. [Online]. Available: http://dx.doi.org/10.1039/B819874H

[88] D. C. Elliott, T. R. Hart, and G. G. Neuenschwander, "Chemical Processing in High-Pressure Aqueous Environments. 8. Improved Catalysts for Hydrothermal Gasification," *Ind. Eng. Chem. Res.*, vol. 45, no. 11, pp. 3776–3781, 2006. [Online]. Available: http://pubs.acs.org/doi/abs/10.1021/ie060031o

[89] R. M. Ravenelle, J. R. Copeland, W.-G. Kim, J. C. Crittenden, and C. Sievers, "Structural changes of γ-Al2O3-supported catalysts in hot liquid water," *ACS Catalysis*, vol. 1, no. 5, pp. 552–561, 2011.

[90] R. M. Ravenelle, F. Z. Diallo, J. C. Crittenden, and C. Sievers, "Effects of Metal Precursors on the Stability and Observed Reactivity of Pt/γ-Al_2O_3 Catalysts in Aqueous Phase Reactions," *ChemCatChem*, vol. 4, no. 4, pp. 492–494, 2012. [Online]. Available: http://dx.doi.org/10.1002/cctc.201100307

[91] R. Ravenelle, J. Copeland, A. Van Pelt, J. Crittenden, and C. Sievers, "Stability of Pt/γ-Al_2O_3 Catalysts in Model Biomass Solutions," *Top. Catal.*,

vol. 55, pp. 162–174, 2012, 10.1007/s11244-012-9785-3. [Online]. Available: http://dx.doi.org/10.1007/s11244-012-9785-3

[92] N. Luo, X. Fu, F. Cao, T. Xiao, and P. P. Edwards, "Glycerol aqueous phase reforming for hydrogen generation over Pt catalyst - Effect of catalyst composition and reaction conditions," *Fuel*, vol. 87, no. 17-18, pp. 3483–3489, 2008. [Online]. Available: http://www.sciencedirect.com/science/article/pii/S0016236108002640

[93] M. F. Johnson, "Surface area stability of aluminas," *Journal of Catalysis*, vol. 123, no. 1, pp. 245 – 259, 1990. [Online]. Available: http://www.sciencedirect.com/science/article/pii/002195179090173H

[94] V. T. Thanh Ho, K. C. Pillai, H.-L. Chou, C.-J. Pan, J. Rick, W.-N. Su, B.-J. Hwang, J.-F. Lee, H.-S. Sheu, and W.-T. Chuang, "Robust non-carbon ti0.7ru0.3o2 support with co-catalytic functionality for pt: enhances catalytic activity and durability for fuel cells," *Energy Environ. Sci.*, vol. 4, pp. 4194–4200, 2011. [Online]. Available: http://dx.doi.org/10.1039/C1EE01522B

[95] Y. Matsumura, X. Xu, and J. M. Antal, "Gasification characteristics of an activated carbon in supercritical water," *Carbon*, vol. 35, no. 6, pp. 819–824, 1997. [Online]. Available: http://www.sciencedirect.com/science/article/pii/S0008622397000183

[96] S. J. Tauster, S. C. Fung, and R. L. Garten, "Strong metal-support interactions. group 8 noble metals supported on titanium dioxide," *Journal of the American Chemical Society*, vol. 100, no. 1, pp. 170–175, 1978. [Online]. Available: http://dx.doi.org/10.1021/ja00469a029

[97] J. B. Butt and E. E. Petersen, *Activation, Deactivation, and Poisoning of Catalysts*. Academic Press, 1988.

[98] R. Hughes, *Deactivation of Catalysts*. London; Orlando: Academic, 1984.

[99] S. I. Sanchez, M. D. Moser, and S. A. Bradley, "Mechanistic Study of Pt–Re/γ-Al2O3 Catalyst Deactivation by Chemical Imaging of Carbonaceous Deposits Using Advanced X-ray Detection in Scanning Transmission Electron Microscopy," *ACS Catal.*, vol. 0, pp. 220–228, 2014. [Online]. Available: http://pubs.acs.org/doi/abs/10.1021/cs4008123

[100] G. W. Huber, J. W. Shabaker, S. T. Evans, and J. A. Dumesic, "Aqueous-phase reforming of ethylene glycol over supported Pt and Pd bimetallic catalysts," *Applied Catalysis B: Environmental*, vol. 62, no. 3-4, pp. 226–235, 2006. [Online]. Available: http://www.sciencedirect.com/science/article/pii/S0926337305002870

[101] M. Salciccioli, Y. Chen, and D. G. Vlachos, "Density Functional Theory-Derived Group Additivity and Linear Scaling Methods for Prediction of

Oxygenate Stability on Metal Catalysts: Adsorption of Open-Ring Alcohol and Polyol Dehydrogenation Intermediates on Pt-Based Metals," *The Journal of Physical Chemistry C*, vol. 114, no. 47, pp. 20 155–20 166, 2010. [Online]. Available: http://pubs.acs.org/doi/abs/10.1021/jp107836a

[102] H.-Y. Ma and G.-C. Wang, "Theoretical study of 1,3-cyclohexadiene dehydrogenation on Pt (111), Pt3Sn/Pt (111), and Pt2Sn/Pt (111) surfaces," *J. Catal.*, vol. 281, no. 1, pp. 63–75, 2011. [Online]. Available: http://www.sciencedirect.com/science/article/pii/S0021951711001151

[103] M.-L. Yang, Y.-A. Zhu, X.-G. Zhou, Z.-J. Sui, and D. Chen, "First-Principles Calculations of Propane Dehydrogenation over PtSn Catalysts," *ACS Catal.*, vol. 2, no. 6, pp. 1247–1258, 2012. [Online]. Available: http://pubs.acs.org/doi/abs/10.1021/cs300031d

[104] A. Iglesias-Juez, A. M. Beale, K. Maaijen, T. C. Weng, P. Glatzel, and B. M. Weckhuysen, "A combined in situ time-resolved UV-Vis, Raman and high-energy resolution X-ray absorption spectroscopy study on the deactivation behavior of Pt and PtSn propane dehydrogenation catalysts under industrial reaction conditions," *J. Catal.*, vol. 276, no. 2, pp. 268–279, 2010. [Online]. Available: http://www.sciencedirect.com/science/article/pii/S0021951710003295

[105] S. Miguel, A. Castro, O. Scelza, J. Fierro, and J. Soria, "FTIR and XPS study of supported PtSn catalysts used for light paraffins dehydrogenation," *Catal. Lett.*, vol. 36, pp. 201–206, 1996. [Online]. Available: http://dx.doi.org/10.1007/BF00807620

[106] Z.-F. Xu and Y. Wang, "Effects of Alloyed Metal on the Catalysis Activity of Pt for Ethanol Partial Oxidation: Adsorption and Dehydrogenation on Pt3M (M = Pt, Ru, Sn, Re, Rh, and Pd)," *The Journal of Physical Chemistry C*, vol. 115, no. 42, pp. 20 565–20 571, 2011. [Online]. Available: http://pubs.acs.org/doi/abs/10.1021/jp206051k

[107] Y.-L. Tsai, C. Xu, and B. E. Koel, "Chemisorption of ethylene, propylene and isobutylene on ordered Sn/Pt(111) surface alloys," *Surf. Sci.*, vol. 385, no. 1, pp. 37–59, 1997. [Online]. Available: http://www.sciencedirect.com/science/article/pii/S0039602897001143

[108] B. K. Vu, M. B. Song, I. Y. Ahn, Y.-W. Suh, D. J. Suh, W.-I. Kim, H.-L. Koh, Y. G. Choi, and E. W. Shin, "Pt-Sn alloy phases and coke mobility over Pt-Sn/Al2O3 and Pt-Sn/ZnAl2O4 catalysts for propane dehydrogenation," *Appl. Catal., A*, vol. 400, no. 1-2, pp. 25–33, 2011. [Online]. Available: http://www.sciencedirect.com/science/article/pii/S0926860X11002444

[109] M. Chiappero, P. T. M. Do, S. Crossley, L. L. Lobban, and D. E. Resasco, "Direct conversion of triglycerides to olefins and paraffins over

noble metal supported catalysts," *Fuel*, vol. 90, no. 3, pp. 1155–1165, 2011. [Online]. Available: http://www.sciencedirect.com/science/article/pii/S001623611000565X

[110] J. Weiguny, H. Borchert, and T. Gerdau, "Applying tin catalyst to oxide support to form catalyst, hydrogenating acid in the presence of catalyst," Dec. 17 1996, uS Patent 5,585,523. [Online]. Available: http://www.google.com/patents/US5585523

[111] A. Corma, M. T. Navarro, L. Nemeth, and M. Renz, "Sn-MCM-41-a heterogeneous selective catalyst for the Baeyer-Villiger oxidation with hydrogen peroxide," *Chem. Commun.*, pp. 2190–2191, 2001. [Online]. Available: http://dx.doi.org/10.1039/B105927K

[112] X. Xu, Y. Matsumura, J. Stenberg, and M. J. Antal, "Carbon-Catalyzed Gasification of Organic Feedstocks in Supercritical Water," *Ind. Eng. Chem. Res.*, vol. 35, no. 8, pp. 2522–2530, 1996. [Online]. Available: http://pubs.acs.org/doi/abs/10.1021/ie950672b

[113] T. Yeh, S. Linic, and P. E. Savage, "Deactivation of Pt Catalysts during Hydrothermal Decarboxylation of Butyric Acid," *ACS Sustainable Chemistry & Engineering*, vol. 2, no. 10, pp. 2399–2406, 2014. [Online]. Available: http://dx.doi.org/10.1021/sc500423b

[114] R. C. Crittendon and E. J. Parsons, "Transformations of cyclohexane derivatives in supercritical water," *Organometallics*, vol. 13, no. 7, pp. 2587–2591, 1994.

[115] N. Ito, H. Esaki, T. Maesawa, E. Imamiya, T. Maegawa, and H. Sajiki, "Efficient and Selective Pt/C-Catalyzed H-D Exchange Reaction of Aromatic Rings," *Bull. Chem. Soc. Jpn.*, vol. 81, no. 2, pp. 278–286, 2008.

[116] A. G. Chakinala, D. W. F. W. Brilman, W. P. van Swaaij, and S. R. A. Kersten, "Catalytic and Non-catalytic Supercritical Water Gasification of Microalgae and Glycerol," *Ind. Eng. Chem. Res.*, vol. 49, no. 3, pp. 1113–1122, 2010. [Online]. Available: http://pubs.acs.org/doi/abs/10.1021/ie9008293

[117] I. Simakova, B. Rozmysłowicz, O. Simakova, P. Mäki-Arvela, A. Simakov, and D. Murzin, "Catalytic Deoxygenation of C18 Fatty Acids Over Mesoporous Pd/C Catalyst for Synthesis of Biofuels," *Top. Catal.*, vol. 54, pp. 460–466, 2011. [Online]. Available: http://dx.doi.org/10.1007/s11244-011-9608-y

[118] P. Duan and P. E. Savage, "Hydrothermal Liquefaction of a Microalga with Heterogeneous Catalysts," *Ind. Eng. Chem. Res.*, vol. 50, no. 1, pp. 52–61, 2011. [Online]. Available: http://pubs.acs.org/doi/abs/10.1021/ie100758s

[119] R. Sotelo-Boyás, Y. Liu, and T. Minowa, "Renewable Diesel Production from the Hydrotreating of Rapeseed Oil with Pt/Zeolite and NiMo/Al2O3 Catalysts," *Ind. Eng. Chem. Res.*, vol. 50, no. 5, pp. 2791–2799, 2011. [Online]. Available: http://pubs.acs.org/doi/abs/10.1021/ie100824d

[120] B. Peng, X. Yuan, C. Zhao, and J. A. Lercher, "Stabilizing Catalytic Pathways via Redundancy: Selective Reduction of Microalgae Oil to Alkanes," *J. Am. Chem. Soc.*, vol. 134, no. 22, pp. 9400–9405, 2012. [Online]. Available: http://pubs.acs.org/doi/abs/10.1021/ja302436q

[121] H. Arai and M. Machida, "Thermal stabilization of catalyst supports and their application to high-temperature catalytic combustion," *Applied Catalysis A: General*, vol. 138, no. 2, pp. 161 – 176, 1996, chemical Engineering and Catalysis. [Online]. Available: http://www.sciencedirect.com/science/article/pii/0926860X95002944

[122] P. Forzatti, "Status and perspectives of catalytic combustion for gas turbines," *Catalysis Today*, vol. 83, no. 1–4, pp. 3 – 18, 2003, 5th International Workshop on Catalytic Combustion. [Online]. Available: http://www.sciencedirect.com/science/article/pii/S0920586103002116

[123] M. Hirano, K. Ota, and H. Iwata, "Direct Formation of Anatase (TiO2)/Silica (SiO2) Composite Nanoparticles with High Phase Stability of 1300 °C from Acidic Solution by Hydrolysis under Hydrothermal Condition," *Chemistry of Materials*, vol. 16, no. 19, pp. 3725–3732, 2004. [Online]. Available: http://dx.doi.org/10.1021/cm040055q

[124] Q. Xia, S. Kawi, K. Hidajat, and L. Li, "Enhancement of thermal and hydrothermal stability of MCM-41 by TiO2 deposition," in *Recent Advances in the Science and Technology of Zeolites and Related Materials Proceedings of the 14th International Zeolite Conference*, ser. Studies in Surface Science and Catalysis, I. C. E. van Steen and L. Callanan, Eds. Elsevier, 2004, vol. 154, Part A, pp. 856 – 862. [Online]. Available: http://www.sciencedirect.com/science/article/pii/S0167299104808954

[125] S. G. Roussis, R. Cranford, and N. Sytkovetskiy, "Thermal treatment of crude algae oils prepared under hydrothermal extraction conditions," *Energy & Fuels*, vol. 26, no. 8, pp. 5294–5299, 2012. [Online]. Available: http://dx.doi.org/10.1021/ef300798b

[126] J. L. Faeth, P. J. Valdez, and P. E. Savage, "Fast hydrothermal liquefaction of nannochloropsis sp. to produce biocrude," *Energy & Fuels*, vol. 27, no. 3, pp. 1391–1398, 2013. [Online]. Available: http://dx.doi.org/10.1021/ef301925d

[127] A. Haiduc, M. Brandenberger, S. Suquet, F. Vogel, R. Bernier-Latmani, and C. Ludwig, "SunCHem: an integrated process for the hydrothermal production of methane from microalgae and CO_2 mitigation," *Journal of*

Applied Phycology, vol. 21, pp. 529–541, 2009, 10.1007/s10811-009-9403-3. [Online]. Available: http://dx.doi.org/10.1007/s10811-009-9403-3

[128] M. Ni, D. Y. Leung, M. K. Leung, and K. Sumathy, "An overview of hydrogen production from biomass," *Fuel Process. Technol.*, vol. 87, no. 5, pp. 461–472, 2006. [Online]. Available: http://www.sciencedirect.com/science/article/pii/S0378382005001980

[129] P. Biller, A. Ross, S. Skill, A. Lea-Langton, B. Balasundaram, C. Hall, R. Riley, and C. Llewellyn, "Nutrient recycling of aqueous phase for microalgae cultivation from the hydrothermal liquefaction process," *Algal Research*, vol. 1, no. 1, pp. 70 – 76, 2012. [Online]. Available: http://www.sciencedirect.com/science/article/pii/S2211926412000057

[130] L. Amer, B. Adhikari, and J. Pellegrino, "Technoeconomic analysis of five microalgae-to-biofuels processes of varying complexity," *Bioresource Technology*, vol. 102, no. 20, pp. 9350 – 9359, 2011. [Online]. Available: http://www.sciencedirect.com/science/article/pii/S0960852411010960

[131] L. B. Brentner, M. J. Eckelman, and J. B. Zimmerman, "Combinatorial life cycle assessment to inform process design of industrial production of algal biodiesel," *Environmental science & technology*, vol. 45, no. 16, pp. 7060–7067, 2011. [Online]. Available: http://pubs.acs.org/doi/abs/10.1021/es2006995

[132] A. F. Clarens, H. Nassau, E. P. Resurreccion, M. A. White, and L. M. Colosi, "Environmental Impacts of Algae-Derived Biodiesel and Bioelectricity for Transportation," *Environmental Science & Technology*, vol. 45, no. 17, pp. 7554–7560, 2011, pMID: 21774477. [Online]. Available: http://dx.doi.org/10.1021/es200760n

[133] O. Jorquera, A. Kiperstok, E. A. Sales, M. Embiruçu, and M. L. Ghirardi, "Comparative energy life-cycle analyses of microalgal biomass production in open ponds and photobioreactors," *Bioresour. Technol.*, vol. 101, no. 4, pp. 1406–1413, 2010. [Online]. Available: http://www.sciencedirect.com/science/article/pii/S0960852409012449

[134] X. Liu, A. F. Clarens, and L. M. Colosi, "Algae biodiesel has potential despite inconclusive results to date," *Bioresource Technology*, vol. 104, pp. 803 – 806, 2012. [Online]. Available: http://www.sciencedirect.com/science/article/pii/S0960852411015653